

transmitting stations established at various sites in the world for communication with submarines. Since the transmission source is in a great distance away from the surveyed area, the primary magnetic field is handled theoretically as plane waves, and the direction of the wave vibration can be regarded as perpendicular to the direction of wave propagation and simultaneously as horizontal as shown in Fig. II - 5 .

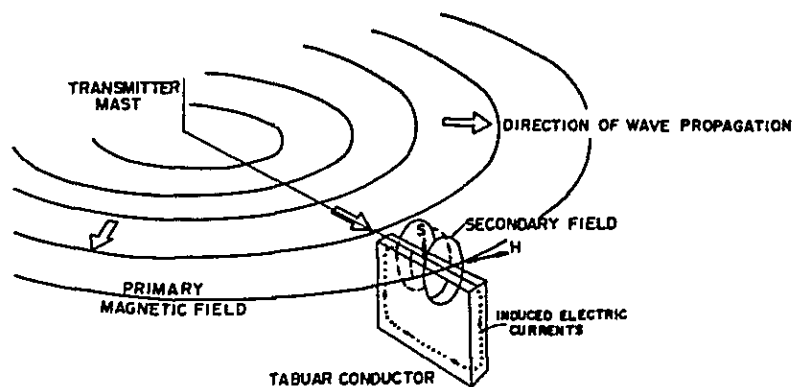


Fig. 5. A picture of primary magnetic field from transmitter and secondary magnetic field generated by conducting body

Fig. II - 6 illustrates, when good conductors exist underground, the relation existent at measuring point P, among the primary magnetic field \vec{H} , the secondary magnetic field $\Delta\vec{H}$, and the resultant magnetic field \vec{C} of the two preceding fields.

Provided that for convenience sake the coordinate axis x, which is set so that it passes p, the measuring point p, coincides with the direction of the primary magnetic field \vec{H} , and there exists a good conductor directly below point 0 on axis x, the eddy current induced within the good conductor by the primary magnetic field \vec{H} , flows perpendicular to the paper plane (toward reverse side of the paper from the front side) at the upper end of

the conductor. As a result, secondary magnetic field $\Delta\vec{H}$ is produced with phase difference ϕ .

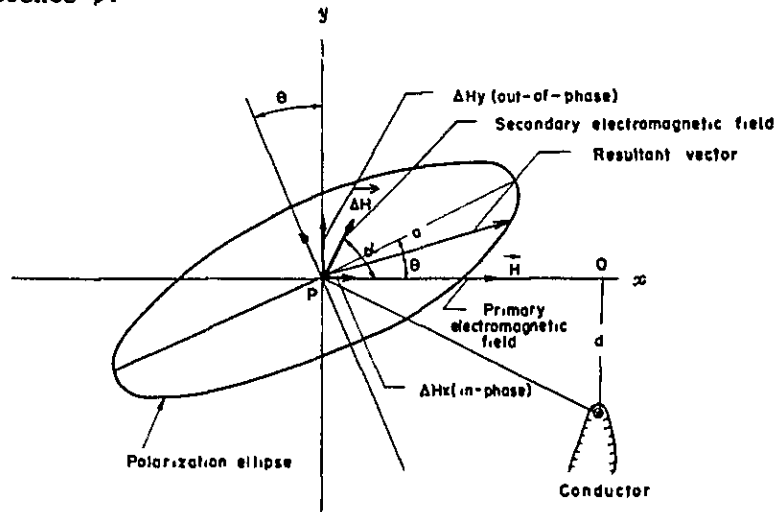


Fig. II - 6. A generalized picture of polarization ellipse

When the vector of $\Delta\vec{H}$ is inclined upward by the angle α from the \vec{H} plane, the components of \vec{H} and $\Delta\vec{H}$ in the directions both of x and y axes are given as follows:

$$H_x = H \cos \omega t$$

$$H_y = 0$$

$$\Delta H_x = \Delta H \cos (\omega t + \phi) \cos \alpha$$

$$\Delta H_y = \Delta H \cos (\omega t + \phi) \sin \alpha$$

Wherein:

H = Amplitude of the primary magnetic field \vec{H} (henry/meter)

ΔH = Amplitude of the secondary magnetic field $\Delta\vec{H}$ (henry/meter)

ω = Angular frequency (radian/sec.)

t = Time (second)

ϕ = Phase difference between primary \vec{H} and secondary $\Delta\vec{H}$ magnetic fields (radian)

Consequently, the component of the resultant magnetic field \vec{C} , of \vec{H} and $\Delta\vec{H}$ in the direction of the x and y axes is expressed in the following:

$$C_x = H \cos \omega t + \Delta H \cos (\omega t + \phi) \cos \alpha = X \cos (\omega t + \phi') \dots (2.1)$$

$$C_y = \Delta H \cos (\omega t + \phi) \sin \alpha = Y \cos (\omega t + \phi) \dots (2.2)$$

Wherein:

$$X = \sqrt{(H + \Delta H \cos \alpha \cos \phi)^2 + (\Delta H \cos \alpha \sin \phi)^2}$$

$$\phi' = \tan^{-1} \frac{\Delta H \cos \alpha \sin \phi}{H + \Delta H \cos \alpha \cos \phi}$$

$$Y = \Delta H \sin \alpha$$

The locus of the vector \vec{C} is given by eliminating ωt from the simultaneous equations (2.1) and (2.2), as follows:

$$\frac{C_x^2}{X^2} + \frac{C_y^2}{Y^2} - \frac{2C_x C_y}{XY} \cos \delta = \sin^2 \delta \dots (2.3)$$

Wherein:

$$\delta = \phi' - \phi$$

The equation (2.3) exhibits that the locus of \vec{C} describes an ellipse. The ellipse is called the polarization ellipse. The inclination θ of this ellipse suffices the following equation:

$$\tan 2\theta = \frac{2XY \cos \delta}{X^2 - Y^2}$$

So far as $\Delta H \ll H$,

$$\theta = \tan^{-1} \frac{\Delta H}{H} \sin \alpha \cos \phi \dots (2.4)$$

$$= \tan^{-1} \frac{\Delta H \sin \alpha}{H} \dots (2.5)$$

Where,

ΔH_{yi} : In-phase of the vertical component of the secondary magnetic field $\vec{\Delta H}$

The eccentricity ϵ is defined as the ratio of minor axis b , to major axis a , i.e. $\frac{b}{a}$;

$$\begin{aligned}\epsilon &= \tan^{-1} \frac{\Delta H}{H} \sin \alpha \cdot \sin \phi \\ &= \tan^{-1} \frac{\Delta H_{yo}}{H} \dots\dots\dots (2.6)\end{aligned}$$

Where,

ΔH_{yo} : Out-of-phase of the vertical component of the secondary magnetic field $\vec{\Delta H}$

As will be clear from expressions (2.5) and (2.6), the tangent ($\tan \theta$) and the eccentricity (ϵ) of polarization ellipse, shown in Fig. II-6, indicate the rate of strength both of in-phase and out-of-phase of vertical component of the secondary magnetic field to the strength of the primary magnetic field. Therefore, they both express the strength of the response from the underground good conductors to the primary magnetic field.

Strength of the response vary according to various conditions such as shape and electric characteristics of the good conductors, positional relationship between the good conductors and measuring point, etc. In general, the smaller is the resistivity of conductor, and the shallower from surface is the location, the stronger the response is obtained. The EM-16 VLF prospector used in the present survey has the design to measure the values of θ and ϵ with simple operation of the machine.

(2) Induction Method

Fig. II-7 describes conceptionally the principles of measurement using horizontal planar loop coil system that was adopted for use with the present survey. The secondary magnetic field is induced by the eddy current that is generated within a good conductor when the primary magnetic field generated in the transmitting coil passes across an underground good conductor. The electromotive force in proportion with the vertical component of the resultant magnetic field of these primary and secondary fields is produced within the receiver coil. As the measuring instrument has been adjusted to counterbalance the electromotive force from the primary magnetic field, only the vertical component of the secondary magnetic field is possible to be measured.

The direction of the vertical component of the secondary magnetic field that passes across a horizontal receiver coil is, as shown in Fig. II-7(a), the same as that of the vertical component of the primary field (positive response) so far as the transmitting and receiving coil system is to one side of the conductor, but is contrary (negative response) to that of the vertical component of primary field, as shown in Fig. II-7(b), in case the transmitting and receiving coil system astride the conductor.

As a simplified case, suppose an instance in which there exists a conductor of a vertical half-plane. At a point far from the conductor, the vertical component of a secondary field indicates a very small positive value, however, the value grows gradually larger as it approaches the conductor and attains the maximum value when the center of the coil system reaches the point about 0.5 to 1.0 time the spacing distance of the coils separated from the point immediately above the conductor. The value decreases as the coil center passes the point until the value attains zero as either of the coils is located immediately above the conductor. When

the coils astride the conductor, as shown in Fig. II-7(b), the vertical component indicates negative response which attains the maximum negative value when the center of the coils comes to immediately above the conductor. A graph showing this variation of the response is called a response curve. In this case, the response curve is horizontally symmetrical centering on the position of the conductor. It is known that maximum positive value on the down-dip side is greater than the maximum positive value on the up-dip side.

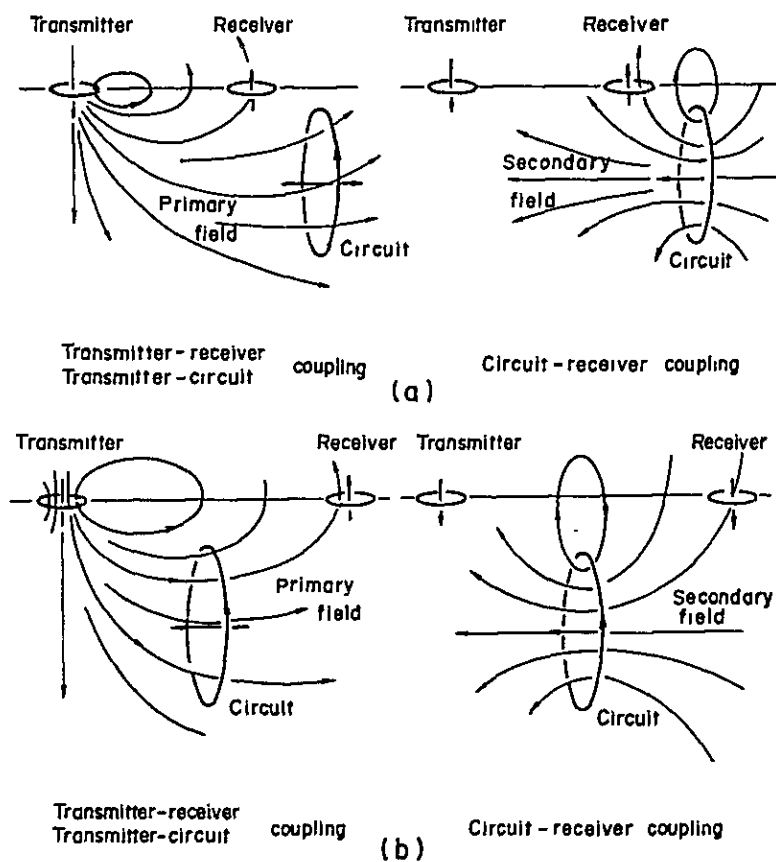


Fig II-7 Coupling of a horizontal-loop prospecting system with a simple circuit (a) prospecting system to one side of the conductor, (b) prospecting system astride the conductor.

2-2-2 Measuring Equipment

(1) VLF Method

Model EM-16, Manufactured by Geonics Limited

Measuring Range: In-phase 0 to $\pm 150\%$

Out-of-phase 0 $\pm 40\%$

Receiver sensitivity: $\pm 1\%$

Frequency: Seven channels (17.8, 24.0, 18.6, 23.4,
21.4, 22.3, and 17.4 KHz)

Power Supply: 9V Battery

Weight: 1.1 kg

(2) Induction Method

Model SE-600, Manufactured by Scintrex Limited

Measuring Range: In-phase: 0 to 200%

Out-of-phase: -50 to 50%

Receiver sensitivity: $\pm 1\%$

Frequency: 1,600 Hz

Coil spacing: 200, & 300 ft.

Coil diameter: 20 inches

Weight: Transmitter - 8 kg

Receiver - 5 kg

Power source: Transmitter - 6V Battery

Receiver - 13.5V Battery

2-2-3 Measuring Method

(1) VLF Method

VLF prospecting was carried out through the measuring stations established at 50 m intervals on C and E survey lines that were selected among the lines on which IP anomaly was detected. As an ideal VLF radio station

for this prospecting, the one which is located in the strike direction of the target conductors should be selected. Accordingly, NAA station (17.8 KHz) was selected as the signal from which was receiver sufficiently clear in the surveyed area and besides it is located almost in the strike direction of the conductor. However, the station's signal was impossible to catch successfully on the day the measurement on survey line E was tried. As a result, NPM station (23.4 KHz) was used, instead.

Table II-2 Main VLF radio-stations

Station	Location	Country	Frequency	Power
NAA	44°39' N 67°17' W	USA	17.8 KHz	1000 KW
NBA	9°04' N 79°39' W	PANAMA	24.0	150
NPG	48°12' N 121°55' W	USA	18.6	250
NPM	21°25' N 158°09' W	USA	23.4	300
NSS	38°59' N 76°27' W	USA	21.4	85
NWC	21°49' S 114°10' E	AUSTRALIA	22.3	1000
NDT		JAPAN	17.4	500

Following procedures were taken for the measurement.

- ① Try to find the direction of the receiver on which the minimum speaker sound is heard through rotating it centered on its vertical axis while keeping its signal coil horizontally as shown in Fig. II-9. The direction thus found is the direction of the VLF station.

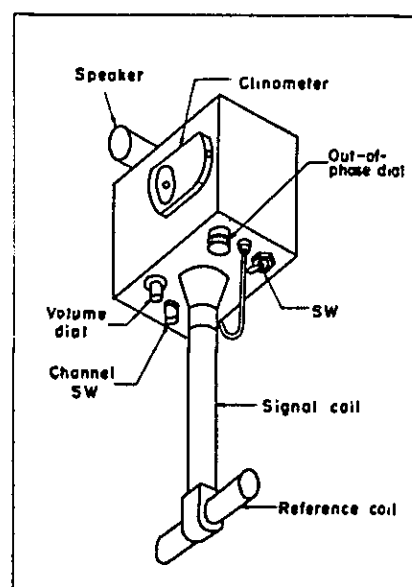
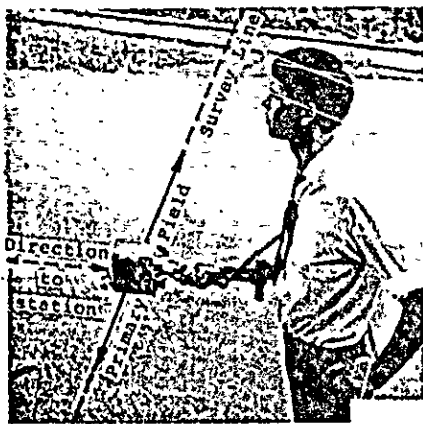


Fig. II-8 EM-16

- ② Hold the receiver in such a way that the signal coil axis stands vertically and the reference coil axis is kept in right angle with the direction of the VLF station, (the vertical plane produced by the axes of both the signal and reference coils at this time is the maximum $\Delta H_y/H$ plane) then, find the position at which the speaker sound is minimized through inclining the axes of the both coils within the vertical plane as shown in Fig. II-9-b. When the position is attained, the signal coil axis coincides with the shorter axis of the polarization ellipse, while the coil inclination represents the tilt angle (θ) of the polarization ellipse.
- ③ Read directly the $\tan \theta(\%)$ at this time with the built-in-clinometer.
- ④ Maintain the tilt angle at θ , while adjust out-of-phase control knob so that almost no speaker sound is audible. Upon completion of this adjustment, the value $\epsilon(\%)$ attained with the control knob represents the ratio of short axis to the long axis, or eccentricity.
- ⑤ Repeat these procedures in (1) to (4) at each measuring station to find θ and ϵ .



(a)



(b)

Fig. II-9 Field operation method of VLF

(2) Induction Method

Induction method can be classified into two, namely, fixed source method (the measuring is accomplished while the receiver is moved although the transmitter is set at a certain position), and moving source method (both the transmitter and receiver are moved for measuring while a certain distance is maintained between the transmitter and receiver). In either method, a handy, lightweight coil is used generally with both the transmitter and receiver. The primary magnetic field is generated when 200 Hz to 5000 Hz range alternating current power is flowed through the coil of the transmitter. Then measure the voltage of the power generated within the receiving coil located in a place separated by a certain distance (20 - 150 m) from the transmitter.

There are various coil configurations. Representative examples are shown in Fig. II-10.

Configurations (a), (b), and (c), are used for measuring the vertical component of the magnetic field, horizontal component of the magnetic field, and inclination of polarization ellipse, respectively.

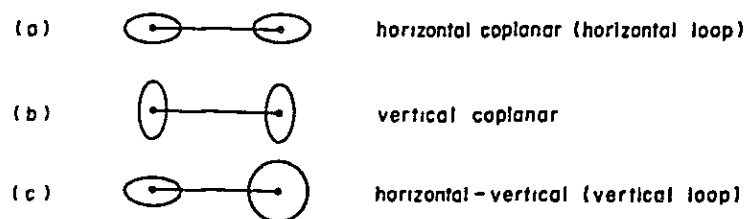


Fig II-10 Configuration of transmitter and receiver coil

In the present survey, IN-LINE MOVING SOURCE METHOD was adopted i.e. measurement was carried out for (a) and (c) coil configurations as shown in Fig. II-10 through moving along respective survey line, while the transmitting and receiving coils were separated from other by a constant spacing of 90 m.

The field operation was carried out in the following procedures:

- o Horizontal Loop Method (See Fig. II-11.)
 - (1) Prior to signal transmission, adjust the balance control in order to minimize the noise level.
 - (2) Set the attitude of coils so that they are on the same plane to form a co-planar coils system before the signal is transmitted.
 - (3) Adjust both the in-phase control knob and out-of-phase control knob so that minimum signal sound is heard.
 - (4) Read out the values of both the in-phase and out-of-phase.
 - (5) Receiver and repeat the procedures as above-mentioned at individual stations.

- o Vertical Loop Method (See Fig. II-12.)
 - (1) Fix the transmitting coil vertically and rotate the receiving coil centering on the co-axis of coils formed by the line connecting the transmitting and receiving coils until the minimum signal sound is heard.
 - (2) Read out the dip angle of the receiving coil when the minimum signal sound is heard.

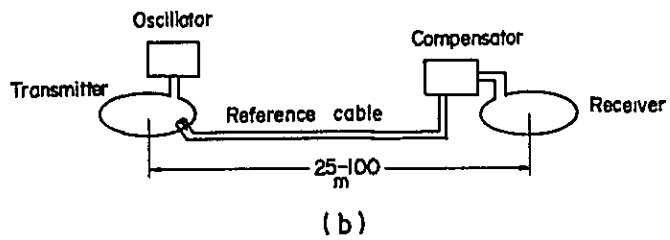
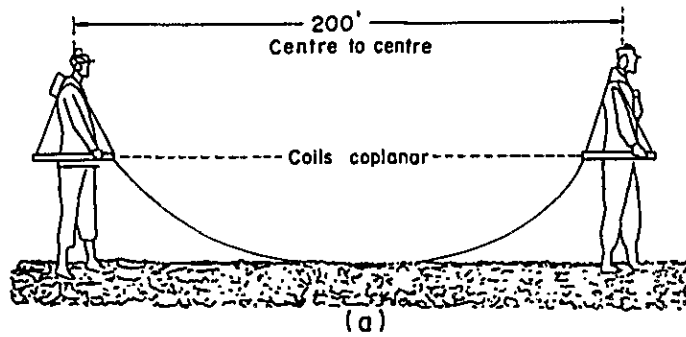


Fig. I-11. Operation method of horizontal loop system

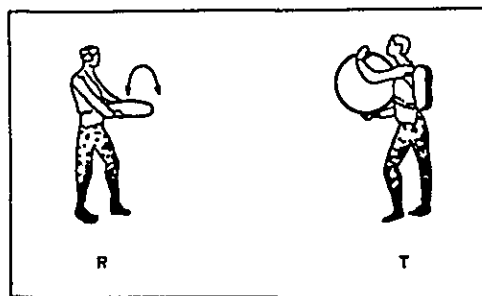


Fig. I-12 Operation method of horizontal-vertical system

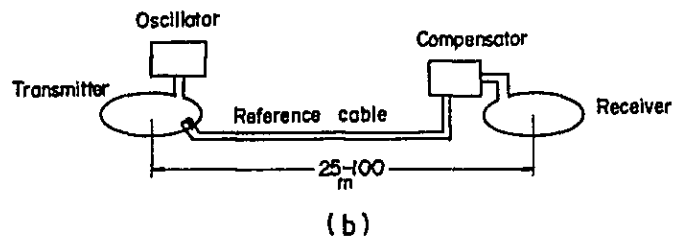
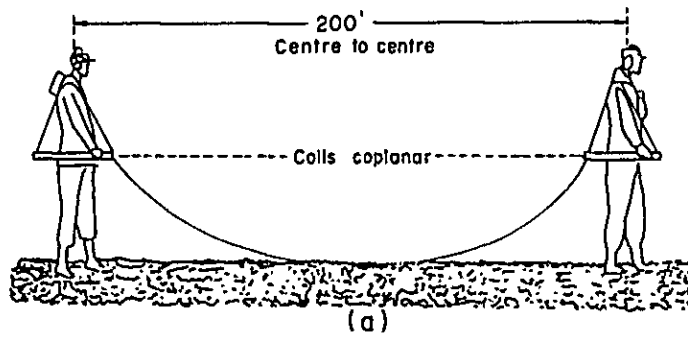


Fig. II-11. Operation method of horizontal loop system

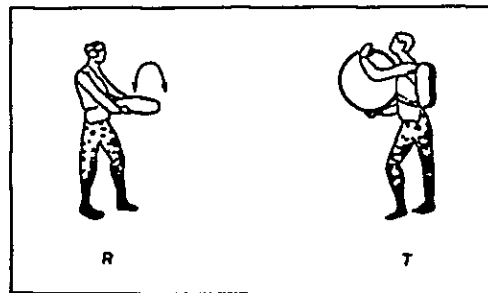


Fig. II-12. Operation method of horizontal-vertical system

Chapter 3. Procedures of Data Analysis

3-1 IP Method

3-1-1 Presentation of Data

The apparent resistivity values, FE values, and MF values for dipole-dipole configuration are plotted according to right-angled isosceles triangle method that is used widely. (See Fig. II - 13.)

3-1-2 Topographic Correction

Apparent resistivity values measured with various electrode arrangements are not uniform so far as the topography of the ground is undulated even if the ground is homogeneous and electrically isotropic. With the cases in which dipole-dipole electrode configuration is employed in an uneven topography, the apparent resistivities measured are generally high in convex relief and generally low in concave relief. When the profile under a survey line can be modelled similarly through a two dimensional model, a topographic correction with the use of the two dimensional model is effective.

In the analysis of the results of this survey, two ways, one to carry out two dimensional topographic correction, and the other to add on topographic effects, respectively, to a part of the measured results attained with dipole-dipole configuration, were employed in combination and in contrast to infer the underground structure. Checking the effectiveness of topographic correction with the afore-mentioned combined use is considered feasible to a certain degree.

3-1-3 Physical Properties of Rocks by Insitu and Laboratory Measurement

(1) Insitu Measurement

Insitu Measurement in the field was accomplished with short spacing electrodes in order to minimize the effect of surrounding rocks affecting the measurements. Electrodes were arranged as a rule, according to pole-dipole configuration as shown in Fig. II - 14.

The apparent resistivity was calculated using expression (2) in the foregoing Item 2-1. The value of K in the expression is $K = 4\pi a = 12.6a$.

(2) Laboratory Measurement

The measurement of physical properties of rock samples was carried out in the ways shown in Fig. II - 15. The sample rocks were shaped almost into rectangular parallelepipeds, and immersed in the water for about 24 hours before they were subjected to the examination. The copper plate electrodes cut to the same size as the cross section of the rock samples were used as sample supporters as shown in Fig. II - 15. The filter paper that was soaked in saturated liquid of copper sulfate was placed between the electrode and a sample rock. During the examination, the current density within sample rocks was reduced in order to attain the density as similar as possible to that in the actual field measurement. However, it was impossible to attain approximately $3\mu\text{s}/\text{cm}^2$ or less due to the capacity of the examining equipment.

3-1-4 Simulation for the Model with An Electronic Computer

Simulation was conducted with an electronic computer for representative case of the models of the underground electric structure inferred from the results of measurement. The simulation method is shown in Fig. II - 16, while the details are given in the following:

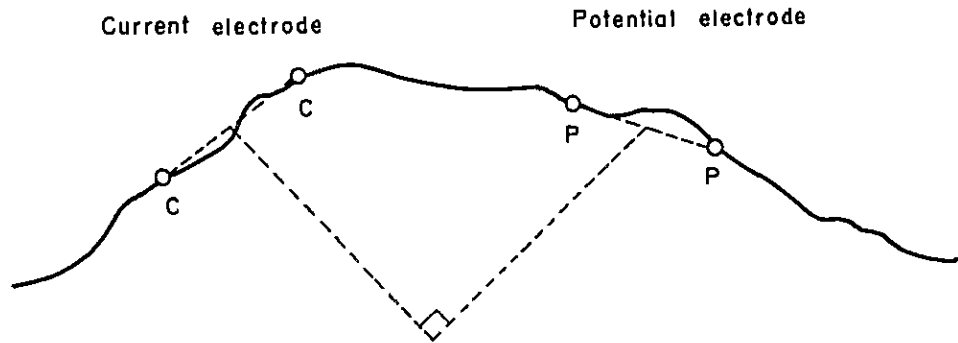


Fig. II-13. Plotting of example

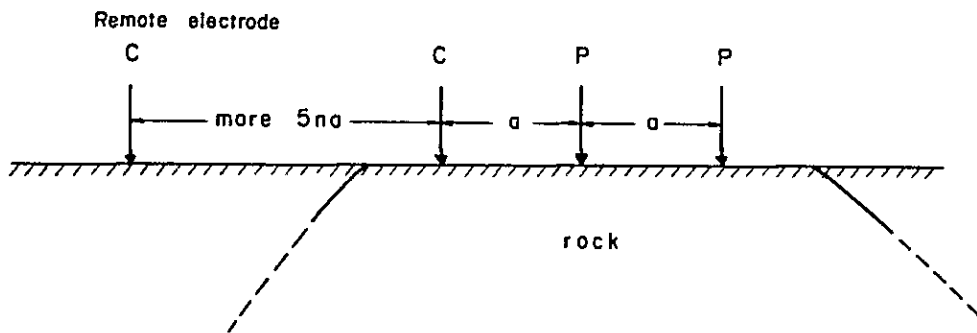


Fig. II-14. Pole-Dipole Configuration

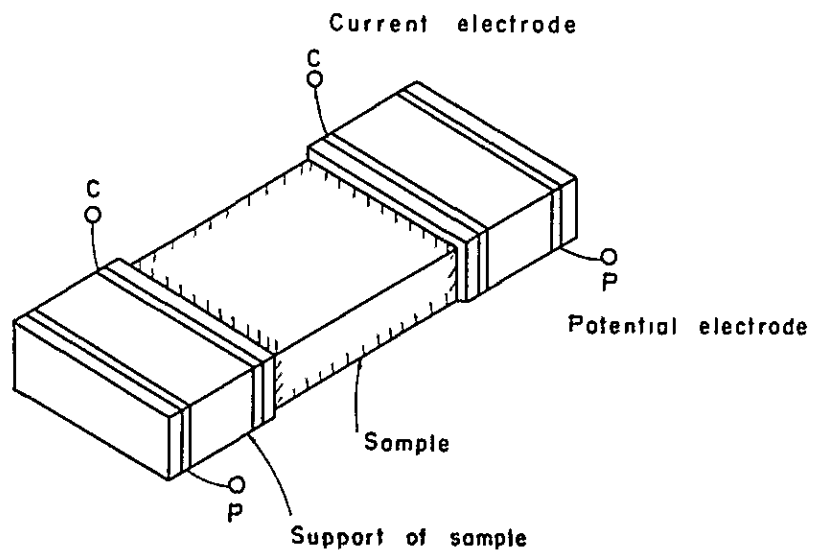
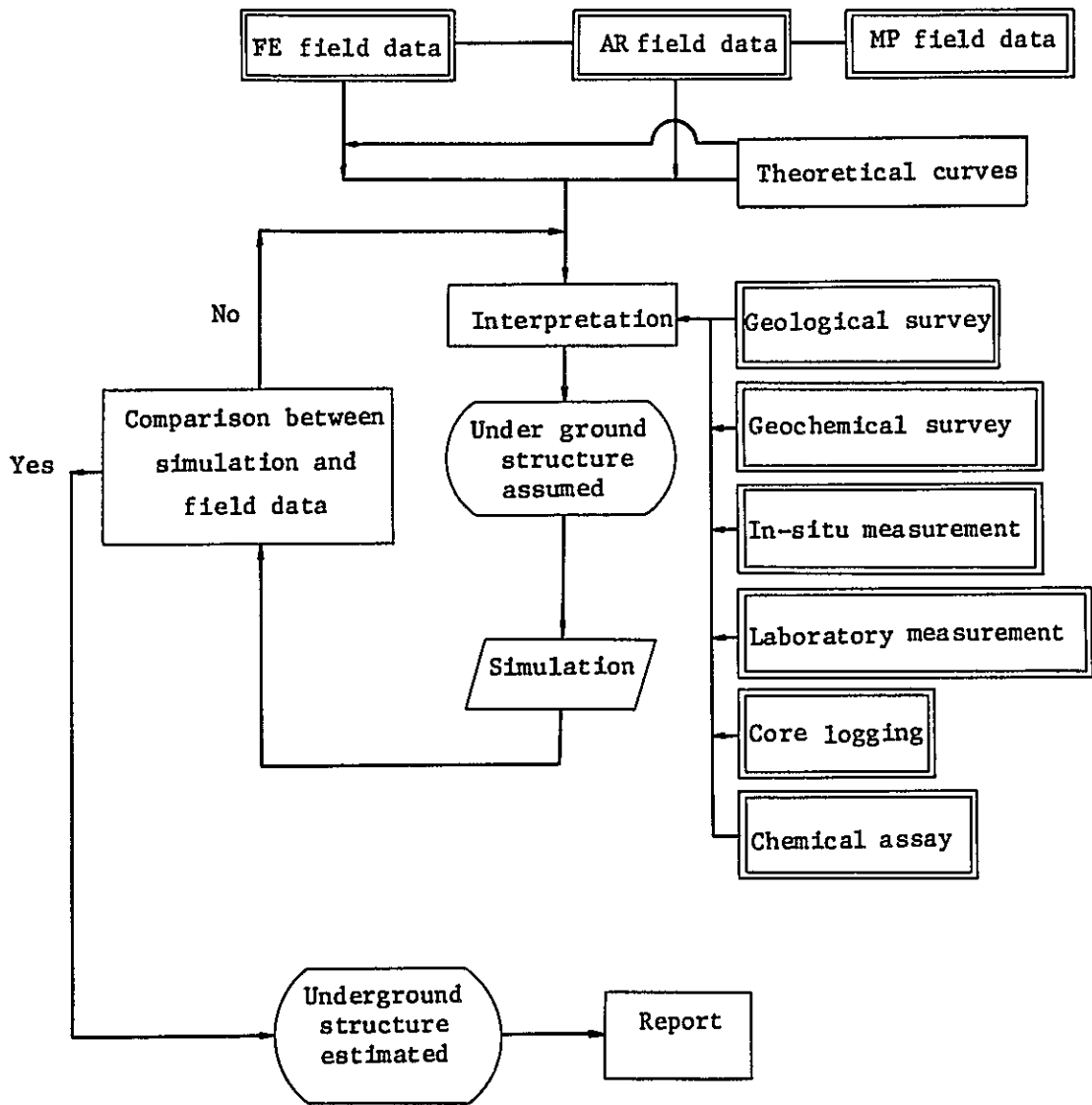


Fig. II-15. Equipment for rocksample measurement

- 1) Eliminate the topographic effect from the measured values (of the apparent resistivity). (See to Item 3-1-2 on topographic correction)
- 2) In view of all the outcome in the past from model calculation and experiments within water tank, make out underground electric structural models that are considered to express best the distribution of apparent resistivity and FE values, and the absolute value thereof with respect to the survey results.
- 3) Carry out approximative calculation with an electronic computer for the apparent resistivity and FE values pertaining to the models made out according to Item 2). In consideration of the capacity and computing time of the electronic computer, a two dimensional model was selected to be used. (Refer to Item 3-1-2 on topographic adjustments concerning the two dimensional model.)
- 4) Compare the calculated results with actually measured values. When the respective distribution and values of the FE and apparent resistivity are similar to each other at this time, the model is considered to represent the underground structure existing along the survey line.
- 5) After the calculation results attain a certain degree of coincidence, simulate an underground structural model in consideration of the topography to compare with the actually measured values in which the topographic effect is contained. Try to correct the model farther in repetition when the two are much different from each other.
- 6) The model is regarded as an underground electric structural model when the calculated results and measured values according to Items 4) and 5) are in an approximate coincidence. Then, make out an underground geological structural model based on geological data as well as on the electric structural model. For making the underground geological structural models from IP data as mentioned in the



Index

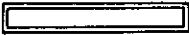
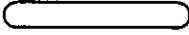
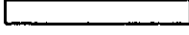

-  Measurement
-  Estimation
-  Analysis, mapping, interpretation
-  Calculation

Fig. II-16. Flow chart of IP survey

foregoing, each 4 - 7 types of underground electric structural models were produced for individual survey lines, then calculation thereof was made with an electronic computer.

3-2 EM Method

3-2-1 Plotting of Measured Results

(1) VLF Method

The reading value of $\tan \theta$ (in-phase) and ϵ (out-of-phase) are plotted on one same cross section, and are connected with solid line and broden line, respectively.

(2) Induction Method

In the case of horizontal loop method, the in-phase and out-of-phase components measured with SE-60 are plotted at the intermediate point between the transmitting and receiving coils, then are connected with solid line and broden line, respectively.

Concerning the vertical loop method, the measured dip angles of the receiving coil are plotted at the intermediate point between the transmission coil and reception coil.

3-2-2 Analysis by means of Curve Matching

In reference of various in-phase and out-of-phase curves of a perfectly conductive half plane model, the depth and inclination of the good conductor with respect to VLF method, and the depth, inclination, position, and ratio of resistivity to thickness of the good conductor with respect to induction method are obtained.

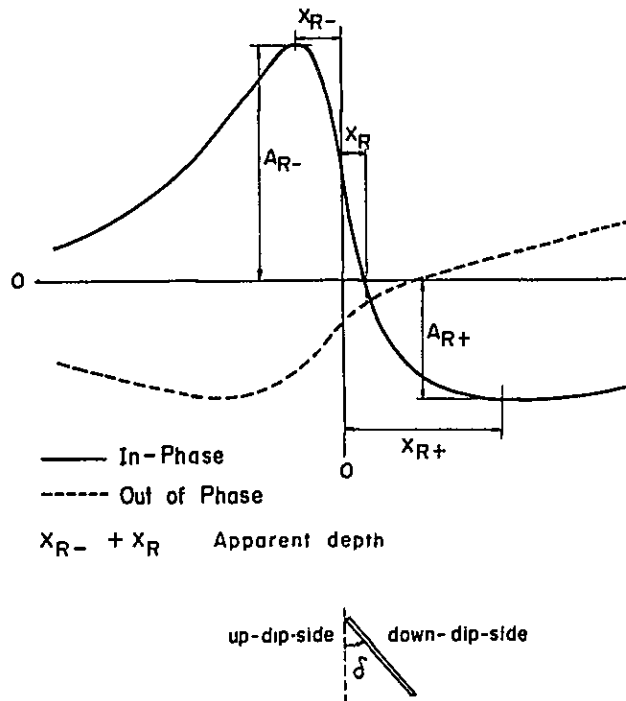


Fig. II - 17. Parameters used for determination of depth to the top of conductor and dip angle

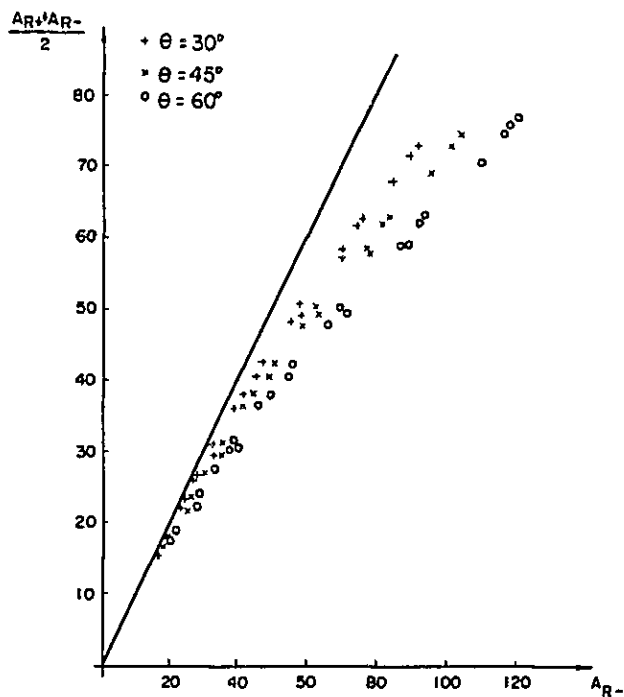


Fig. II - 19. Diagram of half the peak-to-peak anomaly to the up-dip peak anomaly for determination of dip of half plane

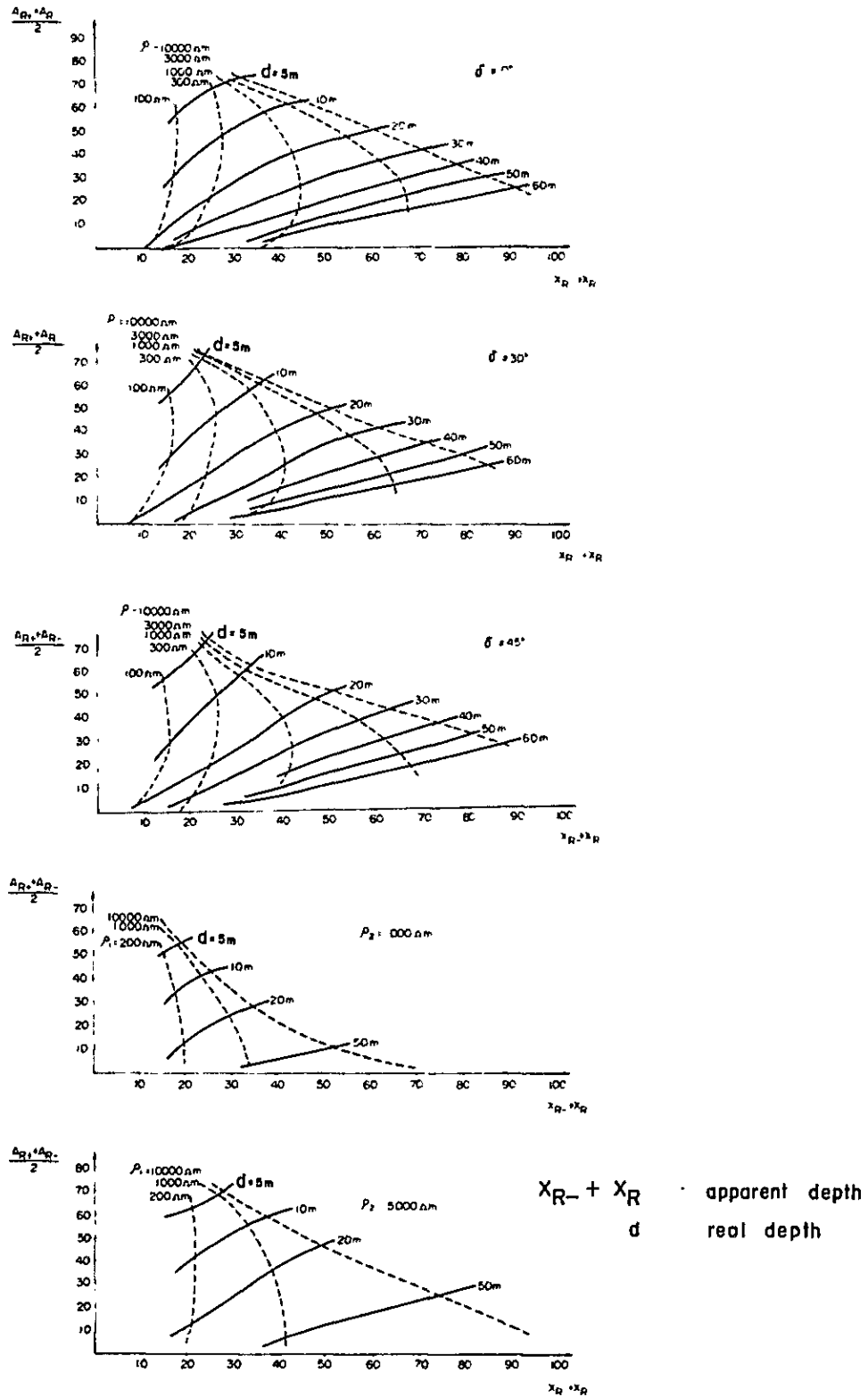


Fig. II-18. Diagram of half the peak-to-peak anomaly to the apparent depth for determination of the real depth to top of conductor

(1) VLF Method

The method proposed by OLSSON (1980) is employed as the analysis method. Fig. II-17 shows the standard type of both in-phase curve and out-of-phase curve. From the inphase curve, the maximum value A_{R-} , the minimum value A_{R+} and the distance $X_{R-} + X_{R+}$ between the points the maximum value and zero response respectively on the survey line, are obtained. These values are plotted on the diagram of Fig. II-18, and Fig. II-19, then the dip angle and depth of the good conductor are found.

(2) Induction Method

From the in-phase and out-of-phase curves given by the horizontal loop method, the positions showing the maximum and minimum values of both the in-phase and out-of-phase are obtained. These values were used as the parameters in the analysis made in reference of the group of curves prepared by the model experiments on perfectly conductive half plane as shown in Figs. II-21 to II-23.

The measurement according to the vertical loop method was employed as the means of reconnaissance survey in a limited scope only of qualitative analysis to infer the position of the good conductors.

M.R. NAIR, S.K. BISWAS AND K. MAZUMDAR

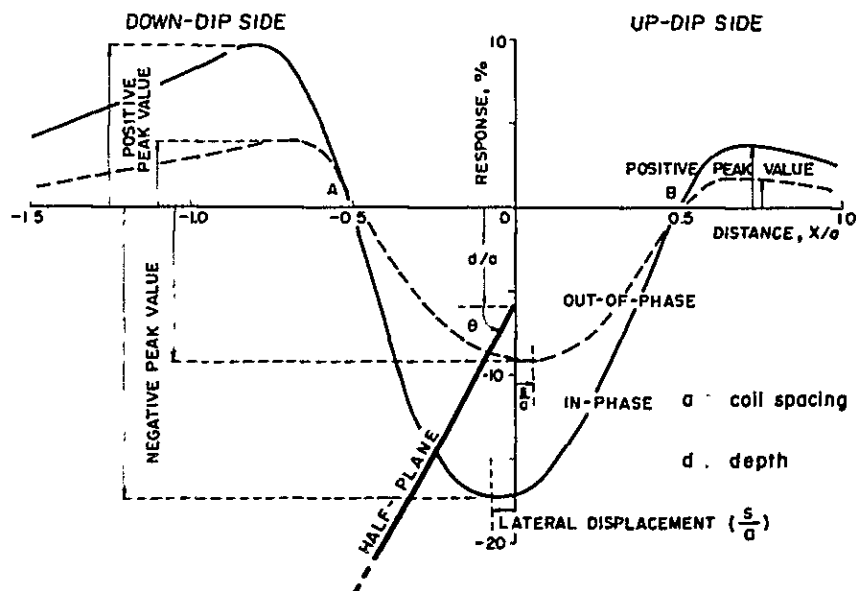


Fig. II-20 A typical profile over a tilted conducting half-plane, $\beta = 60^\circ$, $\lambda/a = 5.0$, $d/a = 0.3$

Chapter 4 Results of Survey

4-1 Geology of the Surveyed

4-1-1 Geology and Geological Structure of the Area near Iscay Cruz ore Deposits

In Iscay Cruz area, there are distributed the sedimentary rocks of Cretaceous era ranging between the Chimu and the Jumasha formations which are intruded by stock or dike form quartz porphyry, dacite and porphyrite.

Sedimentary rocks generally strike in NNW-SSE direction with dips varying between 70°W and 80°E. Santa formation, which is the host rock of the ore deposits, overlies the Chimu formation and ranges 60 m to 105 m in thickness. Some faults and fissures run in the same direction as the formations, and the others across.

4-1-2 Iscay Cruz Ore Deposits

Iscay Cruz ore deposit is embedded in the Santa formation in the west wing of the anticlinal structure which forms the axial trend lying on the Chimu formation. The deposit is embedded in the carbonate rocks and consists of iron-quartz gozzan, disseminated lead-zinc sulfides, skarn, etc. The ore deposit is developed intermittently from the first mineralized zone at the northern end down to the seventh at the southern end. The first mineralized zone consisting of iron-quartz gozzan is of the largest scale among the Iscay Cruz ore deposit and contains two rows of massive ore deposits in its the Santa formation.

The second mineralized zone consists of reticulated iron-quartz gozzan.

The third mineralized zone is dotted with small outcrops of disseminated sphalerite and galena.

The fourth mineralized zone consists of sphalerite and galena into disseminated in, and the mineralization is distributed in two rows.

In its southern part, galena accompanied by massive pyrite is observed. Chupa ore deposit has a dense concentration of ore minerals mainly composed of sphalerite and chalcopyrite in its skarn.

The sixth mineralized zone possess a dense concentration of sphalerite in its dolostone.

The seventh mineralized zone is of a black gozzan.

4-2 IP Measurement with Dipole-dipole Configuration

Profiles of AR(apparent resistivity), FE(frequency effect), and MF(metal factor) on every survey line shown in Pl.II-2-1 to Pl.II-2-8.

4-2-1 AR Measured Results

The apparent resistivity values range from 1 ohm.m to over 100,000 ohm.m. The measured values are classified into five reasonable ranges for convenience of analysis as shown in the following table:

40 Ω m		150 Ω m		650 Ω m		2500 Ω m	
VL	L	M	H	VH			

Explanation is given in the following on the apparent resistivity by each survey line:

(1) Survey Line A (See Pl. II-2-1)

On the line to the north of the station 60, where the first, second, and third mineralized zones are exposed, comparatively high(H) or medium(M) ARs are obtained, in general, while on the southern sector, low AR values

are observed. On the surface, pyrite is observed to increase in content towards the south of the station 62. The medium(M) values of AR indicated to the north of the station 60, where the Santa or the Carhuaz formation is exposed, are distributed widely up to the north end of the survey line.

Very low(VL) AR values are detected near the stations 65 to 71.

"Pant-legs" pattern is indicated mainly near the station 68. From the shape of the pattern, existence of a plate type low AR responding body is presumed near the ground surface. This area belongs to the fourth mineralized zone, and ore minerals such as sphalerite and galena are observed as well as hematite, specular iron, and pyrite. The AR distribution near the stations 71 and 72 shows an extreme variation from very low AR to medium AR.

Low or lower AR is widely distributed near the stations from 76 to 99.

Very low AR distributed between the station 86 (Lagunas tinyag) and the station 99 (Cumbre de Cunsha Punta) is prominent. The surface near this sector has its greater part covered with talus, however, the sector is an argillized area, according to trench survey. An outcrop of skarn is confirmed in the eastern side of the stations 89 and 90 by the geological survey carried out in this year. A great change in AR is observed near the station 99, where the surface is covered with talus and the width of the Santa formation is considered to narrow suddenly.

From the station 100 to the station 112, medium(M) AR is detected, where the Chimu formation, the Santa formation and the Carhuaz formation underlies. Since the geological data shows existence of faults, the area is equivalent to sheared zone. In the southern sector from the station 112, low(L) AR is distributed widely. Very low (VL) AR is distributed about 150 m underneath the surface of the stations 112 to 120. On the surface near the station 115, a good amount of pyrite are observed. Outcrops are

also confirmed near the station 120, a part of which has been skarnized.

(2) Survey Line F (See Pl. II-2-6)

Except for the northern sector from the station 5, and the stations from 15 to 19, where medium (M) AR is detected, high (H) AR is distributed all over the sector. This survey line is situated on the first mineralized zone of the Iscay Cruz ore deposit, and is almost parallel with stations 15-40 on the survey line A. The sector near the stations 8-10, where intense distribution of 1,000 ohm·m or higher apparent resistivity is detected is different in trend from survey line A.

(3) Survey Line G (See Pl. II-2-7)

This survey line intersects F and A survey lines near the stations 7 and 8. Medium(M) AR, high(H) AR is distributed in the western and eastern sector of the line, respectively, bounded by the station 6. On the surface ground to the east of the station 6, the Chimu formation composed of quartzite, sandstone, etc. is exposed, and its land form is steep. The western sector adjoins to the Santa formation and the Carhuaz formation is distributed extensively. To the west of the station 17, sandstone of the Farrat formation, and the limestone of both the Pariahuanca and the Chulec formation occur. However, there is almost no difference in the AR corresponding to all those formations.

(4) Survey Line E (See Pl. II-2-5)

There are distributed very high (VH) AR to the east of the station 9, medium (M) AR to the west of the station 6, and very low (VL) AR in the intermediate sector. In view of "pant-legs" pattern indicated around the station 7, existence of a vertical plate type responding body can be considered. The very low (VL) AR is correlated with the very low (VL) AR detected near the station 68 on the survey line A in locality. On the surface ground east of the station 8, sandstone and quartzite of the Chimu formation are

distributed. The apparent resistivity corresponding to the Chimu formation is very high, or about ten times or more the value of the formation in northern sector. Measured results indicate that the apparent resistivity corresponding to the Chimu formation, the Santa formation and the Carhuaz formation on this survey line has such an extreme difference as very high (VH)- very low (VL)- medium (M).

(5) Survey Line C (See Pl. II-2-3)

Low (L) AR near the stations 6 - 11, very high (VH) AR east of station 11, and medium (M) AR to the west of the station 6 are detected. In consideration of "pant-legs" type very low (VL) AR pattern, existence of vertical responding body can be estimated. Although a greater part of the surface ground is covered with talus, existence of skarn zone and outcrops containing pyrite are confirmed in the Santa formation near the station 10. The high (H) AR obtained to the east of the station 11 corresponds to the distribution of the Chimu formation.

The surface ground to the west of the station 7, where medium (M) AR is obtained, is covered with talus. From the geological data, it is presumed that sandstone of the Farrat formation, the Pariahuanca formation, and the Chulec formation are distributed there. However, they give no recognizable difference in the AR.

(6) Survey Line H (See Pl. II-2-8)

On the eastern sector of the survey line, low and very low (L-VL) AR are detected, while medium and high (M-H) AR are observed on the western sector. The distribution of the very low AR is correlated with the distribution of the limestone of the Pariahuanca formation, sandstone of the Farrat formation, sandstone and shale of the Carhuaz formation, and the Santa formation. The distribution of medium and high (M-H) AR passes across the Chupa ore deposit near the station 5, which is correlated with

the Chulec and the Pariatambo formations distributed in this vicinity. On the surface ground, pyrite, pyrrhotite in addition to sphalerite and chalcopyrite are observed.

(7) Survey Line D (See Pl. II-2-4)

The distribution of apparent resistivity on this survey line is complicated. Although medium AR is distributed on the whole, there observed the AR distribution, from which the "pant legs" pattern of both the low AR and high AR centering on the vicinity of stations 8-9 can be recognized. Very low (VL) AR is distributed in the deep underground along the eastern side of this survey line, and, there is marshy zone on the surface. Medium (M) AR is distributed in correspondence to the Carhuaz formation, the Santa formation, and the Chimu formation, however, the apparent resistivity corresponding to the Chimu formation which is distributed to the east of the station 6, is very low in its value when compared with the AR of northern part of the Chimu formation.

(8) Survey Line B (See Pl. II-2-2)

On the whole, low (L) AR is distributed widely, though medium (M) or higher (H) AR is observed near the surface ground of the stations 3-4, 5-6 and 13-14. Medium (M) to low (M-L) AR in the western sector of survey line to the west of the station 4 is distributed corresponding to the Farrat formation and the Pariahuanca formation etc. Although the low AR to the west of the station 4 is distributed corresponding to the Carhuaz formation, the Santa formation, and the Chimu formation, the medium AR detected near the stations 13-14 is considered to correspond to the Chimu formation in this neighborhood in view of the fact that the location of the AR coincides with the position of the outcrop rock observed on the surface ground. As the result of this year's geological survey, the existence of black gozzan and skarn zone within the Santa formation near the stations 9-10

has been confirmed. The apparent resistivity in the Santa formation and the Chimu formation in this vicinity show very low values when compared with that of the northern black gozzan zone.

4-2-2 FE Measured Results

The maximum value of FE measured is 9%. The measured values are classified into five reasonable ranges for convenience of analysis.

	2%	3%	4%	6%
Back ground	W	M	S	VS

Descriptions are given in the following on FE anomaly detected on each survey line as follows:

(1) Survey Line A (See Pl. II-2-1)

The FE value at 3% or less is a weak anomaly (W) that is detected near the stations 22 and 58. The weak anomaly (W) observed near the station 45 extends up to the south end of the survey line, showing a large scale distribution. This weak anomaly once fades out near the station 86.

Lagunas Tinyag is situated near this station and surrounded by alluvial deposits with limonitized reddish soil. The weak anomaly in and to the north of Cumbre de Suerococha is in a small scale without continuity, yet, particularly large scale of gozzan among the Isca Cruz ore deposit is exposed on the surface ground.

Medium (M) FE anomaly including very strong FE anomaly is widely spreading in the vicinity of the station from 59 up to 71. The strong (S) FE anomaly detected mainly near the station 68 indicates "pant-legs" pattern. The pattern suggests an existence of a large scale plate responding body near

the ground surface. This area belongs to the fourth mineralized zone, limonite, specularite, and pyrite in addition to ore minerals of sphalerite and galena are observed. Near stations 73-78, medium (M) FE anomaly is detected, however its scale is small. The surface is covered with talus, while existence of such ore minerals as sphalerite, chalcopyrite, etc. and some outcrops including that of pyrite are confirmed near the station 75.

Strong (S) FE anomaly is detected near the stations 81-85. This anomaly is located only in shallow underground and is not spreading downwards, however, medium FE anomaly is extended to deep underground.

Weak (W) to Medium (M) FE anomaly is detected around the stations 90-95. Greater part of its surface is covered with talus, however, according to the data obtained by trenching, white argillaceous alteration zone underlies the talus.

Medium (M) FE anomaly is located about 100 m underneath the surface near the stations 100-105. Weak FE anomaly extends toward south, however, the scale of responding body is inferred to be small according to the extent of the medium FE anomaly distribution. Skarn accompanied with pyrite is exposed near the station 103, where a fault is expected.

Strong (S) FE anomaly is located on and the south of the station 111. The distribution of both strong and weak FE anomaly extend as far as 1.5 km. From the anomaly of "pant-legs" pattern centering on the vicinity of the station 115, it can be considered that a plate like responding body exists in shallow underground. The strong FE anomaly located in and to the south of the station 120 lies about 150 m below the surface, while medium FE anomaly overlies it in the shallow underground. Black gozzans and small scale of skarn zones are confirmed to exist near the station 120. A plenty of pyrite is observed on the surface near the station 115.

(2) Survey Line G (See Pl. II-2-7)

Weak (W) "pant-legs" pattern was observed in the vicinity of the station 6. From the pattern, an almost vertical responding body is inferred to exist. This survey line across the gozzan of the Iscay Cruz ore deposit at a point near the station 6. The FE values obtained in the western sector to the west of the station 6 correspond to that of a background. No alteration is observed in sandstone and shales of the Santa formation, the Carhuaz formation and the Farrat formation, which expose on the surface ground.

(3) Survey Line F (See Pl. II-2-6)

Weak (W) FE anomaly is distributed widely over the entire survey line. The anomaly lies in shallow underground to the south of the station 7, while it extends to deep underground in the vicinity of the stations 11-15. This area belong to the first mineralized zone of the Iscay Cruz ore deposit. This survey line passes over gozzans spreading in continuation.

(4) Survey Line E (See Pl. II-2-5)

Strong (S) FE anomaly is located near the stations 6-9, which indicates "pant-legs" pattern. This pattern suggest the existence of an approximately vertical columnar responding body. This strong FE anomaly corresponds to the anomaly obtained in the vicinity of the station 68 of survey line A. The FE anomaly does not extend toward the east and west direction, but shows a narrow distribution. The FE values in the eastern sector of the line to the east of the station 9 and in the western sector to the west of the station 6 indicate the FE values of background, while no FE anomaly is recognizable in the Carhuaz formation. The strong FE anomaly obtained on the intersection point of both the survey lines A and E indicate a pattern extending long on north to south profile but short on east to west profile.

(5) Survey Line C (See Pl. II-2-3)

From the vicinity of station 8 up to the vicinity of station 12, medium to strong FE anomaly (M-S) is obtained. The strong (S) FE anomaly exhibits a trapezoidal form centering on the vicinity of station 9, which suggests the existence of an approximately vertical columnar responding body. Skarn is exposed at the place where this survey line passes over the Santa formation near the station 10. To the west of stations 9-10, the Carhuaz formation is distributed, however, greater part of the formation is covered with talus. Sandstone of the Carhuaz formation exposed on the surface is associated with disseminated pyrite. The distribution of the above-mentioned strong FE anomaly corresponds to that of the Santa formation and partly of the Carhuaz formation adjoining to the Santa formation.

(6) Survey Line H (See Pl. II-2-8)

From the vicinity of the station 5 up to the vicinity of the station 9, medium FE anomaly (M) and partly strong FE anomaly (S) are distributed. The strong FE anomaly (S) indicates "pant-legs" pattern centering on the vicinity of stations 6-7, which suggests the existence of plate-like responding body in shallow underground. This survey line passes across over the Chupa ore deposit at a point near the stations 5-6. Ore minerals such as sphalerite, chalcopyrite, etc, and pyrrhotite, pyrite are observed in the skarn of the pariahuanca formation exposed on the surface ground. Horizontal distribution of the FE anomaly in this shows that the extention of the FE anomaly ranges from the eastward of the Pariahuanca formation up to the Santa formation. On the other hand, the FE anomaly on the survey line C can be observed in the Santa formation and a part of the Carhuaz formation. In the area where the Pariahuanca formation and the Farrat formation are expected presumed to be overlain by talus in the west end of survey line C, there is seen no such FE anomaly as those detected on survey line H

is observed.

(7) Survey Line D (See Pl. II-2-4)

To the west of the station 8, medium FE indication (M) partly with strong FE indication (S) is observed. To all the strong FE indications (S) detected on A, E, E, and H survey lines, low apparent resistivity corresponds. However, the strong FE indication detected on the survey line D is accompanied by medium apparent resistivity (M). Compared with the FE values in the vicinity of stations 100-105 on the survey line A which lies along the Santa formation, which run along the Santa formation, the FE indication on survey line D which intersects the survey line A is strong and extends westward, however, its scale is small. This survey line lies along fault line and over surrounding sheared zone. Skarn zone accompanied with pyrite are recognized near the station 6.

(8) Survey Line B (See Pl. II-2-2)

To the east of the station 6, medium FE anomaly (M) partly with strong FE anomaly (S) is distributed. Vertical columnar responding bodies are expected near the surface ground of the station 13 and under the shallow to deep ground of the station 9. The strong FE anomaly is detected on the survey line B, 150 m under the ground where the similar FE indication is obtained on the survey line A which intersects the survey line B.

However, the scale of the FE anomaly detected on survey line B is not large. The FE anomaly distributed along Santa formation stretches as long as 1.5 km in the north to south profile along the survey line A, however, only it shows a short length of extension on the survey line B. This fact justifies the consideration that the FE responding body stretches long in the north to south direction but short in the east to west bearing. By the measurements on the survey line B, the FE anomaly is detected only on the Santa formation and on its periphery, but is not recognized in the

Pariahuanca formation.

During the geological survey conducted in this year, the existence of outcrops of small scale of skarn and black gozzan are confirmed in the Santa formation near the station 9 - 10.

4-2-3 MF Measured Results

Through the computation of MF, maximum value of 9,000 is obtained. The MF values are classified into five reasonable ranges for the convenience of analysis as mentioned below:

	10	50	100	200
Back ground	W	M	S	VS

Description on MF anomaly calculated on each survey line is given in the following:

(1) Survey Line A (See Pl. II-2-1)

In the area between the station 65 and the station 71, very strong MF anomaly (VS) is obtained. This anomaly corresponds to strong FE or very strong FE anomaly (VS) and very low AR (VL). The MF values attain its maximum of 9,000. Strong MF anomaly (S) is distributed in the area between the station 75 and the station 78. The anomaly corresponds to medium FE indication and very low AR. The foregoing two areas are located within the fourth mineralized zone.

In the area between the station 85 and the station 100, very strong MF anomaly (VS) is obtained. This anomaly corresponds to the weak (W) or medium FE anomaly (M) and very low AR (VL). The highest MF value in this area is 4500. Greater part of the surface ground is covered with talus, however, limonitization in the alluvial deposits near the station 85 and

alteration zone, which consists of white clays, exposed to the south of the station 93 are distributed extensively. Since the FE anomaly corresponding to the MF distribution is not strong, it is conceivable that the MF anomaly is different in its origin from that detected in the foregoing fourth mineralized zone.

Medium MF anomaly is located about 150 m under the ground between the station 113 and the station 120. This anomaly corresponds to the strong (S) or very strong FE indication (VS) and low (L) or very low apparent resistivity (VL). The maximum MF value is 333, which is smaller than the value obtained in the fourth mineralized zone. By the geological survey carried out in this year, mineralization is confirmed on the surface ground.

(2) Survey Line E (See Pl. II-2-5)

Strong (S) and very strong MF anomaly (VS) are distributed between the station 5 and the station 10. This anomaly corresponds to the strong (S) or very strong FE anomaly (VS) and very low apparent resistivity (VL). The maximum MF value of 2,550 is attained. This area belongs to the fourth mineralized zone.

(3) Survey Line D (See Pl. II-2-4)

Weak MF anomaly (W) is distributed corresponding to very low and medium apparent resistivity (L-M). The MF anomaly located in the deep underground to the east of the station 8 corresponds to the FE values less than 2%, and is considered to be quasi-anomaly due to very low apparent resistivity.

(4) Survey Line C (See Pl. II-2-3)

Strong MF anomaly (S) corresponding to strong FE anomaly (S) and very low apparent resistivity (VL) is distributed between the station 7 and the station 9. The MF values obtained to the east of station 11 are

very small.

(5) Survey Line H (See Pl. II-2-8)

Strong MF anomaly (S) is obtained to the east of the station 5 corresponding to strong FE anomaly (S) and very low apparent resistivity (VL). The survey line H passes across the Chupa ore deposit which is exposed on the surface ground.

(6) Survey Line B (See Pl. II-2-2)

A small scale of strong MF anomaly (S) corresponding to strong FE anomaly (S) and low apparent resistivity (L) is shown about 200 m under the ground between the station 8 and the station 11. Outcrops of skarn are confirmed in existence below the surface of the station 9.

4-3 EM Measurement

4-3-1 Measurement Results of VLF Method (See Pl. 4-1 and 4-2)

(1) Survey Line C

In-phase component attains the maximum value of +40% at the west of stations 9-10 and the minimum value of -40% at the east, indicating a remarkable anomaly in response. Since the corresponding out-of-phase component shows, in like manner, the minimum value of -10% at the west and the maximum value of +6% at the east stations 9-10, existence of a conductor near the stations 9-10 can be inferred.

(2) Survey Line E

The types of response changes of both in-phase and out-of-phase components on survey line E are similar to the type on survey line C. In-phase component, shows the maximum value of +20% in response at the west of stations 7-8 and the minimum value of -20% at the east. Although the amplitude of the response is reduced to a half when compared with the case

on survey line C, existence of a conductor is presumed in the vicinity of the stations 7-8. The out-of-phase component corresponding to the in-phase indicates the changes in a range between minimum 0% and maximum +10%.

4-3-2 Measurement Results of Induction Method

(1) Survey Line C

Since definite response anomaly is recognized near stations 10-11, with horizontal loop method, showing maximum +7% and minimum -18% of in-phase component and maximum +4% and minimum -15% out-of-phase component, existence of conductor is inferred in the vicinity of the station 10-11. Also with vertical loop method, remarkable changes in dips angle is recognized near stations 9-11 showing a good coincidence as to the location with the anomaly with horizontal loop method.

(2) Survey Line E

With horizontal loop method, both the in-phase and out-of-phase components indicate the response almost symmetric as to east and west centering on an intermediate point between stations 7 and 8. The maximum and minimum values of in-phase component are +5%, and -15%, respectively, while, the maximum and minimum values of out-of-phase component are +3%, and -10%, respectively. Also with vertical loop method, the dip angle changes from north (east side) to the south (west side) at the intermediate point, a between stations 7 and 8. The coincidence in position with the case of horizontal loop method indicates a high probability of the existence. Subsequently, it is inferred that of a conductor near stations 7-8.

4-4 In-situ Measurement and Laboratory Work

4-4-1 The Results of Laboratory Measurement

56 rocks were provided as rock samples for measurement of electrical property in the laboratory, however, measured values are obtained from 52 rocks as 4 of them crumbled during reforming work and measurement. The measurement values are listed in Table 3, while the values arranged in order by rock types and stratigraphy are shown in Table 4. From the measured values attained, Chart of the Correlation between FE and Resistivity Values is prepared. (See Fig. II-24)

Following are the items pointed out from the results of laboratory measurement.

(1) Limestone (3 samples)

The average FE value and average resistivity value obtained from two samples classified as of the Pariahuanca formation are 0.6%, and 7184 ohm·m, respectively. While another sample belonged to the Santa formation marked FE value of 1.2%, and resistivity value of 7,120 ohm·m. Total average values of FE and resistivity are 0.8%, and 7,162 ohm·m, respectively.

(2) Sandstone (20 samples)

The FE values obtained from 20 samples of sandstone range from 0.3% to 2.5%, showing a small variation comparatively, while, the values mark a large variation with its values ranging from 82 ohm·m to 9,970 ohm·m, and total average value of 2,850 ohm·m. Significant difference in the average value of resistivity can be recognized between formations. The Carhuaz formation (3,225 ohm·m) and the Santa formation (2,254 ohm·m) have average values almost the same as the total average value, while, those of the Farrat formation (1,480 ohm·m), and the Chimu formation (9,970 ohm·m) are lower, and higher, respectively, than the total average value. This state

is considered attributable to the difference in porosity, which is one of the factors having influence on the resistivity of rocks, as every sample from the Farrat formation is porous, while those of the Chimu formation are compact due to silification.

(3) Shale (8 samples)

The FE values attained from samples of shale range from 1.0% to 2.8%, showing small variation, and the total average is 1.8%. In the average by formation the Santa formation (1.1%) is slightly lower than that of the Carhuaz formation (2.1%), however, no significant difference is recognized. FE values of shale within the survey area is considered to be represented by the total average value. Resistivity values range from 568 ohm.m to 43,343 ohm.m showing a very large variation, and total average marks 12,138 ohm.m. The average is 1,802 ohm m when samples A98-1 (42,951 ohm.m) and A98-2 (43,343 ohm.m) of high values are omitted. In the average by formation, the Chimu formation and the Santa formation marks 15,356 ohm.m, and 2,485 ohm.m, respectively.

(4) Dolostone (2 samples)

Dolostone, grouped in the Santa formation, gives its average FE value of 3.8%, which is high compared with those of the foregoing rock types in (1), (2), and (3) items. Average resistivity value of 2,108 ohm.m approximately coincides with those of the sandstone and shale of the Santa formation.

(5) Gozzan (5 samples)

Every gozzan sample is grouped in the Santa formation. Their average FE value is 4.3%, while individual values range from 1.3% to 8.2%, showing a large difference. No large variation can be recognized in resistivity values, and the average value of which marks 555 ohm.m.

(6) Hematite (8 samples)

The FE values of hematite - gozzan range from 5.5% to 13.0%, showing a small variation. The average of the values is 10.4%, while resistivity ranges between 115 ohm.m and 653 ohm.m, and the average value is 343 ohm.m. The resistivity value is low compared with those of the foregoing other types of rocks.

(7) Magnetite (2 samples)

For the small number of samples, average FE value is very high at 41%, while average resistivity is only 12 ohm.m, a low figure. It indicates remarkable correlation between high FE value and low resistivity.

(8) Pyrite - Ore (2 samples)

The samples shows their FE values of 11.5% and 21%, and high average value of 16.3%. The resistivity 8 ohm.m and 10 ohm.m, while the average value is low at 9 ohm.m. They show the same trend as the preceding item (7) of high FE value and low resistivity.

(9) Sphalerite - Ore (2 samples)

The FE value, and average resistivity value are 1.7%, and 99 ohm.m, respectively. They show lower FE value and higher resistivity compared with Item (8). Especially, the FE value shows a definite difference from that of Item (8).

4-4-2 In-Situ Measurement Result

In-Situ measurement was carried out at the three positions namely; (1) The point, where the survey line A and the survey line D intersects to each other, (2) Near the station 5 and (3) At a point near the station 8 on the survey line H. The measured results are shown in Table II-5.

Table II-5 Results of In-situ method

Point of measurement	Electrode configuration	Electrode spacing		F E (%)	A R (Ωm)	Rock
		AB (m)	MN (m)			
Line A No.13	Schlumberger	200	8	6.5	265	Skarn
Line D No. 6	"	200	15	6.5	255	"
Line H No. 5	Pole-dipole	258	21	2.5	707	Lime stone
Line H No. 8	"	263	19	3.2	464	Sand stone

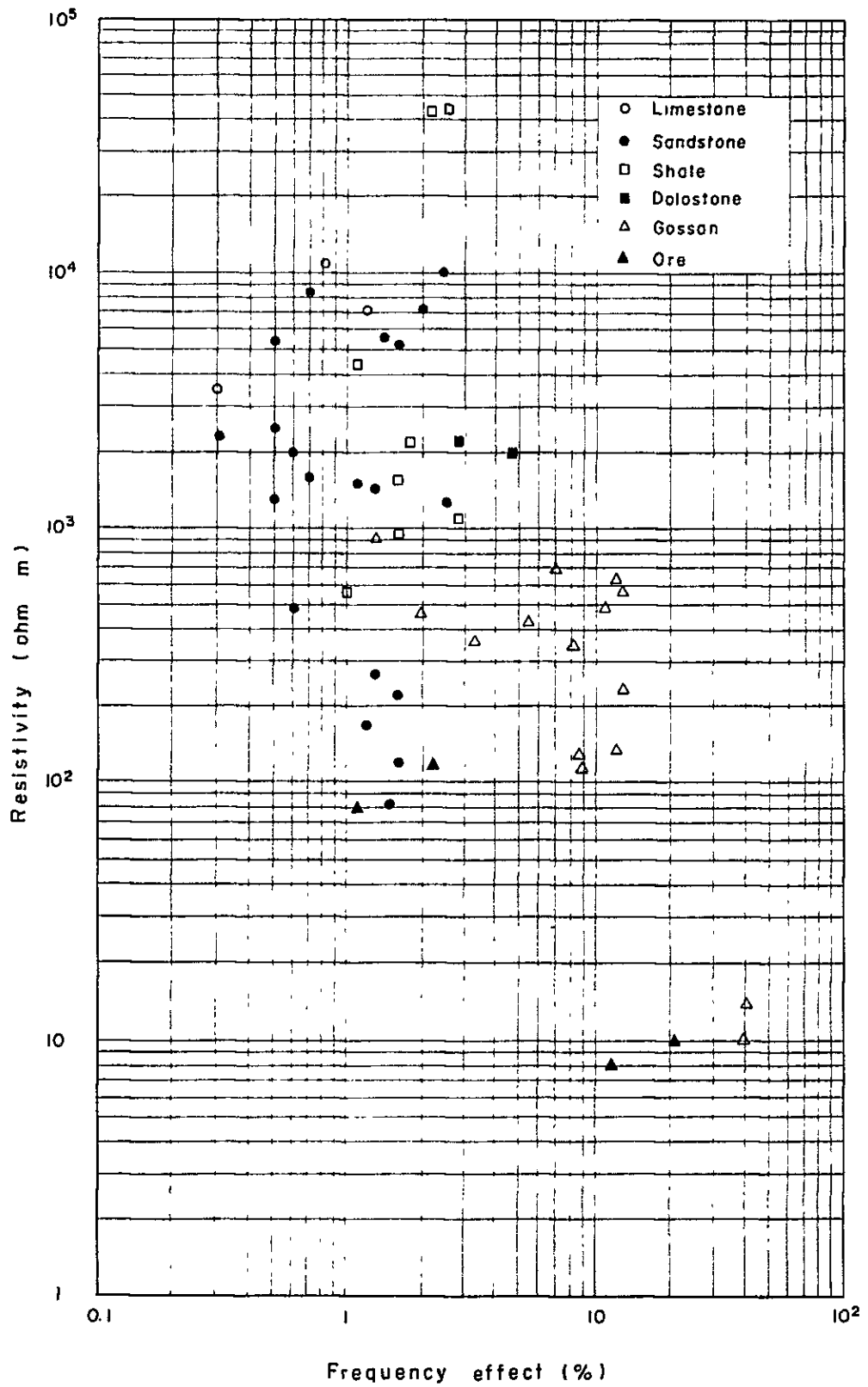


Fig. II -24. Correlation between AR and FE of Laboratory measurement

Table II-3 Results of laboratory measurement

Point No. on survey line	Rock name	Frequency effect (%)	Resistivity (ohm-m)	Note
A22	Dolostone	4.7	1,980	
A24	Gossan	6.9	684	
A25-1	Gossan	8.2	345	
A25-2	Limestone	1.2	7,120	
A43	Dolostone	2.8	2,236	
A64	Sandstone	0.6	1,987	Silified Strong
A65-1	Shale	1.0	568	
A65-2	Sandstone	0.5	2,520	Silified Strong
A65-3	Gossan	3.3	358	Silified Strong
A66-1	Sandstone	2.5	1,281	
A66-2	"	1.3	1,480	
A68-1	Specularite-Gossan	12.8	564	
A68-2	Shale	1.1	4,401	
A68-3	Specularite-Gossan	10.7	490	
A68-4	"	12.0	653	
A68-5	"	13.0	231	
A98-1	Shale	2.1	42,951	Silified Strong
A98-2	"	2.5	43,343	Silified Strong
A103-1	Pyrite-Ore	21.0	10	
A103-2	Zinc-Ore	1.1	79	
A103-3	Pyrite-Ore	11.5	8	
A103-4	Zinc-Ore	2.2	118	
A104-1	Sandstone	1.4	5,629	
A104-2	"	1.6	5,122	
A120-1	Hematite-Gossan	8.8	115	
A120-2	"	8.5	131	
A120-3	"	12.0	136	
A120-4	Shale	2.8	1,128	
A120-5	"	1.6	1,584	
E2-1	Sandstone	1.6	221	Coarse
E2-2	"	1.2	171	Coarse

Point No. on survey line	Rock name	Frequency effect (%)	Resistivity (ohm-m)	Note
E4-1	Sandstone	0.3	1,510	
E4-2	"	0.7	7,211	Massive
E4-3	"	0.7	8.352	Massive
E5-1	"	0.7	1,594	
E5-2	"	0.5	1,302	
F13	Hematite-Gossan	5.5	427	
G7	Sandstone	2.4	9,970	
G8-1	Gossan	2.0	471	
G8-2	"	1.3	918	
G19-1	Sandstone	1.5	82	Coarse grain
G19-2	"	1.6	119	Coarse grain
H5-1	Limestone	0.8	10,913	
H5-2	"	0.3	3,454	
H5-3	Magnetite-Gossan	40.0	10	Massive
H5-4	"	42.0	14	Massive
H5-5	Sandstone	0.6	493	
H5-6	"	1.3	269	
H7-1	Shale	1.6	960	
H7-2	"	1.8	2,169	
H8-1	Sandstone	0.5	5,373	
H8-2	"	0.3	2,306	

Table II-4 Results of laboratory measurement

Rock group	Rock name	Point No. on survey line	F.E (%)	FE average (%)		R (ohm-m)	R. average (ohm-m)	
Ph	Limestone	H5-1	0.8	0.6	0.8	10,913	7,184	7,162
		H5-2	0.3			3,454		
		St	A25-2	1.2		1.2	7,120	
Fr	Sandstone	E2-1	1.6	1.5	1.2	221	148	2,850
E2-2		1.2	171					
G19-1		1.5	82					
G19-2		1.6	119					
Ch		A66-1	2.5	1.1		1,281	3,225	
		A66-2	1.3			1,480		
		A104-1	1.4			5,629		
		A104-2	1.6			5,122		
		H5-5	0.6			493		
		H5-6	1.3			269		
		H8-1	0.5			5,373		
		H8-2	0.3			2,306		
		E4-1	1.1			1,510		
		E4-2	2.0			7,211		
		E4-3	0.7			8,352		
		E5-1	0.7			1,594		
		E5-2	0.5			1,302		
St		A64	0.6	0.6		1,987	2,254	
Cm		A65-2	0.5	2.4		2,520	9,970	
		G7	2.4			9,970		
Ch	Shale	A98-1	2.1	2.1	1.8	42,951	15,356	12,138 (1,802)
		A98-2	2.5			43,343		
		A120-4	2.8			1,128		
		A120-5	1.6			1,584		
		H7-1	1.6	960				
		H7-2	1.8	2,169				
St		A65-1	1.0	1.1		568	2,485	
	A68-2	1.1	4,401					

Rock group	Rock name	Point No. on survey line	F.E (%)	FE average (%)		R (ohm-m)	R. average (ohm-m)	
St	Dolostone	A22	4.7			1,980		
		A43	2.8	-	3.8	2,236	-	2,108
St	Gossan	A24	6.9			684		
		A25-1	8.2			345		
		A65-3	3.3	-	4.3	358	-	555
		G8-1	2.0			471		
		G8-2	1.3			918		
St	Hematite	A68-1	12.8			564		
		A68-3	10.7			490		
		A68-4	12.0			653		
		A68-5	13.0			231		
		A120-1	8.8	-	10.4	115	-	343
		A120-2	8.5			131		
		A120-3	12.0			136		
		F13	5.5			427		
St	Magnetite	H5-3	40.0			10		
		H5-4	42.0	-	41.0	14	-	12
St	Pyrite-Ore	A103-1	21.0			10		
		A103-3	11.5	-	16.3	8	-	9
St	Sphalerite-Ore	A103-2	1.1			79		
		A103-4	2.2	-	1.7	118	-	99

Rock group Ph : Pariahuanca Formation

Fr : Farrat "

Ch : Carhauz "

St : Santa "

Cm : Chimu "

Chapter 5 Analysis Result

Analysis on the six remarkable FE anomalies has been carried out as explained in the following:

5-1 Central Part

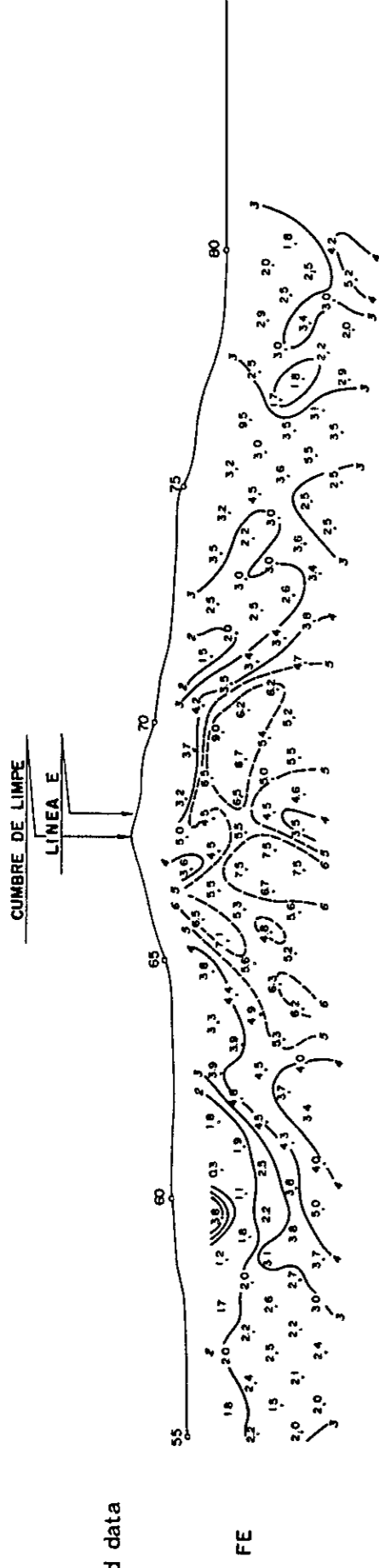
5-1-1 FE anomaly in Cumbre de Limpe

The explanation is related on A and E survey lines as the survey lines are situated in the fourth mineralized area of the Iscay Cruz ore deposit consisting of lead and zinc sulfides.

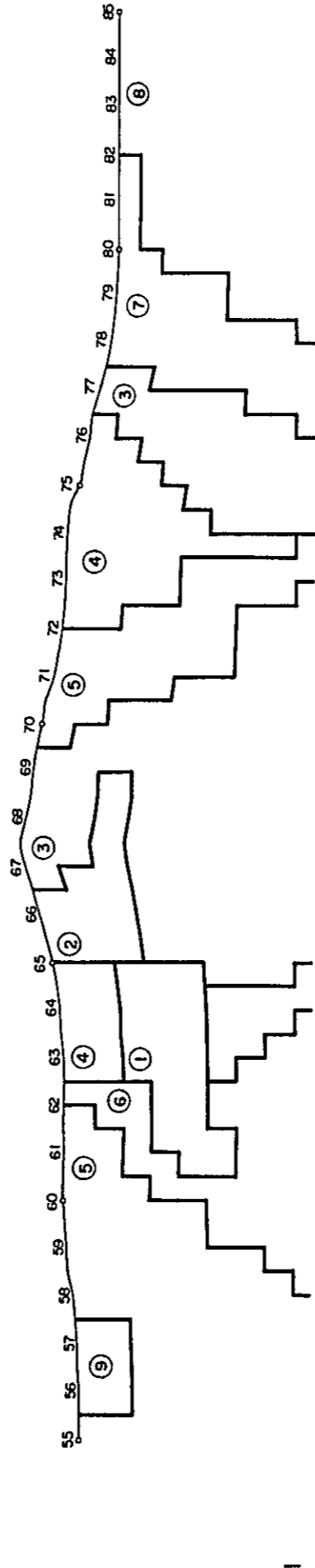
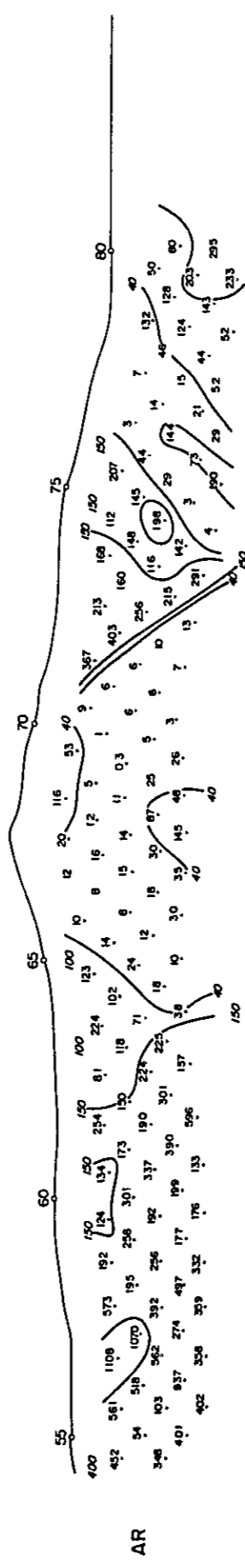
The calculated values and the final models, which shows a comparatively good coincidence with actually measured values as the results of simulation, are shown in Fig. II-25 and II-26.

(1) Survey Line A (See Fig. II-25)

The responding bodies ②, and ①, showing strong FE indications, are estimated to have resistivity of 15 to 100 ohm.m and FE values of 5 to 6.5%. The ② and ① responding bodies suggest a plate-like form with horizontal continuity: The ① is situated about 100 m below the surface ground, and the ② is situated in a shallow underground. In correlation with the mineralization on the surface ground, the responding bodies ③, ④, and ⑥ exist in a wide area and stretching to deep underground. These responding bodies indicate low values of resistivity ranging between 10 and 175 ohms, and FE values ranging between 3.3% and 3.5%. Responding bodies from ① to ④, and ⑥ occupy an area with low resistivity and medium to strong FE. The responding body ⑤, in correlation with the limestone of the Santa formation and the Carhuaz formation in the north of the station 62, indicates a slightly higher resistivity of 230 ohm.m and FE of 1.5% which corresponds to the back ground FE value. Responding body ⑨



Field data



	①	②	③	④	⑤	⑥	⑦	⑧	⑨
AR (Δm)	100	15	10	100	230	175	75	300	1000
FE (%)	50	65	35	33	1.5	35	20	40	15

Results of simulation

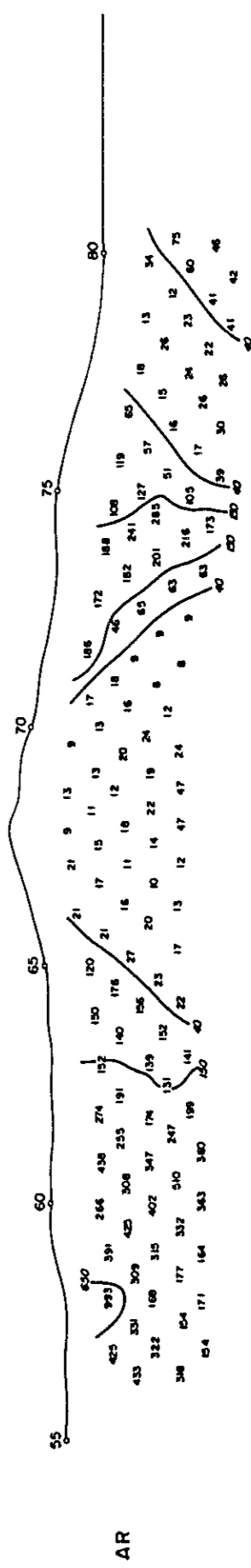
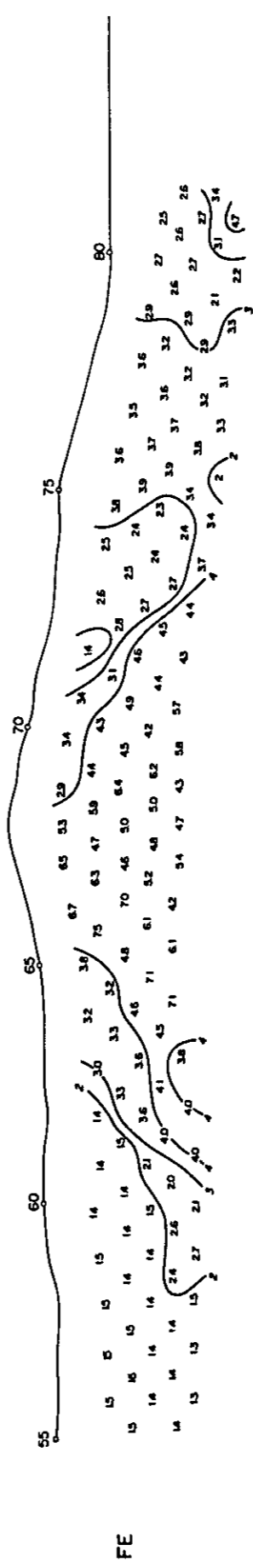


Fig. II -25. Field results and results of computer modeling on line-A



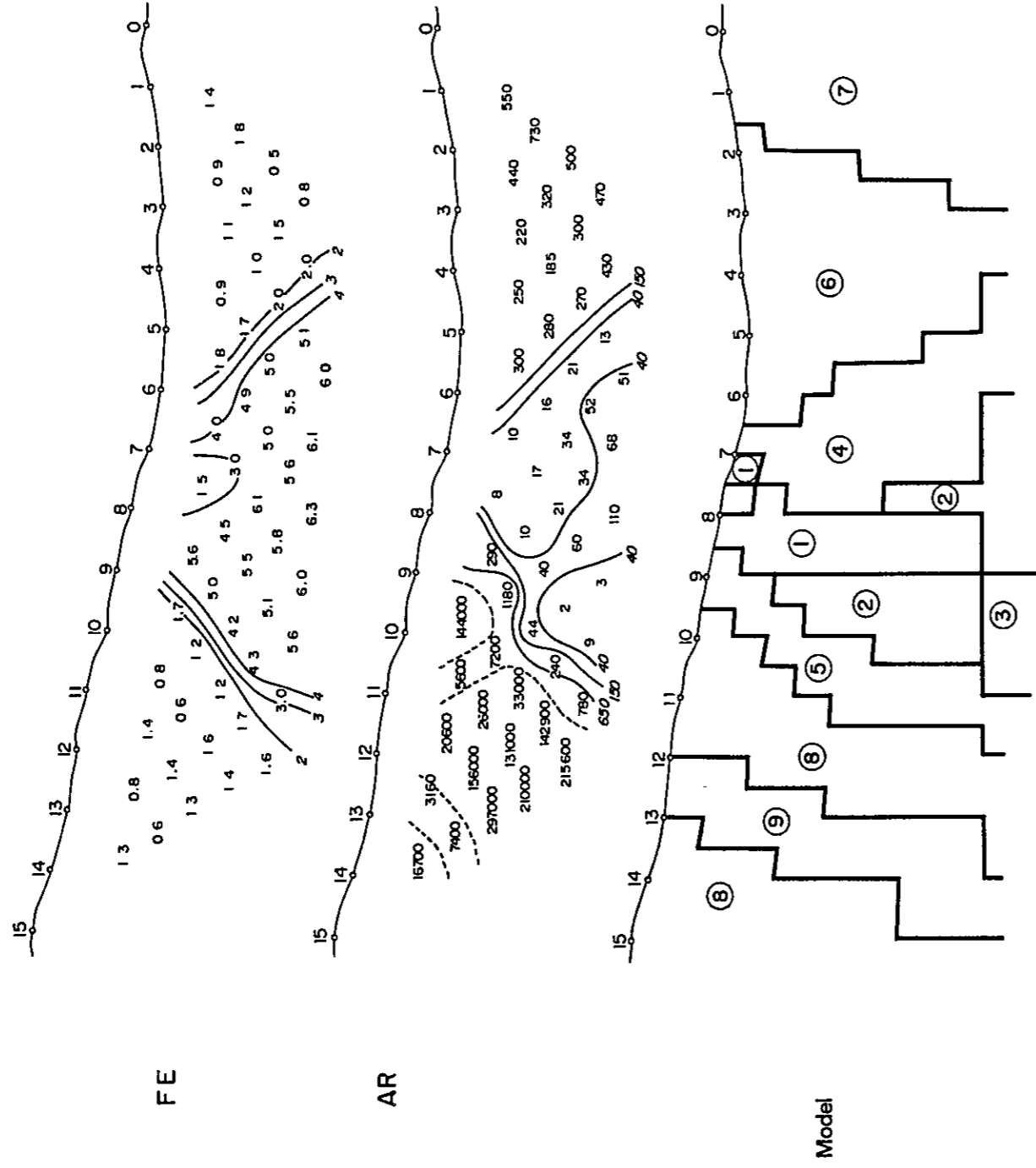
exists in a shallow underground and is correlated with the Santa formation, however, its resistivity is high at 1,000 ohm.m and shows background FE indication of 1.5%. Responding body ⑧ indicates a strong FE value of 4% in correlation with the mineralization on the surface ground, while its resistivity is high at 300 ohm.m.

(2) Survey Line E (See to Fig. II-26)

The responding bodies ①, ②, and ③, showing strong FE indications, are calculated to have resistivity, ranging from 10 to 50 ohm.m and FE values of 5 to 6.5%. Responding body ① extends from a shallow ground to deep part in a vertical columnar shape. The responding body ③ underlies the responding body ① in deep part. The responding body ② has its top about 100 m under the ground and adjoins to the responding bodies ① and ③. The bodies ①, ② and ③ form a large vertical columnar body which extends from shallow to deep underground. Responding body ④ has low resistivity of 15 ohm.m and 3.5% FE indication. The body extends to deep underground with westward dip. The responding bodies from ① to ④ occupy a low resistivity and strong FE indication area. Responding bodies ⑥ and ⑦ indicate a comparatively high resistivity range between 300 and 500 ohm.m and FE value ranging between 0.5% and 1.5%, which correspond to the value of background, and are correlated with the Carhuaz formation. Responding bodies ⑤, ⑧, and ⑨ show very high resistivity values between 4,000 and 100,000 ohm.m, and FE values between 1.5% and 3.5%. They are correlated with the Chimu formation.

From the above results of analysis, on the area in which survey lines A and E intersect in Cumbre de Limpe, it is indicated that the responding body with a strong FE anomaly has a plate-like form in north to south section and vertical columnar shape in east to west section.

Field data



	①	②	③	④	⑤	⑥	⑦	⑧	⑨
AR (Δm)	15	50	10	15	4000	300	500	100000	5000
FE (%)	6.5	6.5	5	3.5	3.5	1.5	0.5	1.5	0.5

Results of simulation

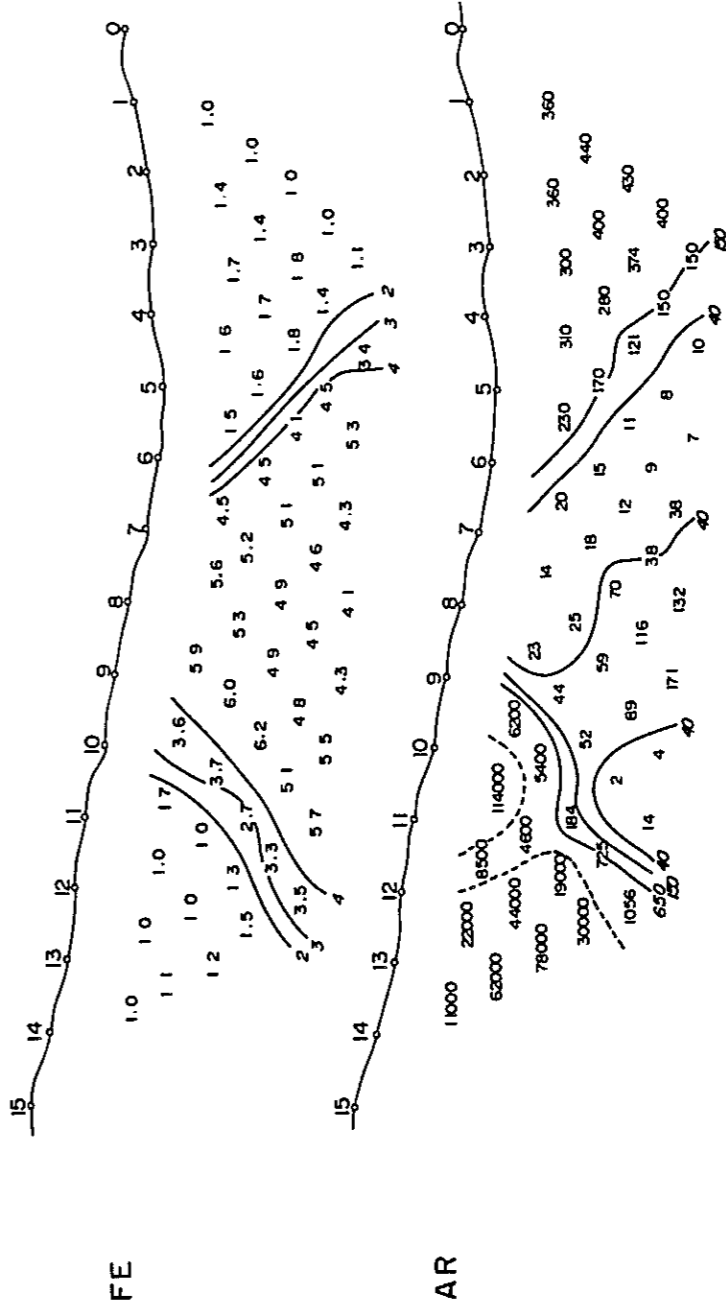


Fig. II -26. Field results and results of computer modeling on line-E

5-1-2 EM Indication on Survey Line E

(1) VLF Method

A quantitative analysis was made in accordance with the method described in Section 3-2-2 on the in-phase component of EM anomaly detected around the stations 7-8 on survey line E. The in-phase component shows a sudden change around the station 8 to indicate maximum positive value of 13% at the intermediate point between stations 7 and 8, and minimum negative value of -20% at about 25 m to the east of the station 8.

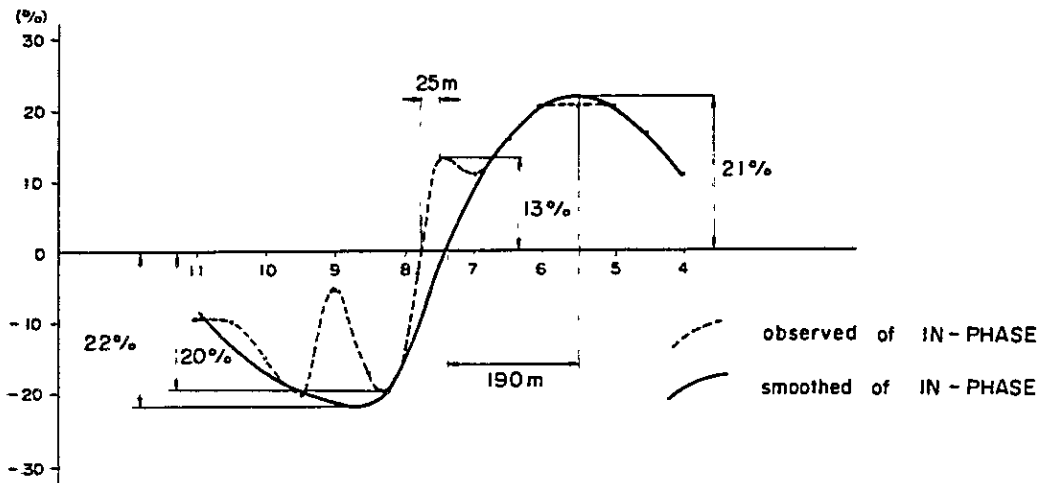


Fig. II-27. Determination of parameters for depth to top of conductor and dip angle. Line-E

From the curve shown in Fig. II-27, the following analytical parameters are obtained: $A_{R-} = 13\%$, $A_{R+} = 20\%$, $X_{R-} + X_{R+} = 25$ m, and

$$\frac{A_{R-} + A_{R+}}{2} = 16.5 .$$

From the graph shown in Fig. II-19 against the values,

it is concluded that the good conductor is almost a vertical body.

The diagram in Fig. II-18 against the values and $\theta = 0^\circ$ gives the depth to the good conductor at $d = 25$ m. The in-phase curve indicated by the solid line shown in Fig. II-27 is obtained when the original in-phase curve is smoothed through elimination of local anomaly. This curve indicates a

symmetric aspect taking the approximate intermediate point between stations 7-8 and at the same time indicates the values such as, $A_{R-} = 21\%$, $A_{R+} = 22\%$, and $X_{R-} + X_{R+} \approx 190$ m. The depth to this good conductor is considered to be 60 m or deeper from the diagram in Fig. II-18. Also, the dip of the conductor is approximately vertical. It is concluded from all the above that the conductor is located about 25 m, or 60 m or more below the surface ground of the stations 7-8, and that the conductor stands vertically with its plate-like shape.

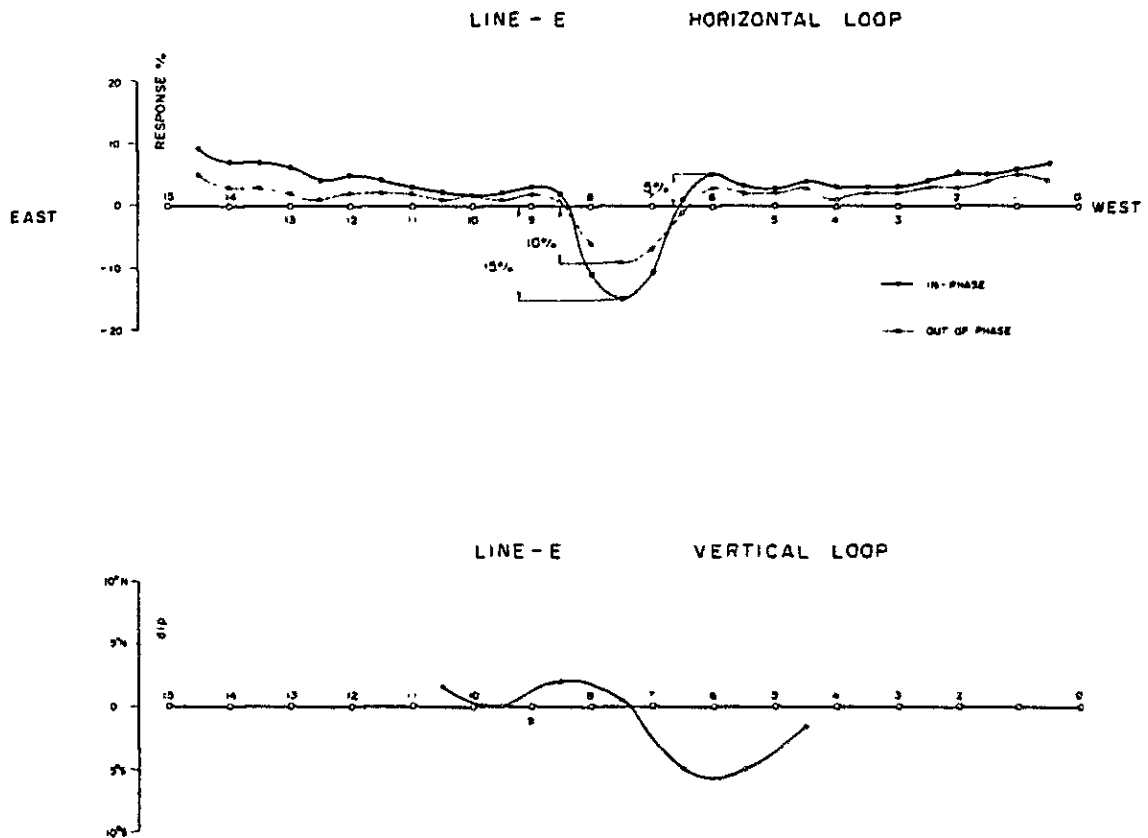


Fig. II - 28 - (a) Observed magnetic field curves of In-phase and Out-of-phase components

(2) Induction Method

Quantitative analysis was carried out on the anomaly of in-phase and out-of-phase curves obtained in the vicinity of the station 7-8. On the response curve obtained by horizontal loop coil system in Fig. II-28, the minimum values of in-phase and out-of-phase are -15% and -10%, respectively, while, the maximum in-phase value is 5%. The sequence of the analysis is explained in the following:

Step 1

Locate the point (-15, -10) in the phase diagrams, Fig. II-21 and read off the corresponding values of λ/a and d/a .

Tabulate as in Table II-6.

Table II-6 Response parameter and depth determined from various phase diagrams

θ	λ/a	d/a
90	6.79	0.29
80	6.87	0.292
60	7.17	0.30
40	8.25	0.316
20	9.67	0.342

Let us plot $\theta^{*\textcircled{1}}$ against $\lambda/a^{*\textcircled{2}}$ and θ against $d/a^{*\textcircled{3}}$ as shown in Fig. II-29. It is understood from Table II-6 that the true value of λ/a takes the value within the range $\lambda/a = 5$ to 15.

Step 2

Locate the θ corresponding to a series of a/d correlated with maximum in-phase value of +5% from Fig. II-22, with respect to $\lambda/a = 5, 7.5, 10,$ and 15.

Table II-7 Depth and dip corresponding to various response parameters

λ/a	d/a	θ
5.0	0.35	90°
	0.40	81°
7.5	0.35	85°
	0.40	73 1/2°
10.0	0.25	90°
	0.30	79°
	0.35	69 1/2°
	0.40	62 1/2°

λ/a	d/a	θ
15.0	0.25	75°
	0.30	67°
	0.35	60°
	0.40	53 3/4°

The values in Table II-8 are obtained when the intersection point of curve ① and ② is found, and further the values of θ and d/a pertaining to the intersection point is found after having plotted into Fig. II-29 the graph of d/a pertaining to θ with respect to respective values of each λ/a .

Step 3

Find in Fig. II-29 the graph of $\lambda/a = 5$ to 30, and the intersection point of curve ① of d/a .

Table II-8 Depth and dip corresponding to various values of response parameters

λ/a	d/a	θ
10	0.292	81°
15	0.297	67 1/2°

Step 4

Plot into Fig. II-29 the θ pertaining to each λ/a in Table II-8, then connect the points to make it ③

Step 5

Through finding the intersection point of curves (1), and (2), with curve ③, the values $\lambda/a = 6.8$, and $d/a = 0.292$ will be obtained. The angle θ is almost close to 90° . Since θ is almost close to a right angle, the position of the good conductor on the survey line is considered to be near the station indicating the minimum value of in-phase component, or near the intermediate point between the stations 7 and 8.

$$\frac{\lambda}{a} = \frac{10^5}{a\mu f} \cdot \frac{\rho}{t} \dots\dots\dots (1)$$

$$\frac{\rho}{t} = \frac{\frac{\lambda}{a}}{\frac{10^5}{a\mu f}} = \frac{\lambda}{a} \cdot \frac{a\mu f}{10^5}$$

Since the unit at this time is ohm cm for ρ , it is converted into ohm.m now.

$$\frac{\rho}{t} = \frac{a\mu f}{10} \cdot \frac{\lambda}{a} \text{ (Ohm)} \dots\dots\dots (2)$$

- ρ : resistivity (ohm.m)
- a : coil spacing (m)
- μ : relative permeability (μ/μ)
- f : frequency (Hz)
- t : thickness (m)

In the present survey, $a = 90$ m, $f = 1,600$ Hz. When $\mu = 1$, $\rho/t \doteq 0.10$ ohm, and $d \doteq 26$ m are obtained. The depth and tilt of the good conductor obtained are almost coincident with the result from VLF Method.

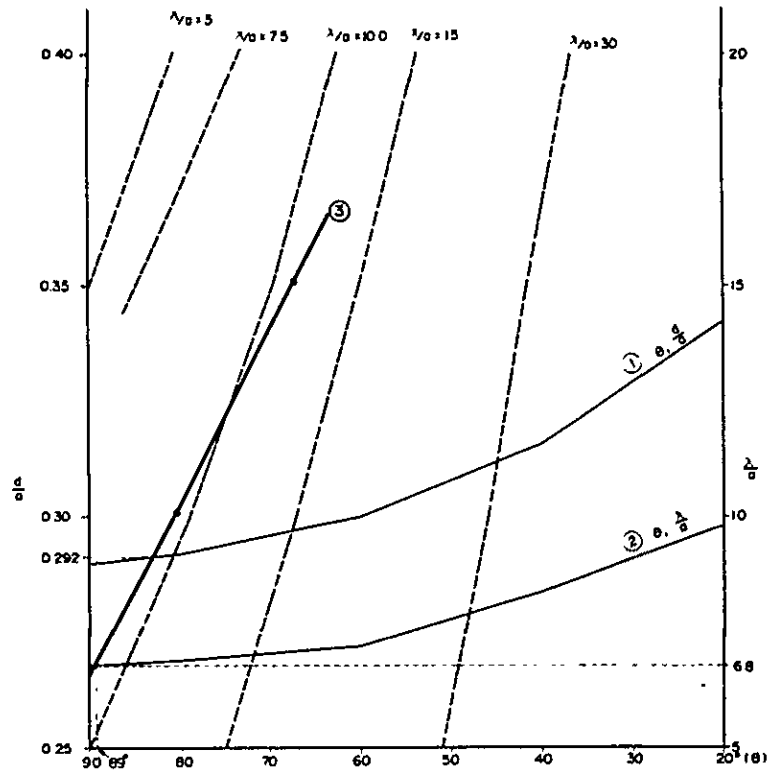


Fig. II - 29. Determination of the unknown parameters of Conducting half-plane

5-1-3 The Relation between AR Anomaly and EM Anomaly

Here are related the relation between AR and EM anomaly on Survey

Line E. Orderly collection of every anomaly is listed in Table II-9 below:

Table II-9 AR anomaly and EM anomaly

AR anomaly	EM anomaly	
IP method	VLF method	Induction method
The responding body ① with vertical attitude obtained near the station 8 indicating 15 ohm·m resistivity	The anomaly is obtained near the stations 7 and 8, and conductor exists about 25 m or 60 m or more below the surface ground. The dip of the conductor is almost vertical	It is an anomaly obtained near the stations 7 and 8, and its depth is about 26 m, $\rho/t = 0.1$ ohm, and its attitude is almost vertical.



Both the AR anomaly and EM anomaly are detected in one same place. The conductor relative to the EM anomaly is considered to correlate with responding body ①, according to the IP model simulation. When it is a case of $\rho/t = 0.1$ ohm according to EM, the following relation exists between resistivity and width of the responding body.

ρ (Ωm)	t (m)
1	10
5	50
10	100
15	150

The depth to responding body ① is 50 m from the surface ground, and the figures coincides approximately with the result from EM. In the case of $\rho = 10$ to 15 ohm.m, as specified with the EM results, the width of the responding body is 100 m to 150 m. The figures of the width coincides approximately with the width of responding body ①.

5-2 Southern Part of Iscay Cruz

5-2-1 FE Anomaly in Surrounding Area of Chupa Mine

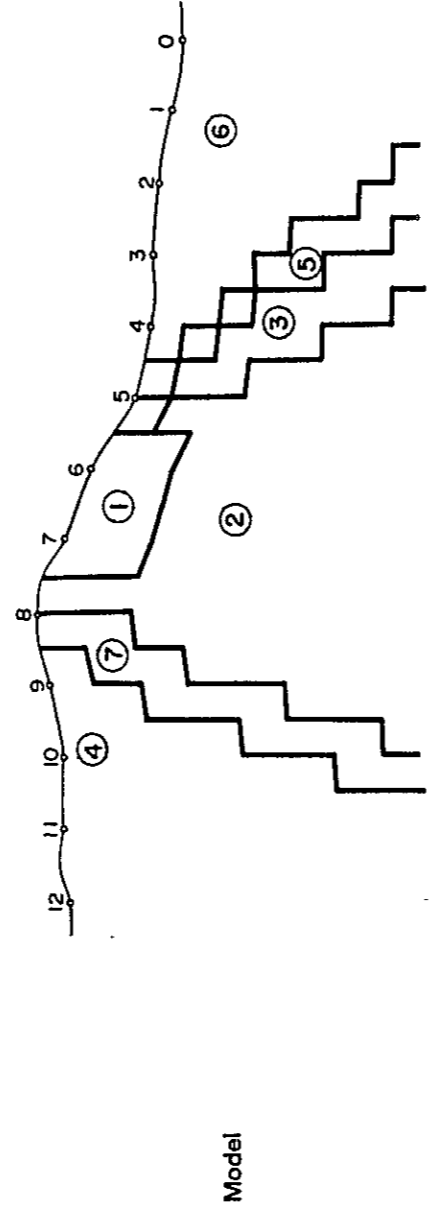
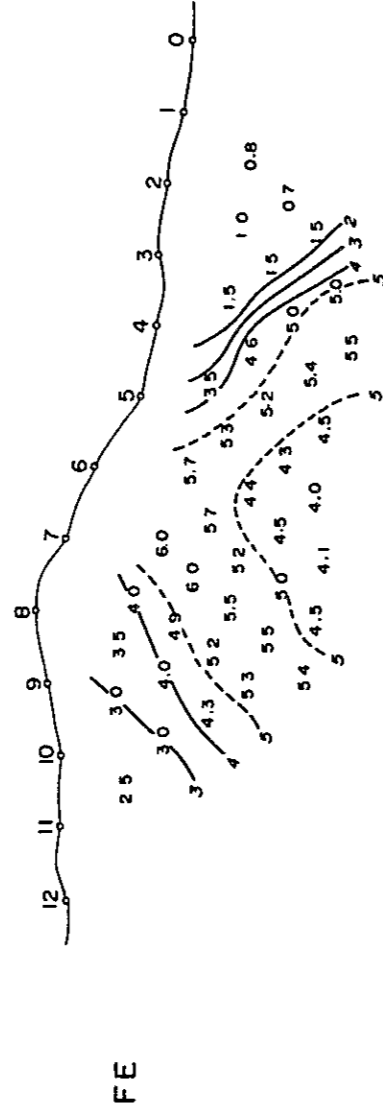
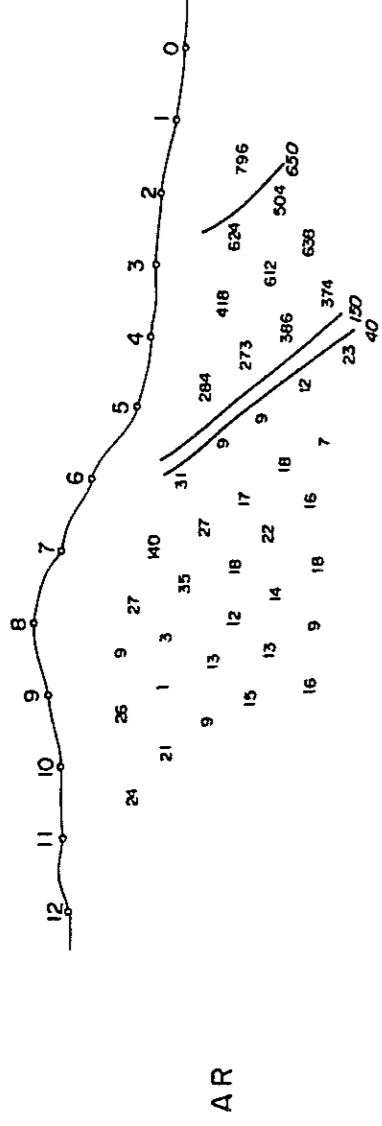
Since Chupa mine deposit is regarded as a ore deposit formed relative to the mineralization phenomenon of Iscay Cruz ore deposit, explanation is made on survey lines C and H that lie on the both deposits.

The calculation value and the final model, that provided a comparatively satisfactory coincidence with the actually measured values as a result of simulation, are shown in Fig. II-30, and Fig. II-31.

(1) Survey Line H (See Fig. II-30)

The responding body ① showing strong FE anomaly, is calculated to have resistivity of 5 ohm.m and 6% FE value indicates a good approximation.

Field data



	①	②	③	④	⑤	⑥	⑦	⑧
AR (Δm)	5	15	50	20	250	650	10	
FE (%)	6	4.5	3.2	2.5	2	1	3.2	

Results of simulation

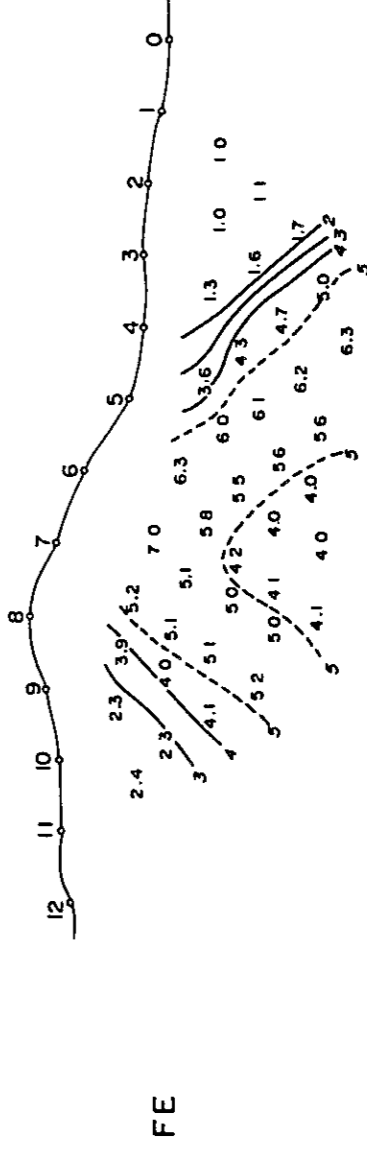
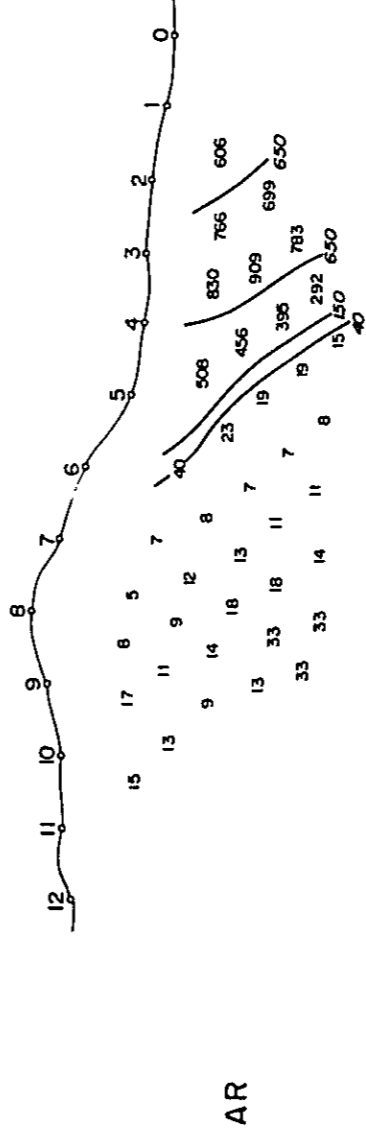
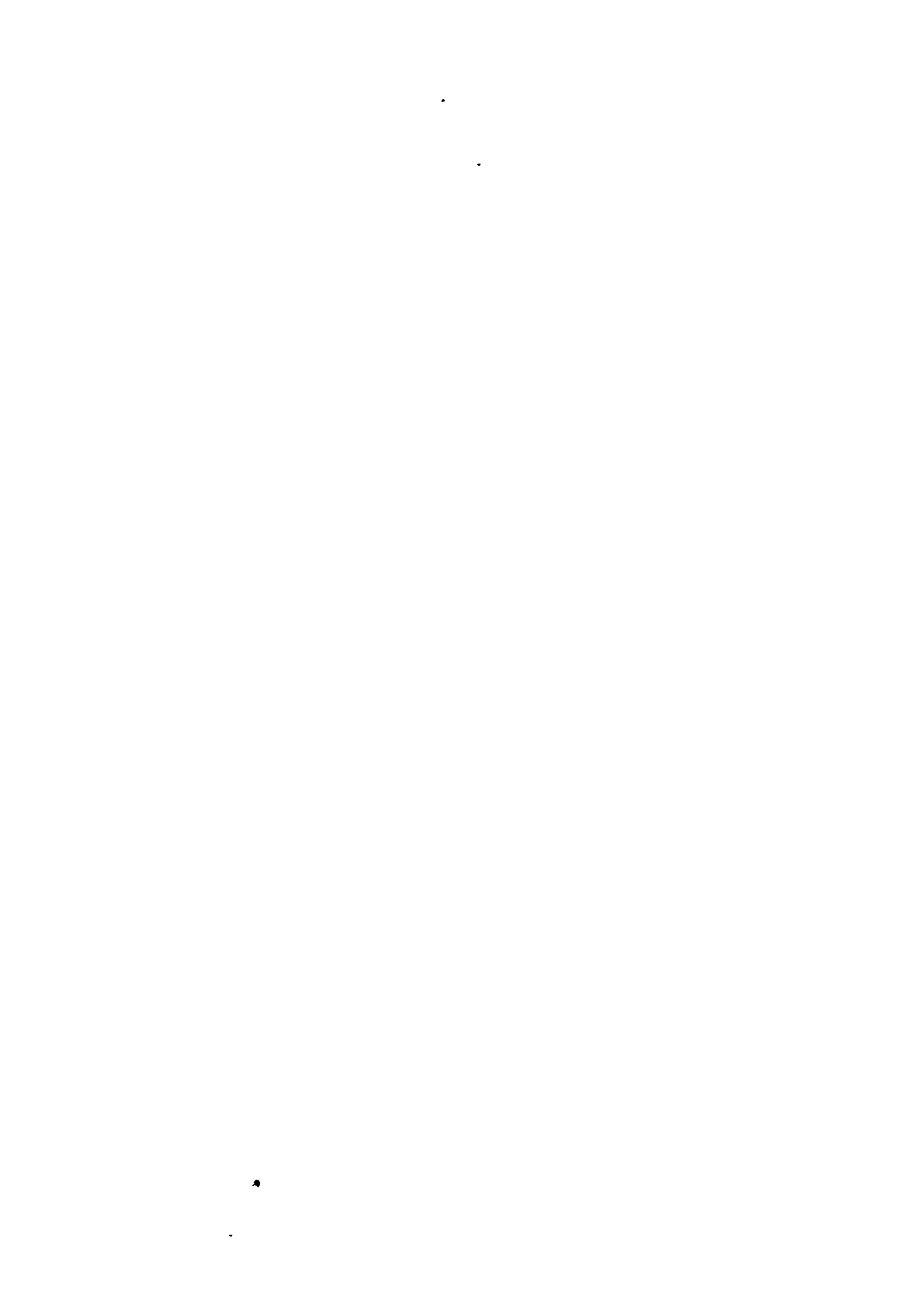


Fig. II-30. Field results and results of computer modeling on line-H



The responding body indicates a plate-like structure in shallow under the ground from the surface ground. Responding body ② indicates 15 ohm·m resistivity and 4.5% FE value, and extends to deep part in continuation to responding body ①. The responding bodies ① and ② can be put together to form a large scale of single body. Its location is correlated with the Chupa Mine. Responding bodies ④ and ⑦ indicate resistivity values ranging between 10 and 20 ohm·m and FE values ranging between 2% and 3.2%. The strata correlated with responding bodies ④ and ⑦ is the Carhuaz formation consisting of clayey alteration zone.

Responding body ⑥ indicates 650 ohm·m resistivity and 1% FE value, a background. It is correlated with the Chulec formation and the Pariatambo formation.

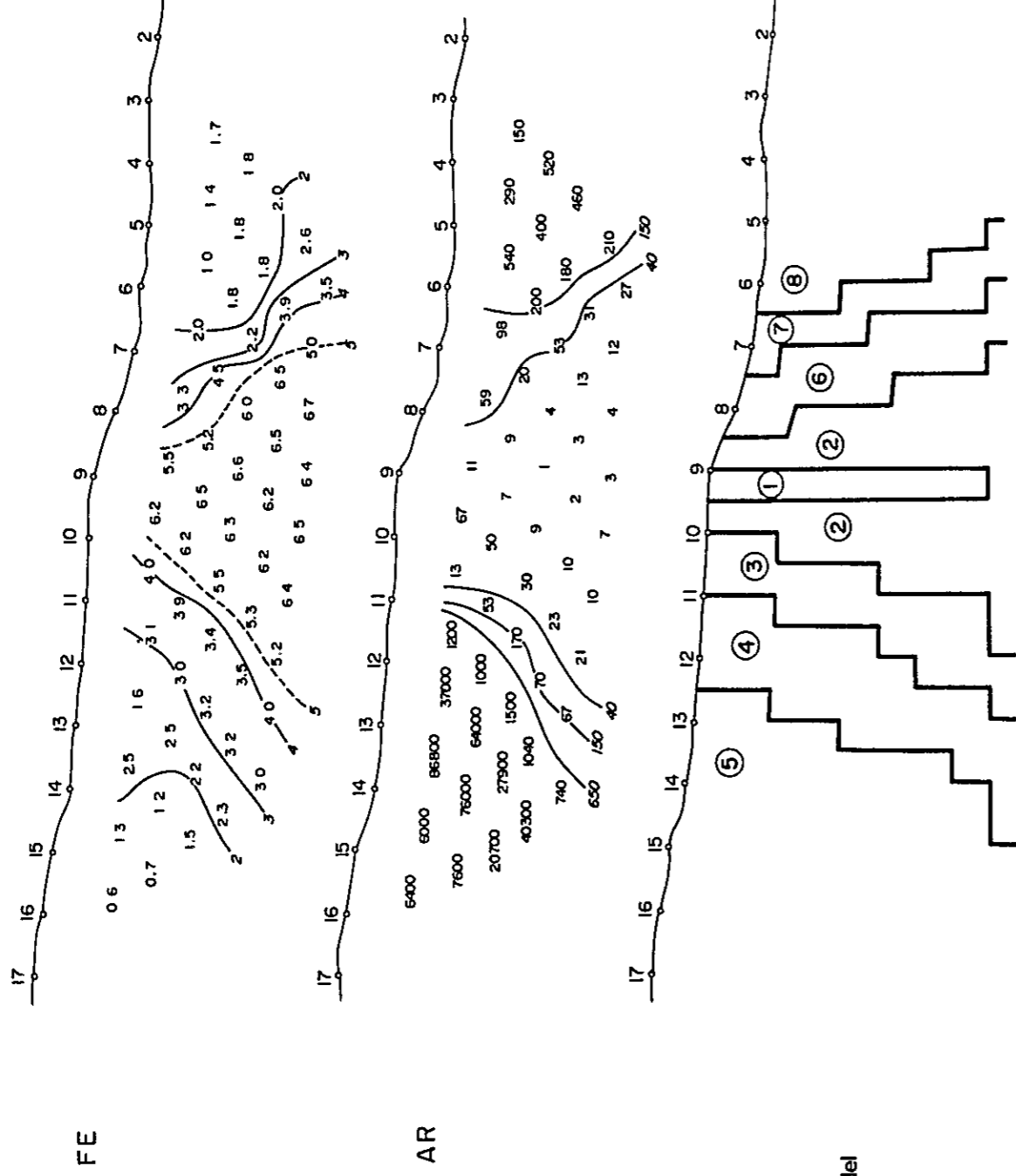
Responding body ③ indicates 50 ohm·m resistivity and 3.2% FE value, and extends below the responding body ⑥, with westward dip.

(2) Survey Line C (See Fig. II-31)

The responding body ① shows strong FE values of 6.5% indication, and 5 ohm·m resistivity. The responding body indicates a vertical columnar form stretching from the surface ground. Responding body ② indicates 15 ohm·m resistivity and 5% FE value. The body extends into deep part from the surface ground in such a way that responding body ① is surrounded by this body. The bodies ① and ② form a medium scale of vertical columnar body extending from shallow under ground.

Responding body ③ indicates 50 ohm·m resistivity and 3.0% FE values. The body extends to deep underground with eastward dip. This is correlated with the Santa formation. Responding bodies ⑥ and ⑦ indicate high resistivity values ranging between 400 and 750 ohm·m and close to background FE values of 1.5% to 2.5%. These bodies are correlated with the Carhuaz formation.

Field data



	①	②	③	④	⑤	⑥	⑦	⑧
AR (Δ.m)	5	25	50	700	50000	100	400	750
FE (%)	6.5	5	3	2	1.5	3.3	2	1.5

Results of simulation

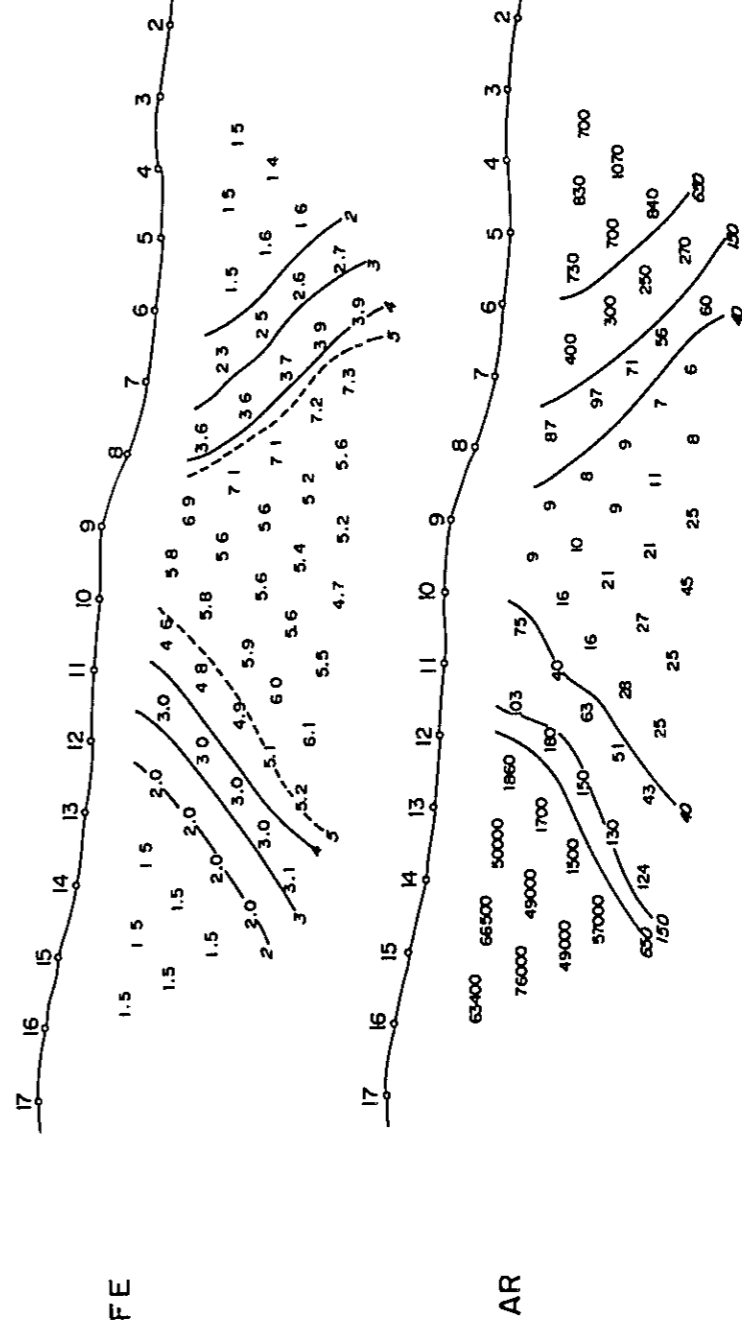


Fig. II-31. Field results and results of computer modeling on line-C

Responding bodies ④ and ⑤ indicates a very high resistivity values ranging between 700 and 50,000 ohm·m and background FE values between 1.5% and 2.0%, and is correlated with the Chimu formation.

The analysis results relating to the Chupa Mine and its surrounding areas, can be summarized that the responding body with strong FE anomaly is a vertical columnar responding body stretching to the Santa formation, and part of the Carhuaz formation which adjoins to the Santa formation, on survey line C. On survey line H, there is a trapezoidal responding body that is obtained in the Carhuaz and Farrat formations and Chupa ore deposit.

5-2-2 EM Anomaly on Survey Line C

(1) VLF Method

Quantitative analysis was carried out on EM anomaly of in-phase component detected in the vicinity of the station 10 on survey line C.

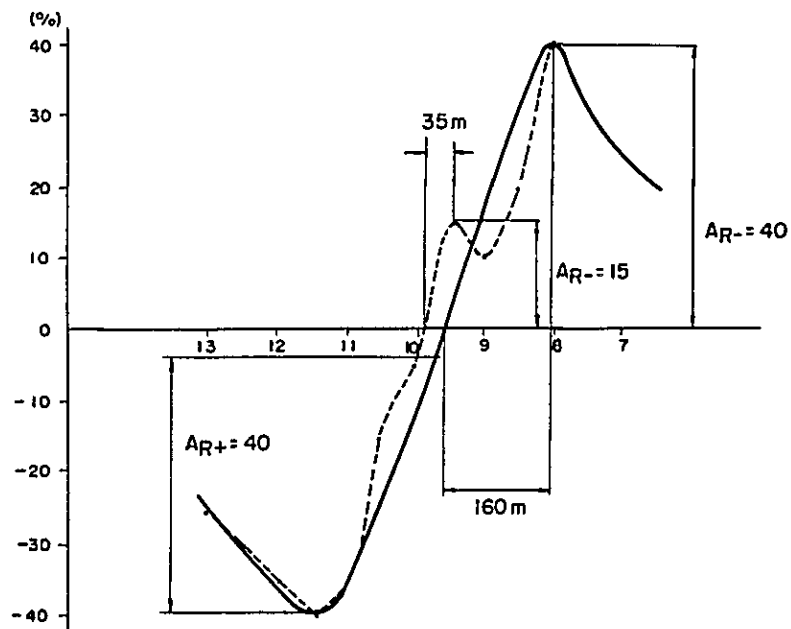


Fig. II-32. Determination of parameters for depth to top of Conductor and dip angle, Line-C

From the in-phase curve in Fig. II-32, the following parameters are obtained:

$$A_{R^-} = 15\%, \quad A_{R^+} = 40\%, \quad \frac{A_{R^-} + A_{R^+}}{2} = 27.5\%, \quad \text{and} \quad X_{R^-} + X_{R^+} = 35 \text{ m.}$$

From the diagram in Fig. II-18, and Fig. II-19, the depth to the good conductor, $d = 25 \text{ m}$, and dip angle $\theta = 0^\circ$ are obtained.

With respect to smoothed curve, the followings are obtained:

$$\frac{A_{R^-} + A_{R^+}}{2} = 40\%, \quad X_{R^-} + X_{R^+} = 160 \text{ m}, \quad A_{R^-} = 40\%, \quad \text{and} \quad A_{R^+} = 40\%.$$

From Fig. II-18, and Fig. II-19, the followings are given:

Depth $d = 60 \text{ m}$ or deeper, and dip angle $\theta = 0^\circ$.

Therefore, the anomaly is considered to have been caused by a vertical plate-like conductor situated in 25 m depth or 60 m or more depth.

(2) Induction Method

Quantitative analysis was carried out on the anomaly of in-phase and out-of-phase curves centering on stations 10 and 11. From Fig. II-28, the minimum values of in-phase, and out-of-phase, are -18%, and -15%, respectively, while the maximum value of in-phase is +7%.

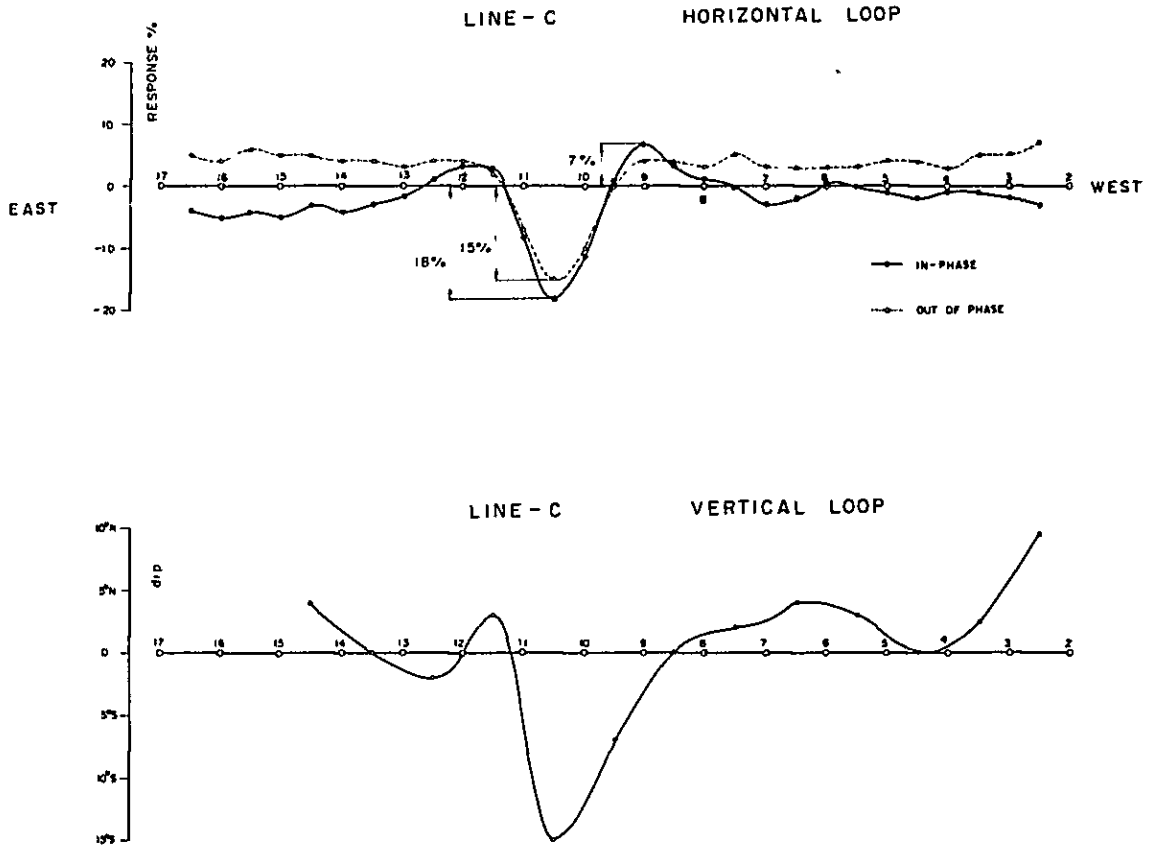


Fig. II-28-(b) Observed magnetic field curves of In-phase and Out-of-phase components

The curves ① and ② in Fig. II-33 are drawn when λ/a and d/a pertaining to each dip angle (θ) are obtained from the foregoing -18%, and -15%, and illustration thereof is made.

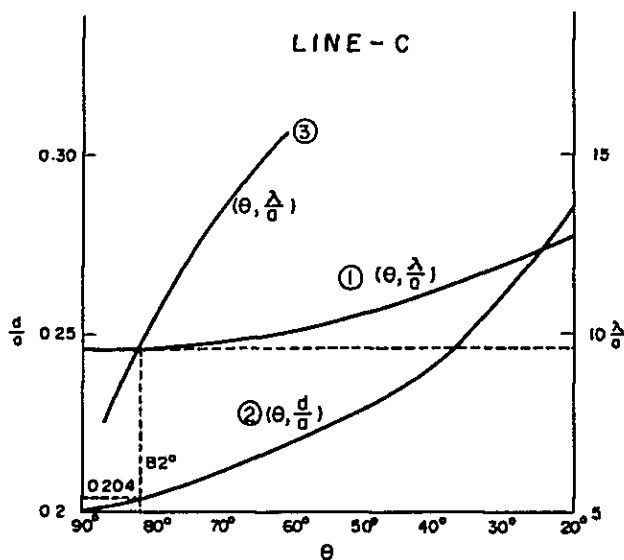


Fig. II-33. Determination of the unknown parameters of Conducting half-plane, Line-C

The results as mentioned in the following Table are attained when the intersection points with λ/a curve ① and the series of d/a and θ corresponding to the 7% from Fig. II-22 found with respect to $\lambda/a = 7.5$, 10, and 15, are found.

Table II-10 Depth and dip corresponding to various values of response parameters

λ/a	d/a	θ
7.5	0.202	86
10	0.204	81
15	0.217	64

Curve ③ is obtained through plotting into Fig. II-33 the relationship between λ/a and θ according to this Table. When this curve is intersected with the previously plotted λ/a curve ① to find their intersection points, $\lambda/a = 9.6$, and $d/a = 0.204$ are obtained. The dip angle θ is 82° which is almost vertical. In addition, since the dip angle of the conductor is almost vertical, the top point of the good conductor is considered to exist near the station at which, the indication of the minimum in-phase component value is indicated.

When $a = 90$ m, $f = 1,600$ Hz, and $\mu = 1$, $\rho/t = 0.14\Omega$, and $d = 18$ m are obtained from expression (2) of Section 5-1-2, (2).

Wherein, ρ/t : the ratio of resistivity to the width of the strata. Now, the depth and dip of the conductor are approximately coincident with the results of VLF method.

5-2-3 Relationship between AR anomaly and EM anomaly

Explanation is given in the following on the relationship between AR anomaly and EM anomaly on the survey line C: Each anomaly is brought together and arranged as mentioned in Table II-11.

Table II-11 AR anomaly and EM anomaly

AR anomaly	EM anomaly	
IP method	VLF method	Induction method
The responding body ① with vertical attitude near the station 9 - 10 indicating 5 ohm.m resistivity.	The anomaly is obtained near the station 10, and conductor exists about 25 m or 60 m or more below the surface ground. This dip of the conductor is almost vertical.	It is an anomaly obtained near the stations 10 and 11, and its depth is about 18 m, $\rho/t = 0.14$ ohm, and its attitude is almost vertical.

Both the AR and EM anomaly was detected at the same place. The EM anomaly of the conductor is considered to be correlated with conductor ① according to the IP model simulation. When the expression, $\rho/t = 0.14$, is justified from EM result, the following relation exists between the resistivity and width of the conductor.

ρ (Ω m)	t (m)
1	7
5	36
10	71
15	107

When $\rho = 5 - 10$ ohm.m is justified from EM result, the width of the conductor is from 36 to 71 m, which coincides approximately with the width

of responding body ①.

5-2-4 FE Anomaly in Cunsha Punta and Antapampa

The FE value is detected at two points. Specially definite FE indication was detected at south end of Iscay Cruz ore deposit, about 2.5 to 3 km south of Chupa Mine. In each of them, limestone or dolostone of the Santa formation are mineralized, which fact is confirmed with the geological survey carried out this year. The calculated values and final models, which showed a good coincidence with the actually measured values are indicated in Figs. II-34 and II-35.

(1) Survey Line A (See Fig. II-34)

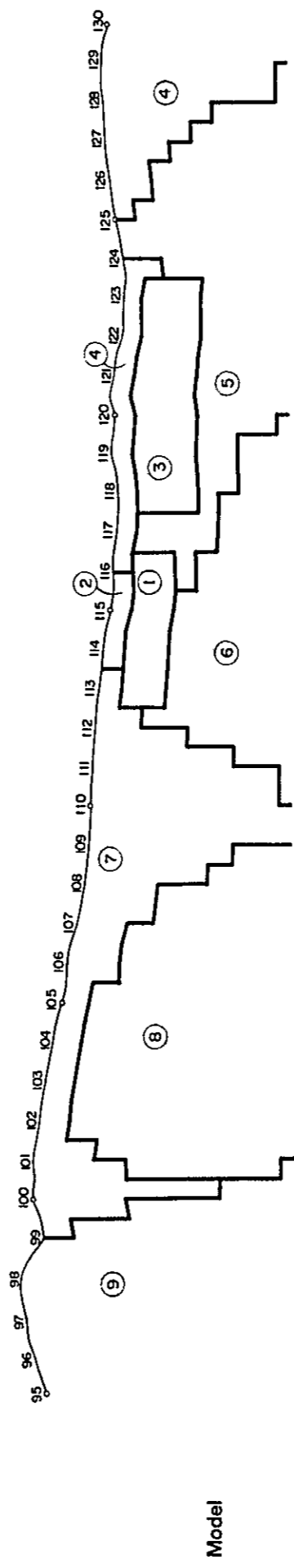
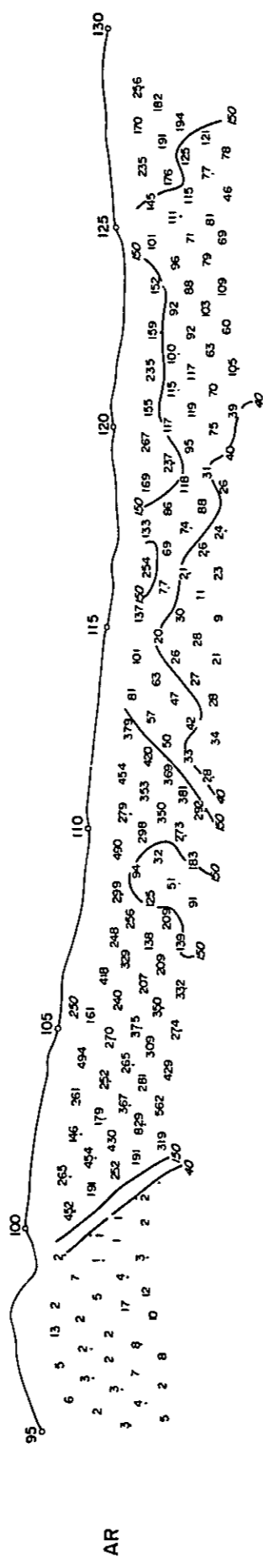
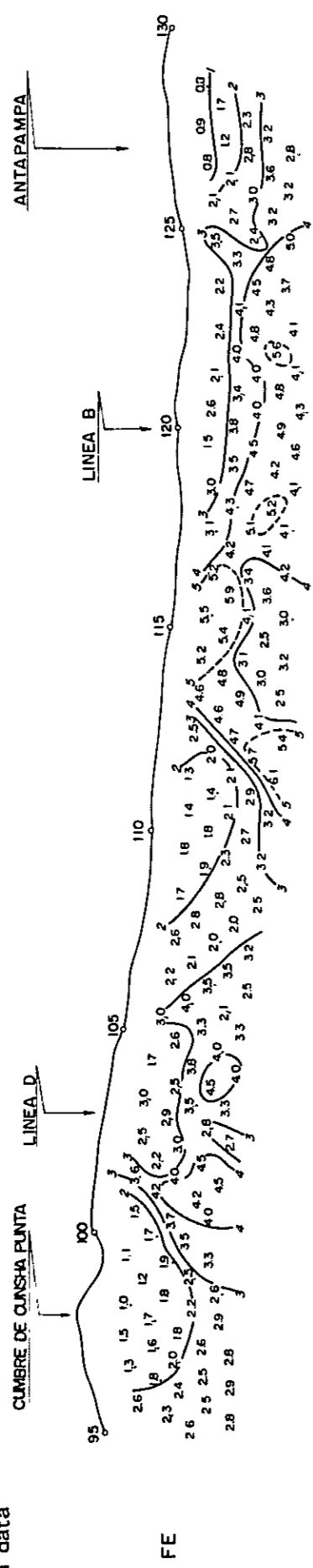
The responding bodies showing strong FE anomaly, are estimated to have resistivity of 20 ohm·m and FE of 5% with the body ①, resistivity of 150 ohm·m and FE of 6.5% with the body ②, and resistivity of 80 ohm·m and FE of 4.5% with the body ③.

The responding bodies of both ① and ③ plate like shapes are located about 50 m below the surface ground. Responding body ② is located in shallow underground and is of a small scale plate-like shape. Responding bodies ① and ② are correlated with non-mineralized limestone and the Cauhuaz formation. Responding body ⑥ indicates 10 ohm·m resistivity and 3% FE, and extends into deep part in a large scale body adjoining to responding body ①. Responding body ⑤ indicates 90 ohm·m resistivity and 3.2% FE, and is distributed adjoining to the responding bodies ①, ③, and ⑥. Responding bodies ⑤ and ⑥ are of low resistivity though not the same in value, and approximately the same in FE value.

Responding bodies ①, ②, ③, ⑤ and ⑥ are of low resistivity, and from medium to strong FE anomaly area in a very large scale.

Responding body ④ indicates 200 ohm·m resistivity and 2% FE, and extends

Field data



	1	2	3	4	5	6	7	8	9
AR (m)	20	150	80	200	90	10	250	300	3
FE (%)	50	65	45	20	32	30	20	35	22

Results of simulation

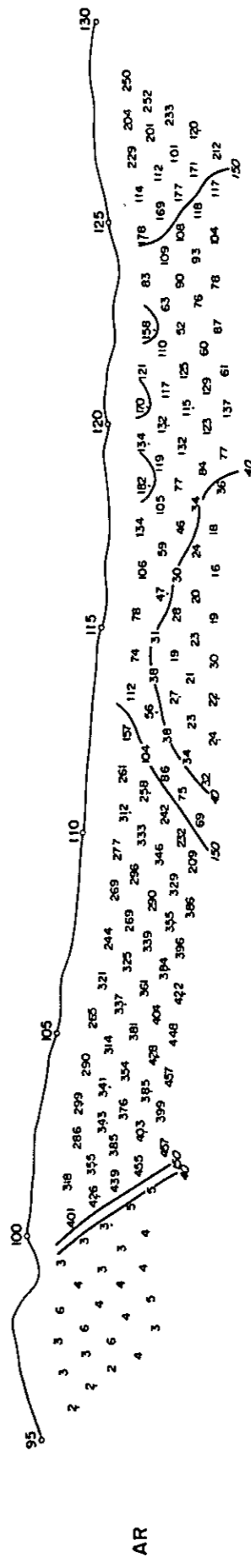
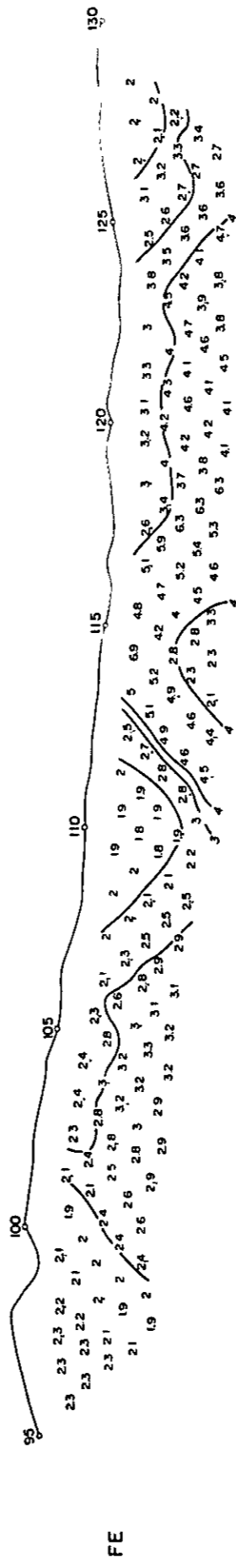


Fig. II -34. Field results and results of computer modeling on line-A

from shallow underground to south side stretching to deep part in its south end. This responding body is correlated with the Carhuaz formation.

Responding body ⑦ indicates 250 ohm.m resistivity and 2% FE, and is located in shallow underground stretching to north side correlating with the Carhuaz formation, the Santa formation, and the Chimu formation.

Responding body ⑧ indicates 300 ohm.m resistivity and 3.5% FE. It is situated about 50 m below the surface ground on which the Santa formation accompanied with are minerals are exposed. Responding body ⑨ showing 3 ohm.m resistivity and 2.2% FE is located to the north side of responding bodies ⑦ and ⑧. This responding body is correlated with the Carhuaz formation.

(2) Survey Line B (See Fig. II-35)

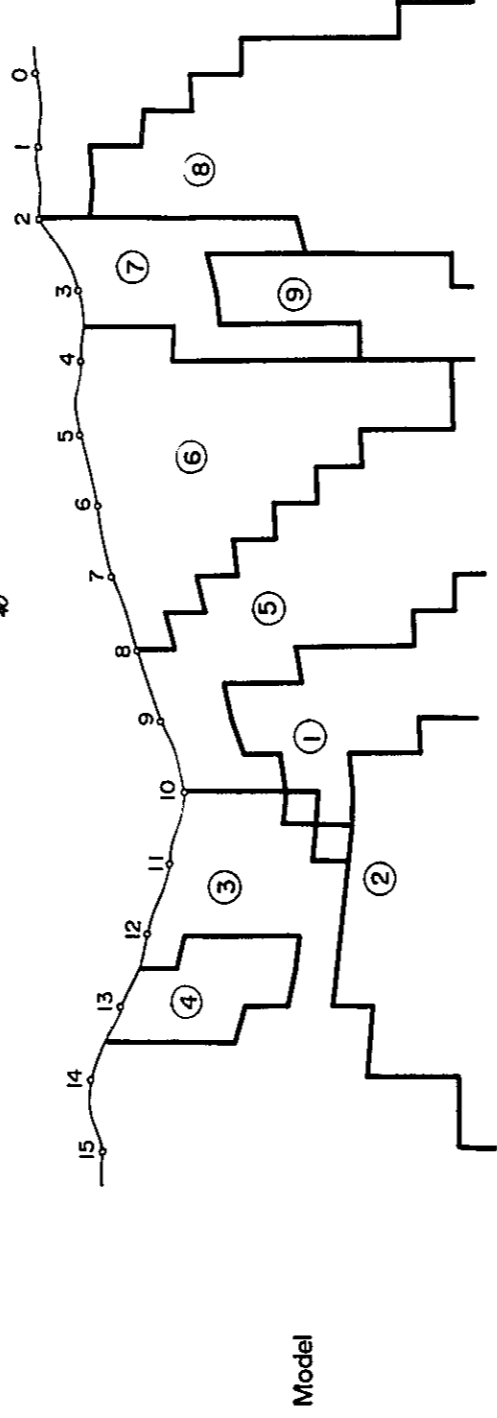
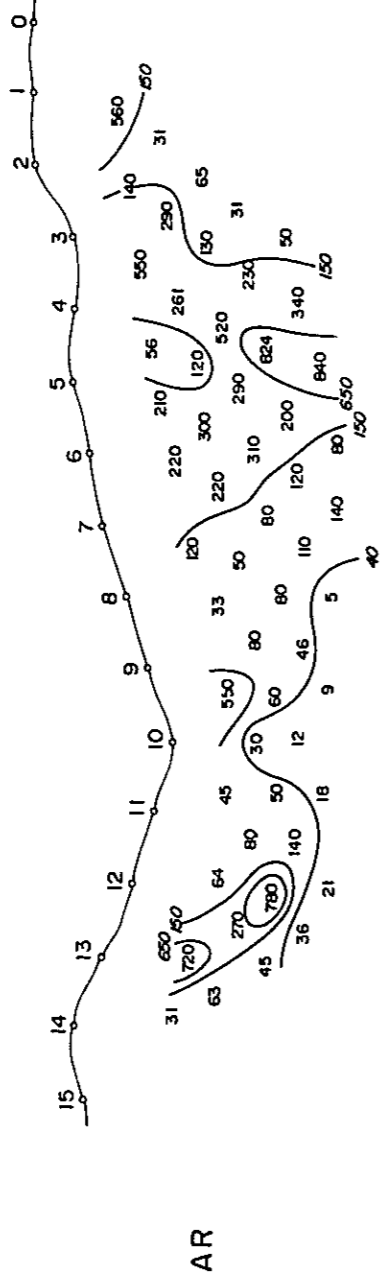
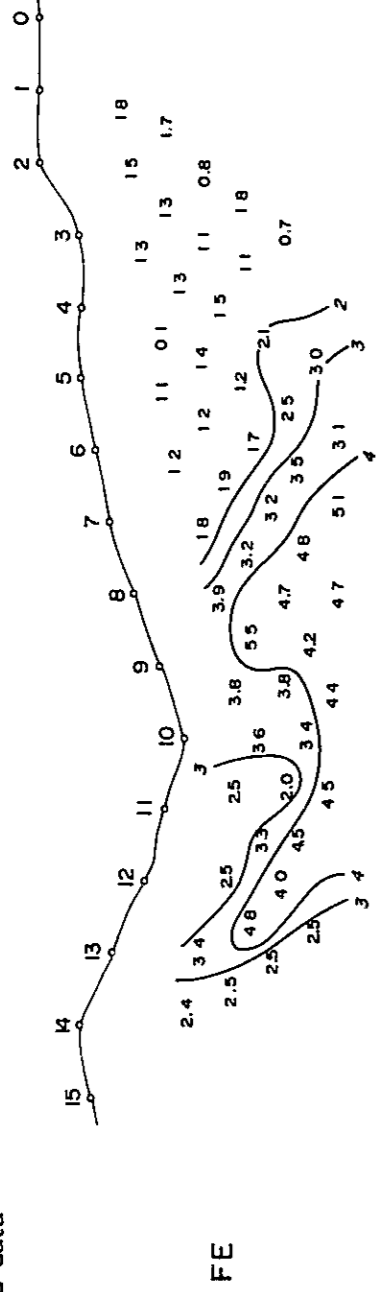
The responding bodies showing strong FE anomaly, are estimated to have resistivity of 80 ohm.m and FE of 8% with the body ①, and resistivity of 5 ohm.m and FE of 5.5% with the body ②. Responding body ① is almost a vertical structure situated about 100 m below the surface ground near the station 9. Responding body ② extends deeper and widely adjoining to responding body ①. Mineralized part of the Santa formation is distributed over the surface ground above responding body ①.

Responding bodies ③ and ⑤ indicate 100 ohm.m resistivity and FE values ranging from 3 to 3.2%, and stretch extensively. These bodies are correlated with the Carhuaz formation, the Santa formation, and the Chimu formation. Responding body ④ indicates 1,000 ohm.m resistivity, and 5.5% FE, and is located in shallow underground. Responding bodies ⑦ and ⑨ indicate from 700 to 3,000 ohm.m resistivity and background FE value of 1.5%.

On the Surface ground above this responding bodies, quartziters are exposed. These responding bodies are correlated with the Farrat formation and the Pariahuanca formation.

Summarization as to the FE values in Antapanpa are given as follows:
The responding bodies which indicated the strong FE anomaly exhibit plate like structure in the north to south profile, and approximately vertical structure on its east to west profile. The depth of the responding body in the north to south profile is in shallow near the station 115 and about 50 m below the surface ground near the station 120, while on the east to west profile, the responding body is located about 100 m below the surface ground at the intersection near station 120. The both responding bodies are coincide in situation.

Field data



	①	②	③	④	⑤	⑥	⑦	⑧	⑨
AR (Ωm)	80	5	100	1000	100	150	700	35	3000
FE (%)	8	5.5	3.2	5.5	3	1.8	1.5	1	1.5

Results of simulation

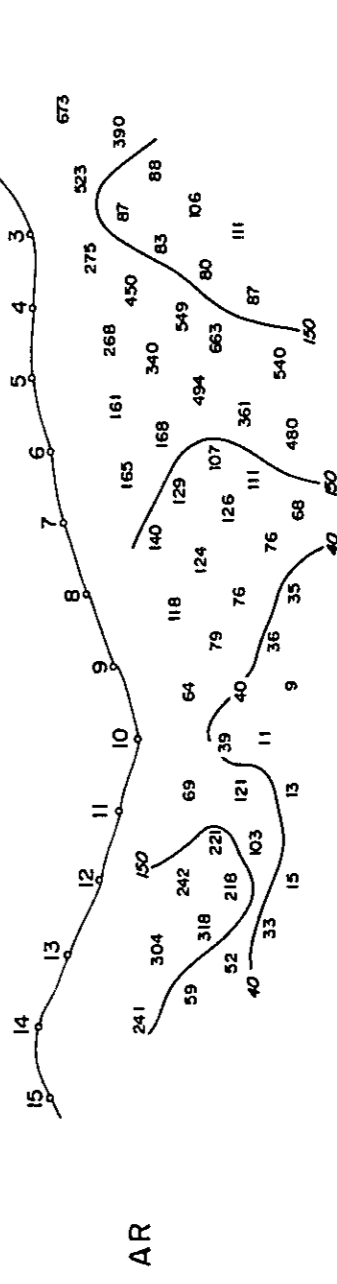
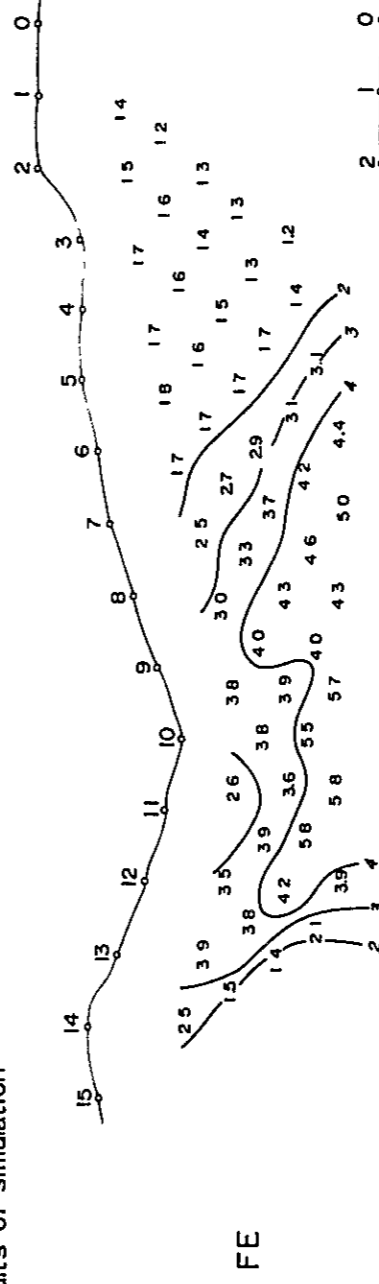


Fig. II-35. Field results and results of computer modeling on line-B

Chapter 6. The Underground Structure Inferred from the Results of
Geophysical Prospecting (IP and EM Methods)

The entire surveyed area is divided into three parts for discussion. The underground structure inferred from the result of the geophysical prospecting is as follows.

6-1 The Northern Part of Iscay Cruz (See Pl. II-2-1, II-2-6, II-2-7, and from II-3-1 to II-3-6.)

This is the special area in which a large scale gozzan are exposed unlike various other mineral deposits of Iscay Cruz. According to the results of physical property examination (see Tables 3 and 4, and Fig. II-24) of rock samples, the limestone, and dolostone of the Santa formation embedding ore deposits indicate resistivity of 7000 ohm·m and FE value 1.2%, and resistivity of 2000 ohm·m and FE value of 4.7%, respectively. Also the gozzan shows such variation as resistivity from 360 to 900 ohm·m and FE values from 1.3% to 8.2%. When inferred from the results of the IP measurement in consideration also of the results of the physical property examination, the Santa formation in this part of the area is considered to correlated with medium to high apparent resistivity (M to H).

The weak FE anomaly detected on the gozzan and on the survey lines running along the Santa formation correlate with the distribution of gozzan. High FE anomaly is detected from highly limonitified gozzan samples which are among the gozzan samples collected on surface ground, however, the limonitified samples are only of a partial factor in number. They are black gozzan on the whole, and not as high as sulfides in FE value. In view of general distribution of weak FE anomaly existence in this vicinity of sulfides or the like to cause high FE anomaly is considered small in

quantity. Also, the fact that the apparent resistivity in this area is higher than that in Central Part and Southern Part suggests that less sulfides exists in this area. The apparent resistivity correlating with the Chimu formation is much higher than that of the Santa formation according to the apparent resistivity cross section on survey line G.

6-2 The Central Part (See Tables 3, and 4, and Fig. II-24.)

This part consists of the fourth mineralized zone and its periphery. Remarkable anomaly of, very low apparent resistivity, and high FE and MF values detected near stations 67-68 (North to South profile) on survey line A and on survey line E (East to West profile) are of the highest intensity detected within the present surveyed area. Explanation is given in the following grouping largely into North to South profile, East to West profile, and the Lagunas Tinyag and its periphery near station 85.

6-2-1 Cumbre de Limpe

(1) East to West Profile (Survey Line E) (See Fig. II-26)

According to the data on geology, the width of the Santa formation is confirmed to be around 100 m, therefore, the responding body ① (or a conductor) is considered to correlate with the Santa formation embedding the fourth mineralized zone. The ground surface near the station 7 is almost covered with hematite, however, there exists much of pyrite as well as ore minerals including galena, sphalerite, etc. Since the afore-mentioned responding body indicates low resistivity and strong FE anomaly, the body is considered to be a mineralized zone accompanied by sulfides within the Santa formation. As the existence of another responding body with the same electric properties as the body ① is estimated in deep part and adjacent to responding body ①, the above-mentioned mineralized zone is

inferred to continue to stretch further downward. In addition, the existence of the conductor estimated at 60 m or deeper inferred through VLF method suggests that the mineralized zone stretches underneath the Santa formation.

(2) North to South Profile (Survey Line A) (See Fig. II-25)

In comparison with the apparent resistivity values in the first, second and third mineralized zone on the north side, the apparent resistivity value in this vicinity is very low on the whole. The difference in the apparent resistivity is inferred to be related with the amount of pyrite, which is observed on the surface ground in this vicinity. The responding body estimated to exist according to the IP method model simulation is the plate-form responding body situated immediately under the surface ground near stations 65-67, and another responding body located about 100 m under the surface ground near stations from 61 to 65, and they both lie to north to south direction. The responding bodies ① and ② indicate the existence of the mineralized zone accompanied with sulfides. It is considered to extend as far as about 600 m from the station 61 to the station 67.

On the surface ground to the south side from station 72, hematite decreases and pyrite increases. The Santa formation is covered almost with talus deposits with little exposures and the formation slides to the east near station 76 due to a fault. Responding body ⑤ obtained by the model simulation indicates the FE values, which correspond to that of the background, near stations 70-72. Responding body ③ indicates values in a range from 3.3% to 3.5% near the station 72 to the station 77. Responding body ⑤ is considered to be connected with the responding body ③ on the north in deep part. As to the fact that the FE values of the responding body near stations from 70 to 77 are weak following reasons are considered to be attributable; i.e. i) The extent of sulfide mineralization is weak on the

whole; ii) The surface ground is covered with talus deposit, and also the survey line located slightly remote from the Santa formation; iii) The mineralized zone is small in its scale.

6-2-2 The Lagunas Tinyag and its Periphery (Survey Line A) (See Pl. II-2-1.)

In the vicinity the Lagunas Tinyag near station 85, medium to high FE anomaly are indicated. The periphery of the lake is covered with alluvial deposits and almost limonitized. Mineralized zone associated with sulfides in the Santa formation is observed in the north side of the station 76, and also skarn zone accompanied by sulfides with the Santa formation is exposed in the south side of the station 87. However, in general the Santa formation is not well exposed in this vicinity due to the existence of the lake and coverage by talus. The FE values detected is considered to be caused by the sulfides such as limonite and the ore minerals embedded in the Santa formation.

6-3 Southern part of Iscay Cruz (See Tables 3, and 4, and Fig. II-24.)

Explanation is given in the following by dividing the area into the three parts of surrounding areas of Chupa Mine, Cunsha Punta, and Antapampa, respectively.

6-3-1 Surrounding Area of Chupa Mine

(1) Chupa Mine (Survey Line H) (See Fig. II-30)

The Chupa ore deposit is a skarn type ore deposit metamorphosed limestone of the Pariahuanca formation. According to the IP method model simulation, the responding body ① showing plate-form is located directly under the stations 6-7. The Chupa Mine situated near the station 5. The skarn zone of the mine yields disseminated ore minerals mainly of sphalerite

and pyrite. In the vicinity of the stations 6-7, pyrite is embedded along the boundary of the Pariahuanca formation and the Farrat formation, and partly in the Carhuaz formation. A sample of magnetite collected near the station 5 gives very strong FE value of 41% and very low resistivity value of 12 ohm·m.

The afore-mentioned plate form responding body ① is located within the Farrat formation and the Carhuaz formation, and is considered to be caused by pyrite on and below the surface ground. In adjacent to this responding body ② with low resistivity and strong FE value is represented by the simulation model. The responding body ② is considered to correspond to the Chupa ore deposit and its periphery, which plunges to east by 70° to 80°. The two responding bodies ① and ② suggest that the skarn zone accompanied with sulfides within the Pariahuanca formation is stretched to downwards. The continuance of the Chupa ore deposit, to the southward is unknown. The continuance to the northward is studied from apparent resistivity distribution as follows; low apparent resistivity and medium apparent resistivity continue almost along the strata from survey line H to survey line C, showing homogeneity of the rocks. While the FE values and responding bodies detected on the Farrat formation and the Pariahuanca formation on survey line H are not detected on each formation on survey line C. Therefore, the possibility is very low that the Chupa ore deposit stretches to the northward to survey line C.

(2) Survey Line C (See Fig. II-31.)

Responding body ① based on IP model simulation gives a vertical columnar shape directly below the surface ground, its resistivity of 5 ohm·m. On the other hand, the dip angle of the conductor calculated on its EM anomaly mark 82°W showing almost vertical. In addition, the depth to the conductor is estimated at about 18 m below the surface ground. According

to the geological data, the width of the Santa formation is confirmed to be about 60 m. Compared with the position of responding body ① according to IP model, the position of the conductor obtained by EM method is a little shifted from the former, yet, the both are considered to correlate with the Santa formation. Skarn accompanied with sulfides occurs within the Santa formation on the surface ground near the station 10-11. The responding body ① showing strong FE value is considered to be correlated with the skarn accompanied with sulfides within the Santa formation. Since the responding body ② with 25 ohm·m resistivity and 5% FE is accompanied by the responding body ① in its periphery, the skarn accompanied with sulfides is inferred to extend downwards. The conductor which is inferred by VLF method to exist in the depth of 60 m or more suggests the possibility of stretching itself below the Santa formation. Responding body ⑧ situated in the west end part of the survey line C, where in the distribution of limestones of the Pariahuanca formation is presumed, indicates weak resistivity value of 750 ohm·m and FE value of 1.5%.

(3) Survey Line A (See Pl. II-2-1.)

The very low apparent resistivity detected near the stations 86-99 is considered to be the indication of alteration. The surface ground near the stations 90 to 99 is covered with talus deposits, however, it is inferred to be a weak clay alteration zone through the investigation conducted by trenching near the stations 96 and 97.

FE indication is weak near the station 89 on survey line A, however, FE indication is strong where survey line C goes across the Santa formation. Therefore the possibility is high that mineralizing alteration is distributed to the east side of east-west profile in this vicinity. Survey line A is a little separated from the Santa formation in the vicinity of the stations from 90 to 97. The weak FE and medium anomaly detected is not

known whether it is caused by the skarn accompanied with sulfides within the Santa formation or by weak clay alteration.

With all the above, the explanation has been given on the Surrounding Area of Chupa Mine. It is considered that this area is sufficiently interesting due to eminent low apparent resistivity and the strong FE anomaly in its east-west profile.

6-3-2 Cunsha Punta

(1) Survey Line A (See Fig. II-34.)

Responding body ⑧ based on the IP model simulation indicates a large scale of distribution with high resistivity at 300 ohm-m and weak FE value of 3.5% in shallow underground near the station 104. According to geological data, the occurrence is confirmed of a mineralized zone accompanied with sulfides within the Santa Formation on the surface ground near the station 103, and of black gozzan near the station 106, which gozzan is also observed in the north area of Iscay Cruz. Responding body ⑧ is considered to be correlated with the afore-mentioned mineralization, and at the same time the extent of sulfide mineralization within the Santa formation on the north to south profile is considered to be low in view of the resistivity value and FE value.

(2) Survey Line D (See Pl. II-2-4.)

From the strong FE anomaly distributed in the west side of the station 6, existence of a responding body with a columnar shape tilted to west can be considered. On the surface ground near the station 6, the occurrence of a mineralized zone accompanied by sulfides in the Santa formation is confirmed. Also, the existence of pyrite in the Carhuaz formation in the west of the station 5 is observed. Strong FE anomaly are detected in correspondence to the Santa formation and a part of the Carhuaz formation.

Therefore sulfide mineralization or alteration may extend to the Santa formation and the Carhuaz formation. However, as the strong FE anomaly is accompanied with the medium apparent resistivity and weak MF anomaly, it is conceivable that the extent of mineralization is still low or that the mineralization is of pyrite without strong alteration.

6-3-3 Antapampa

(1) Survey Line A (See Fig. II-34.)

The responding body that extends in north-south direction is such a scale body that it extends as long as about 1100 m from the station 113 to the station 123.

On the surface ground near the station 115, a good quantity of pyrite is exposed. Gozzan occurs more in amount in the Chimu formation rather than in the Santa formation. According to the geological data, small scale of skarn accompanied with sulfides in the Santa formation and black gozzan mainly composed of manganese oxide, which are observed in the north of Iscay Cruz, are exposed on the ground surface near the station 120.

Responding body ② located directly under the surface ground near the station 115 is considered to indicate mineralization of pyrite which is exposed in a good amount on the surface ground. Responding body ① that adjoins to the lower part of responding body ② is estimated to be correlated with the skarne which accompanied with sulfides in the Santa formation from its FE values and resistivity values.

Responding body ② in the vicinity of the station 120 is correlated with the Santa formation. The FE value is high unlike the FE values caused by the manganese oxide in the north part of Iscay Cruz. Inferred from the FE values and resistivity values of the responding body ③, skarn accompanied with sulfides extends almost continuously with the afore-mentioned responding

body ① is located in shallow underground in a large scale. In addition, two responding bodies ((5) and (6)) of low resistivity and approximate FE value of 3% are obtained by the simulation under the preceding two responding bodies ① and ③. Therefore, the mineralized zone may extend to deeper parts.

(2) Survey Line B (See Fig. II-35.)

Responding body ① given by the IP model simulation exhibits a plate form vertical structure existing about 100 m below the surface ground near the stations 9 and 10. This responding body ① corresponds to the responding body ③ on the survey line A.

On the surface ground, as already mentioned in the preceding Item on survey line A, the existence thereon of small scale of skarn accompanied with sulfides and black gozzan is exposed within the Santa formation. Responding body ① belong to the Santa formation and stretches to deep part from shallow underground. In adjacent to this responding body ①, responding body ② indicating 5.5% FE value and 5 ohm·m resistivity is located in the deep part on the east side. The two responding bodies suggest that the skarn which is accompanied with sulfides and belong to the Santa formation extends to the deep part from shallow underground, and that it expands to deep part towards east side.

On survey line B, a responding body with low resistivity and strong FE value is obtained in deep part near the stations 9-10 on which the survey line B intersects with the survey line A. Therefore, skarn accompanied with sulfides may extend to deep part. The limestone, which is inferred to be located near the station 2-3, in the Pariahuanca formation, gives no indication of FE which is detected on the Chupa Mine. According to the fact, the possibility is little that the Chupa ore deposit extends to this vicinity.

Chapter 7. Conclusions and Guidance for Future Exploration

(See Fig. II-36)

7-1 Conclusion

Following are summarized results obtained with the present geophysical exploration (IP Method and EM Method) in the surveyed area:

(1) The noteworthy FE anomaly zones in the surveyed area are the following three zones:

- i) Cumbre de Limpe : Anomaly Zone I
- ii) Surrounding Area of Chupa Mine: Anomaly Zone II
- iii) Antapampa : Anomaly Zone III

1) Anomaly Zone I

The anomaly zone is an area centering on stations 66-67 on survey line A, and stations 8-9 on survey line E, and is located in the fourth mineralization area. The zone indicates strong FE value (5 to 6.5%) and low resistivity (10 to 100 ohm.m), and is the most promising area within the Santa formation with its mineralization potentiality accompanied with sulphide. The mineralization belt stretches long with south to north profile but short with east to west profile. It is expected to possess the scale of about 600 to 850 m in length, about 50 to 100 m in width, and about 100 to 150 m in thickness, based on the model calculation. As the width of the conductor is calculated to attain about 150 m according to EM analysis, the both calculation results almost coincide. The dip of the Santa formation on east to west profile is construed to be almost vertical from the IP model calculation and EM analysis, the responding body is considered to continue from shallow underground to deep part.

ii) Anomaly Zone II

There are included two component areas in the extent of this zone. One from Chupa ore deposit(a) near stations 6-7 on survey line H to the east side the Santa formation (b) and the other covering the area which surrounds the point at which survey line A intersects survey line C. Within the extent each is correlated with low resistivity to strong FE anomaly. The responding body detected on survey line H on the basis of the model calculation is about 300 m in length, related with Chupa ore deposit, and in trapezoid. Also, the responding body detected on survey line C on the basis of the model calculation is about 50 m long and in vertical plate shape. As the conductor indicated, on EM analysis, dip of 82°W, an almost vertical attitude, and was construed as to its formation width of 36 to 71 m, the results from both of the above calculation and analysis almost coincide. Concerning the potential depth, both (a) and (b) indicate good possibility of extending to deep part from a small depth below the surface ground. From the FE indications detected on the east to west profile, correlation is inferred to exist between the mineralization of Iscay Cruz ore deposit and Chupa ore deposit. When the low resistivity zone which extends extensively including the anomaly zone II is considered to be under the complete influence of the mineralization caused by both the intrusive rocks seen on the east side of this zone and the fault which develops in the east to west direction and intersecting in a right angle with the intrusive rock, the area from the Lagunas Tinyag to Chunsha Punta may be called a very interesting area.

iii) Anomaly Zone III

This anomaly zone is situated in the vicinity of stations 115 and

120 on survey line A and the station 9 on survey line B, and is located in the seventh mineralized zone which is confirmed in the preceding geological survey. It indicates strong FE values (5 to 8%) and low resistivity (5 to 80 ohm·m), from which the potential of the mineralized zone accompanied by sulphides is promising. Estimated scale of the zone based on model calculation is ①, about 400 m in length and about 100 m in thickness in the vicinity of the station 115, and ② about 600 m in length, about 150 m in thickness, and about 100 to 150 m in width in the vicinity of the station 120. In the total of ① and ②, the length is expected to attain as long as 1000 m. Its depth is considered to extend from a small depth from surface ground to deep part.

7-2 Guidance for Future Exploration

- (1) As explained in the foregoing, promising ore deposits are expected to exist in the vicinity of the three anomaly zones which are grasped within the surveyed area. In addition, the potential depth is expected to range from near ground surface to about 250 m. Therefore, it is desirable that exploration drilling should be carried out in the anomaly zone I and II.
- (2) The survey lines had to be established slightly deflected from inferred location of the Santa formation because of the talus deposits covering the south sector from station 90 up to Cunsha Punta and obstructive land form. This sector, which runs along the south to north profile, is correlated with low to medium FE values and low apparent resistivity, and it is worthy of attention from geological structural point of view. However, there are places difficult to effectuate electrode grounding in this sector, and it is



desirable that the existence of conductors should be confirmed rather with EM method than with IP method through arranging a 9 km (1.5 km by 6 survey lines) survey lines over the east to west profile intersecting with the south to north profile.

- (3) The existence of mineral deposits potential next to anomaly zone I is pointed out with anomaly zone III through the IP survey. Although, the plate type responding bodies is expected to exist near the stations 112 to 116, only non-mineralized limestone on the surface ground and black gozzan on its south sector are recognized in existence. Therefore, it is least clear whether or not what scale of mineralized zone can be estimated below the ground at this time. Under the circumstances, it is desirable to carry out exploration drilling in this zone only after having clarified the conditions of underground mineralization through execution of IP method over the survey lines intersecting with the Santa formation in the area including survey lines D and B.

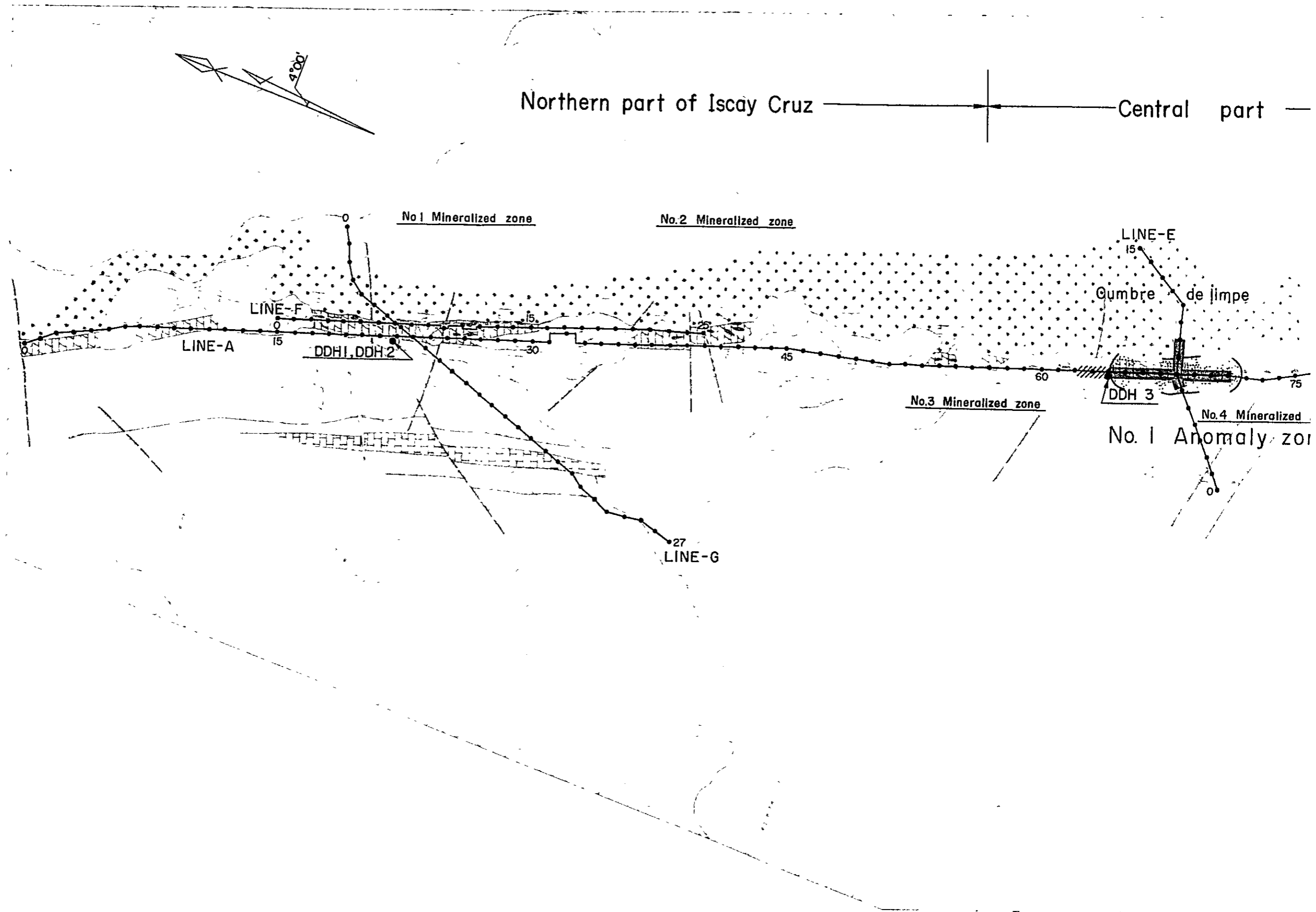
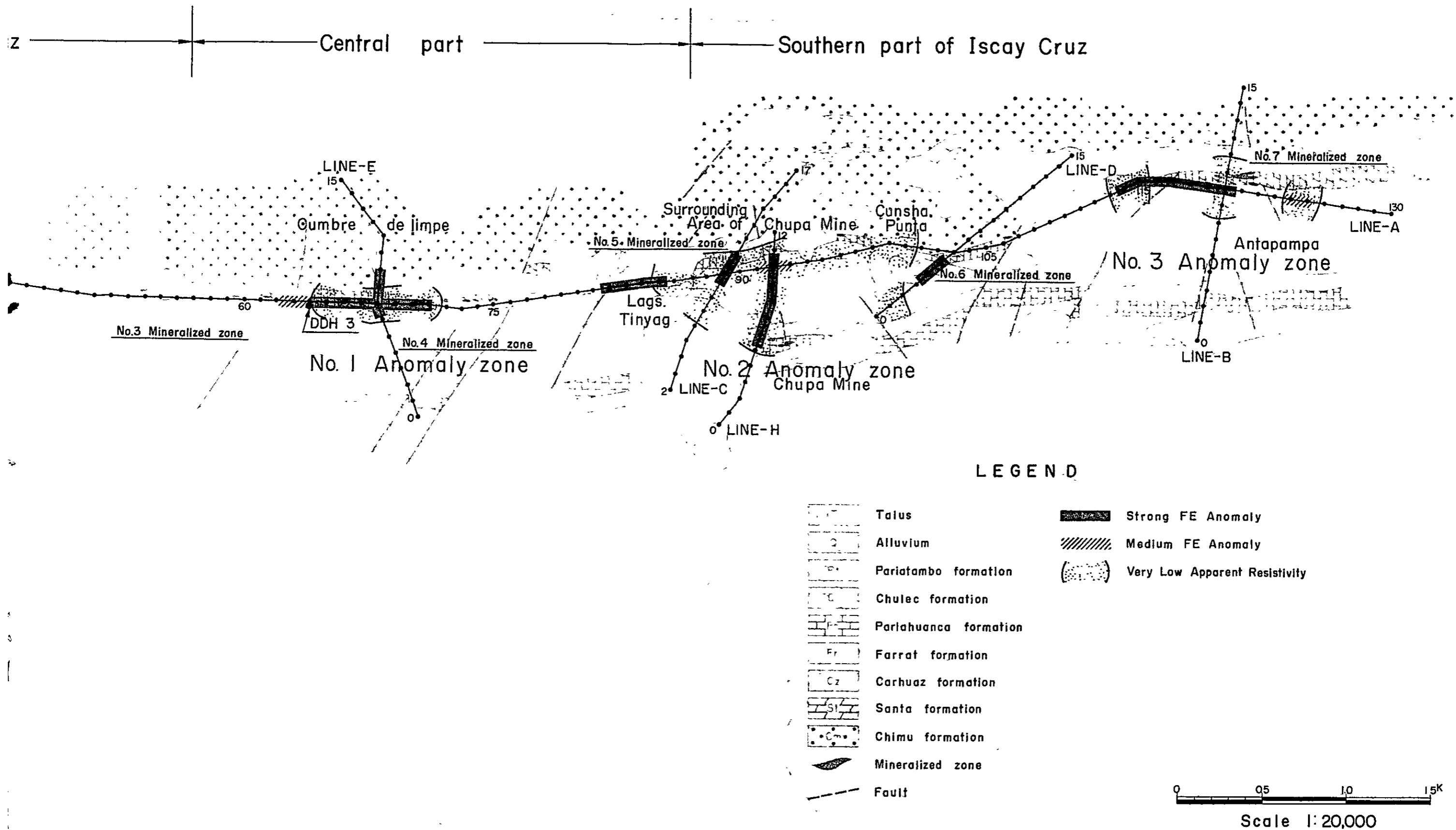


Fig II-36 Relationship between geology and the locatio



relationship between geology and the location of the IP anomalies

REFERENCE LITERATURE

- CONEY, D.P. 1977, Model studies of the VLF-EM method of geophysical prospecting, *Geoexploration* 15, 19-35
- GEONICS LTD. 1964, EM-16 Operating Manual, Geonics Ltd., 2 Thorncliffe Park Drive, Toronto 17, Ont., Canada
- PAAL, G. 1965, Ore prospecting based on VLF-radio signals, *Geoexploration* 3, 139-147
- PAAL, G. 1968, Very low frequency measurements in northern Sweden, *Geoexploration* 6, 141-149
- PATERSON, N.R. and RONKA, V. 1971, Five years of surveying with the very low frequency electromagnetics method, *Geoexploration* 9, 7-26
- HELLAND, C.A. 1946, *Geophysical Exploration*, Prentice Hall, New York
- GRANT, F.S. and WEST, G.F. 1965, *Interpretation Theory in Applied Geophysics*, McGraw-Hill Book Co., New York
- KAIKKONE, P. 1977, A finite element program package for electromagnetic modeling, *J. Geophys.* 43, 179-192
- KAIKKONEN, P. 1979, Numerical VLF modeling, *Geophysical prospecting*, 27 815-834
- NAIR, M.R. etc., 1968, Experimental studies on the electromagnetic response of tilted conducting half-plane to a horizontal-loop prospecting system, *Geoexploration* 6, 207-244
- PHILLIPS, W.J. and RICHARDS, W.E. 1975, A study of the effectiveness of the VLF method for the location of narrow-mineralized fault zones, *Geoexploration* 13, 215-226
- OLSSON, O. 1980, VLF anomalies from a perfectly conducting half plane below an overburden, *Geophysical prospecting* 28, 415-434
- S.E.G. 1967 *Mining geophysics, Volume II*
- SCINTREX LTD. SE-600 Electromagnetic horizontal-vertical loop system
- TATSUGAMI, M. 1970, The VLF E.M method and instrument, *BUTSURI-TANKO* 23, No. 5
- S.E.G.J. 1968, The latest progress in geophysical prospecting (20th anniversary) P. 193-196
- S.E.G. 1966, *Mining geophysics, Volume I*

- J.S, Sumner 1976, Principles of Induced polarization for geophysical exploration
- M.M.A 1980, Republic of Peru report on geological survey of the Oyon Area Vol. I

PARTICULARS

PART III

DRILLING EXPLORATION

PART III DRILLING EXPLORATION

CONTENTS

Chapter 1	Outline of Diamond Drilling	III - 4
1-1	Purpose of the Survey	III - 4
1-2	Outline of Operation	III - 4
1-3	Core Evaluation and Analysis Works	III - 5
Chapter 2	Diamond Drilling Works	III - 6
2-1	Access Road for Transporting Equipment & Materials	III - 6
2-2	Location of the Drill Holes	III - 6
2-3	Preparatory Works	III - 7
2-4	Drilling Works	III - 8
2-5	Mobilization and Demobilization	III - 12
2-6	Progress Records	III - 12
Chapter 3	Geology and Mineralization of the Drill Holes	III - 14
3-1	DDH-1	III - 14
3-2	DDH-2	III - 16
3-3	DDH-3	III - 17
3-4	Evaluation of the Mineralization	III - 19

LIST OF FIGURES

- Fig. III-1 Progress record of diamond drilling, DDH-1
- Fig. III-2 Progress record of diamond drilling, DDH-2
- Fig. III-3 Progress record of diamond drilling, DDH-3
- Fig. III-4 Geological section for DDH-1 and DDH-2
- Fig. III-5 Geological section for DDH-3

LIST OF TABLES

- Table III-1 List of drilling equipment used
- Table III-2 Supplies and drilling parts consumed
- Table III-3 Preparation and removal
- Table III-4 Operational results of drill hole, DDH-1
- Table III-5 Operational results of drill hole, DDH-2
- Table III-6 Operational results of drill hole, DDH-3
- Table III-7 Summary operational data of each drill hole
- Table III-8 Working time of each drill hole
- Table III-9 Drilling meterage of diamond bits
- Table III-10 Specifications of diamond bits
- Table III-11 Assay results of the drilled core
- Table III-12 Assay results of rock forming elements in the drilled core
- Table III-13 Summary of X-ray diffraction test in the drilled core

LIST OF APPENDICES

- A. III - 1 Microscopic observation of the thin sections
- A. III - 2 Microscopic observation of the polished sections
- A. III - 3 Photomicrographs
 - 3 - 1 Polished section
 - 3 - 2 EPMA analysis
- A. III - 4 Charts of X-ray diffraction test

LIST OF PLATES

- Plate III - 1 Geologic drill log, DDH - 1
- Plate III - 2 Geologic drill log, DDH - 2
- Plate III - 3 Geologic drill log, DDH - 3

Chapter 1 Outline of Diamond Drilling

1-1 Purpose of the Survey

Basing upon the results of first year's geological survey in the Oyon area of the Republic of Peru, the Iscay Cruz area was selected as the area to be surveyed for the second year.

The diamond drilling was performed to determine and clarify the relation between the geological structure and the mineralization in the Iscay Cruz area.

1-2 Outline of Operation

One member, as an advance survey member, left Japan on June 1, 1980 and arrived at the Oyon area on June 5. Then, he began to construct a 20 km long access road for materials transportation by using One Fiat-AD7 bulldozer on June 9 and completed it on August 19.

Four additional members of the survey team also arrived at Peru and engaged in the construction of the access road from July 24 to August 3.

Also, drilling equipment and materials shipped from the Port of Yokohama late May, 1980 were unloaded at the Port of Callao, and transported to the drilling site by trucks after August 4. Then, preparatory work was started from DDH-3.

The drilling equipment used was one TGM-3C (drilling capacity: NQ 510 m, BQ 660 m), and three drill holes with a total drilled depth of 564.00 m were made.

As a rule, work was performed on the basis of three 8-hour shifts, and one driller and three helpers worked for each shift. The drilling method adopted was the wire-line method and it was tried to improve the core recovery and to make rapid progress.

The amount of performance are listed below.

<u>Hole No.</u>	<u>Drilled depth (m)</u>	<u>Core length (m)</u>	<u>Core recovery (%)</u>
DDH-1	155.00	109.10	71.8
DDH-2	252.00	206.60	82.0
DDH-3	157.00	145.85	93.3
Total	564.00	461.55	82.5

NOTE: No talus deposit is included for the core recovery.

Drilling work was performed for a period of 80 days from August 20 to November 7.

1-3 Core Evaluation and Analysis Works

All cores of every drill hole were evaluated with respect to lithology, alteration and mineralization, and the data were recorded on the core-logging charts with 1/200 scale.

Cores containing ore minerals were split into halves or one-quarters to produce samples for analysis, and the analyses were made for each element of copper, lead, zinc, silver and so forth. For the geological analysis, thin sections and polished sections of every rock and each mineralized part were prepared and observed through microscope. Also, determination of lithological names of the rocks were completed with the help of X-ray diffraction analysis and electron probe microanalysis.

Main items and quantities of analysis work are listed below.

- (1) Microscopic observation of thin sections of rock: 13 samples
- (2) Microscopic observation of polished sections of ore: 11 samples
- (3) Analysis of ore (Ag, Cu, Pb, Zn, Fe, S): 72 samples
- (4) Rock analysis (Ca, Mg, Mn Fe, Si, Ba, Sr, Co): 18 samples
- (5) X-ray diffraction: 10 samples
- (6) Electron probe microanalysis: 1 sample

Chapter 2 Diamond Drilling Works

2-1 Access Road for Transporting Equipment & Materials

One member who arrived at the Oyon area on June 6, 1980 as an advance survey member of the survey team visited the drilling site for the field investigation. Then, he made plans for construction of access road and for transporting equipment and materials basing upon the results of the field investigation, and then he employed several helpers. In addition, he visited the Oyon City Hall, the Police Department and the Joint Land Ownership Association, and obtained permits and approvals for using site of drilling work, for entering into pastures and for constructing access road.

Access road, 20 km long and 3 m wide, was constructed by about 20 local workers and one Fiat-AD7 bulldozer, for which 9.5 km long existing road was repaired and earth cutting by bulldozer and blasting of exposed rocks were performed.

Since the access road was located on highland with altitude between 4,030 m and 4,980 m above sea level and talus deposit was widely distributed below the mountain pass with an altitude of 4,980 m, landslides and falls of boulders occurred frequently, resulting in many problems in maintaining the road and driving vehicles.

About 10 to 20 workers were always kept mainly at the mountain pass to assure the smooth travelling of vehicles while the repair work was being conducted.

2-2 Location of the Drill Holes

The Isca Cruz area is located at a place approximately 28 km away from the Oyon village via Pampahuay village, and it takes about 2 hours and 30 minutes by drive for one-way trip between them.

The geographical location and elevation of the drilling holes are as follows.

<u>No. of Holes</u>	<u>Longitude</u>	<u>Latitude</u>	<u>Elevation</u>
DDH-1	308.96E	813.07N	4,643 m
DDH-2	308.96E	813.07N	4,643 m
DDH-3	310.41E	809.12N	4,695 m

2-3 Preparatory Works

2-3-1 Transportation of Equipment and Materials

After the customs clearance, equipment and materials were transported by two 6-ton trucks and one 8-ton truck from the warehouse at Port of Callao on August 5, 1980 to Pampahuay on August 6 via Churin and Oyon villages. Then, they were transported for a distance of about 11.4 km between Pampahuay and the site of DDH-3 in the Iscay Cruz area by two 1-ton pickup trucks in accordance with the following schedule:

August 6 to 7: Accept, Unpacking, checking & preparation for transport of equipment and materials

August 8 to 11: Transporting equipment and materials (DDH-3)

August 12 to 16: Transporting equipment and materials (DDH-3)

Setting up drilling machine (DDH-3)

Setting up derrick (DDH-3)

August 17 to 19: Transporting equipment and materials (DDH-3)

2-3-2 Development of Drilling Bases

Development of drilling base began from DDH-3. About 50 m long access road was first constructed with bulldozer and the earth was graded manually to provide the drilling ground base.

For holes DDH-1 and DDH-2 (same location), about 40 m long access road and drilling ground base were constructed.

2-3-3 Water Supply

Water supply pipe about 200 m long was installed for DDH-3 and water was supplied with a pump from a lake in the north of Cumbre de Limpe.

For DDH-1 and DDH-2, 900 m long piping was made and water was supplied with a pump from Laguna Mancacuta.

2-4 Drilling Works

The hole was drilled in the talus deposit with a single tungsten carbide bit of 116 mm dia. When the holes reached the rock face, drilling was continued with HQ wire-line method, then casing pipes were sequentially installed and BQ wire-line was used for the final bore.

The drilling progress of each hole was as follows.

2-4-1 DDH-1

Drilled depth: 155.00 m

Drilled rock core length: 109.10 m

Rock core recovery: 71.80% (except talus deposit)

Starting date of drilling: September 17, 1980

Completion date: October 6, 1980

0 to 4.00 m :

The hole was drilled with a single tungsten carbide bit of 116 mm dia. and feeding mud water. After drilling the talus deposit down to 4.00 m depth, HW casing pipe 4.00 m in length was installed.

4.00 to 9.00 m :

Drilling was carried out in the shale formation with HQ-WL diamond bit and feeding mud water. Since the rock was stable at the depth of 7.30 m, NW casing pipes 9.00 m in total length were installed.

9.00 to 124.70 m :

The hole was drilled down to the depth of 124.70 m in the shale

formation interbedded with clay with NQ-WL diamond bit and feeding mud water. From the depth of 117.20 m, the shale formation with many cracks interbedded with clay began to continue and hole conditions became very poor. NQ-WL diamond bit was replaced. Then, while the rod was being lowered, cavings of the hole caused and swelling occurred at the depth of about 124.70 m, NQ-WL rods were tightly jammed up. It was tried to correct the trouble but the recovery became impossible. Thus, NQ-WL rods were used instead of BW casing pipes and BQ-WL was adopted.

124.70 to 155.00 m :

Shale formation with many cracks interbedded with clay was drilled down to the depth of 155.00 m with BQ-WL diamond bit and feeding mud water, and drilling was completed as planned. Incidentally, jamming occurred again at the depth of 153.00 m because of the residual slime while the rod was being lowered after replacing the BQ-WL diamond bit. For correcting the trouble, the drill hole was reamed with NW casing shoe and BW casing shoe, and both NQ-WL rods and BQ-WL rods were recovered.

2-4-2 DDH-2

Drilled depth: 252.00 m

Drilled rock core length: 206.60 m

Rock core recovery: 82.00% (except talus deposit)

Starting date of drilling: October 9, 1980

Completion date: October 23, 1980

0 to 3.10 m :

The hole was drilled with a single tungsten carbide bit of 116 mm dia. and feeding mud water. Talus deposit with 10 to 50 mm particle size was drilled down to the depth of 3.10 m. Since the rock was stable, HW casing pipes 3.10 m in length were installed.

3.10 to 30.50 m :

Relatively stable shale, dyke and limestone formation was drilled down to the depth of 30.50 m with HQ-WL diamond bit and feeding mud water. Since the rock was stable, NW casing pipes were installed down to the depth of 30.50 m.

30.50 to 122.00 m :

Shale formation with many cracks interbedded with clay and altered limestone formation were drilled with NQ-WL diamond bit and mud water circulation down to the depth of 122.00 m. Since the drilling became more difficult in poor formation generally, BW casing pipes were installed down to the depth of 122.00 m. During this drilling, two layers of Pb and Zn impregnation between 103.40 m and 104.60 m and between 107.70 m and 121.00 m were confirmed.

122.00 to 252.00 m :

Shale formation with many cracks interbedded with clay and altered limestone formation were drilled with BQ-WL diamond bit and mud water circulation down to the depth of 252.00 m, and the drilling was completed as planned. During this drilling, shattered zone with many cracks were found near the depth of 122.00 m and 166.70 m, then installation of additional casing pipes was tried but was impossible beyond the depth of 125.60 m. Also, because of existence of cavities, each 0.4 to 1.50 m deep, at several places below the depth of 202.20 m, water circulation was lost and then drilling was made while carefully controlling the water pressure and mud water circulation. During this drilling, three layers of Pb and Zn impregnation between 121.80 m and 122.70 m, between 125.50 m and 131.00 m and between 164.70 m and 183.90 m were confirmed.

2-4-3 DDH-3

Drilled depth: 157.00 m

Drilled rock core length: 145.85 m

Rock core recovery: 93.30% (except talus deposit)

Starting date of drilling: August 20, 1980

Completion date: September 9, 1980

0 to 3.10 m :

Surface soil of talus deposit was drilled with a single tungsten carbide bit of 116 mm dia. and feeding clear water down to the depth of 3.10 m. Since the rock was stable, HW casing pipes were installed down to the depth of 3.10 m.

3.10 to 30.10 m :

Relatively stable shale formation was drilled with HQ-WL diamond bit, clear water and mud water circulation down to the depth of 30.10 m. Then, the rock was stable and NW casing pipes were installed down to the depth of 30.10 m.

30.10 to 63.60 m :

Mainly the shale formation was drilled with NQ-WL diamond bit and mud water circulation down to the depth of 63.60 m. It encountered a shattered zone of shale interbedded with clay in the layer between 54.60 m and 63.60 m and then drilling was continued while preventing loss of circulation. BW casing pipes were installed down to the depth of 63.60 m.

63.60 to 157.00 m :

Shale interbedded with clay, sandstone, marl and limestone formations were drilled down to the depth of 157.00 m with BQ-WL diamond bit and mud water circulation, then drilling was completed as planned. During this drilling work, there were many cracks and the core frequently blocked so that the mud water circulation was carefully controlled. Ores of lead,

zinc and pyrite were confirmed in the layer between 104.60 m and 118.90 m.

2-5 Mobilization and Demobilization

2-5-1 Mobilization

DDH-1 and DDH-2 are located at an area about 5.5 km north of DDH-3, and four days were needed for moving and preparatory work prior to the drilling.

2-5-2 Demobilization

Since the conditions of access road became very poor because of bad weather during the moving from DDH-2, drilling equipment and materials were transported to the camp (3 km) and stored there while the road was being repaired by 15 to 20 workers. Boring cores were stored in a warehouse of INGEMMET in Lima.

2-6 Progress Records

2-6-1 Productivity

As shown Table III-7, the productivity achieved was 3.20 m/shift with respect to the total manshifts totalling to 564.00 m of drilled length, and also 5.37 m/shift with respect to the drilling manshifts.

Rate of advance and the bit speed (r.p.m.) are indicated below.

	<u>Rate of advance</u>	<u>Bit speeds (r.p.m.)</u>
Hard rock:	1.5 to 2.0 cm/min.	500 to 600 r.p.m.
Semi-hard rock:	2.0 to 3.0 cm/min.	400 to 500 r.p.m.
Soft rock:	3.0 to 4.0 cm/min.	300 to 400 r.p.m.

Productivities shown above are low because the rocks generally had shattered zones with many cracks interbedded with clay.

2-6-2 Core Recovery

As shown in Table III-7, the rock cores about 457.90 m long were obtained out of the total drilled depth of 555.10 m excluding the talus deposit. Average core recovery was 82.5%.

Table III-1 List of drilling equipment used

Item	Model	Quantity	Capacity, Type, and Specification
Drilling Machine	TGM-3C	1	Capacity NQ 510m, BQ 660m Inner Diameter of Spindle 93mm Weight (except engine) 2,300kg
Engine for Drill	F4L-912	1	Diesel Engine 1,800 rpm/55 PS ~ 1,500 rpm/41 PS
Pump	NAS-3C	1	Piston $\phi 75$ mm Capacity 130,72,39,22 ℓ /min Pressure 26 ~ 40 Kg/cm ²
"	NES-100B	1	Piston $\phi 60$ mm Capacity 100,50,71,35.5 ℓ /min Pressure 18 ~ 50 Kg/cm ²
"	MS-303	1	Piston $\phi 25$ mm Capacity 25 ~ 41 ℓ /min Pressure 35 Kg/cm ²
Engine for pump	2T-90L	1	Diesel Engine 1,800 rpm/20 PS
"	NS-130C	1	Diesel Engine 1,800 rpm/8.5 PS
"	NS-65C	1	Diesel Engine 1,800 rpm/5.5 PS
Generator	YSG-3.5	2	3.5KVA, 220V, 60c/s
Engine for Generator	NS-65C	2	Diesel Engine 1,800 rpm/5.5 PS
Mud Mixer	MCE-200	1	Volume 200 ℓ , 800 ~ 1,000 rpm/min
Derrick	DCP9-6A	1	Steel structural derrick (Vertical, inclination) Weight 2.4 ton Lifting 6m height
Rod Holder	RH-85	1	Hand Type
Drill Rods	HQ-WL	11	3.00 m/PC
"	NQ-WL	41	3.00 m/PC
"	BQ-WL	91	3.00 m/PC
Casing Pipes	HW	3	3.00 m/PC
"	NW	11	3.00 m/PC
"	BW	41	3.00 m/PC

Table III-2 Supplies and drilling parts consumed

Description	Specification	Unit	Quantity		
			DDH-1	DDH-2	DDH-3
Light oil		ℓ	1,200	1,800	950
Mobil oil		ℓ	35	50	90
Hydraulic oil		ℓ	-	-	121
Grease		kg	0.5	0.5	4
Bentonite	50kg/bag	Bag	75	26	60
Libonite		kg	55	33	60
Tel-cellose		kg	17	15	18
Cement	40kg/bag	Bag	2	2	3
Tel-stop		kg	-	-	-
Emale 20C		ℓ	20	20	20
Metal crown	116mm	Pc	1	1	1
Single core tube	114mm x 0.5m	Set	-	-	1
Double core tube	114mm x 1.5m	"	-	-	-
Wire line core barrel	HQ x 1.50m	"	-	-	1
"	NQ x 3.00m	"	-	-	1
"	BQ x 3.00m	"	-	-	1
Inner tube assembly	HQ x 1.50m	"	-	-	1
"	NQ x 3.00m	"	-	-	1
"	BQ x 3.00m	"	-	-	1
Outer tube	HQ x 1.50m	Pc	1	-	-
"	NQ x 3.00m	"	-	1	-
"	BQ x 3.00m	"	1	1	-
Inner tube	HQ x 1.50m	"	-	1	-
"	NQ x 3.00m	"	-	1	-
"	BQ x 3.00m	"	1	1	-
Casing metal shoe	HW	"	1	1	1
"	NW	"	1	1	1
"	BW	"	-	-	1
Rag		kg	4	10	5
Core box		Pc	23	46	32
Wire	10#	kg	5	5	25
"	12#	"	4	4	10
Nail		"	5	5	5
Wire rope	6mm x 550m	Roll	0.5	0.5	0.5
"	12mm x 40m	"	1	1	1
Manila rope	18mm x 30m	Pc	1	1	2
Vinyl rope	8mm x 100m	"	1	1	1
Pump packing		"	4	4	4
Valve steel ball	38.1ϕ	"	8	8	-

Supplies and Drilling Parts Consumed-Continued

Description	Specification	Unit	Quantity		
			DDH-1	DDH-2	DDH-3
Piston rod		Pc	2	-	-
Guide pipe	HQ	"	-	1	-
"	NQ	"	1	1	-
"	BQ	"	1	1	-
Guide coupling	HQ	"	1	1	-
"	NQ	"	1	1	-
"	BQ	"	1	1	-
Suction hose	50mm x 4.5m	"	-	1	-
Water swivel packing		"	-	3	3
Water swivel spindle		"	1	1	-
V-belt	TGM-3Cx4L912	Set	1	1	-
"		Pc	-	4	-
Core lifter	HQ	"	1	1	1
"	NQ	"	2	3	2
"	BQ	"	1	3	2
Core lifter case	HQ	"	1	1	1
"	NQ	"	1	2	1
"	BQ	"	1	2	1

Table III-3 Preparation and removal

Item	Hole No.		DDH-1		DDH-2		DDH-3		Man-shifts	Days	Man-shifts	Days	Man-shifts	Days	Man-shifts	Days	Man-shifts	Days		
	In	Out	1st Sep. '80	16th Sep. '80	8th Oct. '80	7th Oct. '80	4th Aug. '80	19th Aug. '80											11th Sep. '80	12th Sep. '80
Preparation	Access road																			
	Haulage			2	30							7	70							
	Installation			5	60	0.5	8					2.5	20							
	Water pipe																			
	Test run, etc.			4	40	0.5	4					6.5	76							
	Total		11	130	1	12					16	166								
Removal	Dismounting		1	10							2	20								
	Pipe removal																			
	Haulage																			
	Road reinforcement																			
	Others																			
		Total		1	10	-	-					2	20							
		Grand Total		12	140	1	12					18	186							

Table III-4 Operational results of drill hole, DDH-1

Working Period	Period			Number of Days	Actual Working Days	Day Off	Total Number of Workers	
	Preparation	1st Sep.'80 ~ 16th Sep.'80			16	11	5	130
	Drilling	17th Sep.'80 ~ 6th Oct.'80			20	20	-	518
	Removing	7th Oct.'80			1	1	-	10
	Total	1st Sep.'80 ~ 7th Oct.'80			37	32	5	658
Drilling Length	Planned Length	150.00 ^m	Over-burden	7.30 ^m	Core Recovery for each 100 m section			
	Increase or Decrease in Length	^m	Core Length	109.10 ^m	Depth of Hole	Section	Total	
	Length Drilled	155.00 ^m	Core Recovery	71.8%	0 ~ 100 ^m	95.1%	95.1%	
Working Time	Drilling	107°00'	16.6%	15.8%	100 ~ 155 ^m	37.7%	71.8%	
	Hoisting & Lowering Rod	7°30'	1.2%	1.1%				
	Hoisting & Lowering I.T.	40°00'	6.2%	5.9%				
	Miscellaneous	105°30'	16.3%	15.6%	Efficiency of Drilling			
	Repairing	188°00'	29.1%	27.6%	155.00 m/Working Period	4.19 m/day		
	Others	198°00'	30.6%	29.2%	155.00 m/Working Days	4.84 m/day		
	Sub Total	646°00'	100%	95.2%	155.00 m/Drilling Period	7.75 m/day		
	Removing	Preparation	16°00'	-	2.4%	155.00 m/Net Drilling Days	7.75 m/day	
		Moving	16°00'	-	2.4%	Total workers/ 155.00 m	4.25 Man/m	
	Grand Total	678°00'	-	100%	Total Drilling Workers/ 155.00m	3.34 Man/m		
Casing Pipe Inserted	Pipe Size & Meterage	Inserted Length (%) Drilling Length	Recovery of Casing Pipe		Hoisting & Lowering Rod	15 Times	Hoisting & Lowering I.T.	156 Times
	HW 6.00 m	3.9%	100%		Remarks			
	NW 9.00 m	5.8%	100%		I.T.: Inner Tube			
	BW 123.00 m	79.4%	100%					

Table III-5 Operational results of drill hole, DDH-2

Working Period	Period		Number of Days	Actual Working Days	Day Off	Total Number of Workers		
	Preparation	8th Oct.'80		1	1	-	75	
Drilling	9th Oct.'80 ~ 23th Oct.'80		15	15	-	319		
Removing	24th Oct.'80		1	1	-	36		
Total	8th Oct.'80 ~ 24th Oct.'80		17	17	-	430		
Drilling Length	Planned Length	250.00 m	Overburden	0.70 m	Core Recovery for each 100 m section			
	Increase or Decrease in Length	m	Core Length	206.60 m	Depth of Hole	Section	Total	
	Length Drilled	252.00 m	Core Recovery	82.0 %	0 ~ 100 m	95.7 %	95.7 %	
Working Time	Drilling	131°00'	25.8 %	25.2 %	100 ~ 200 m	82.6 %	89.5 %	
	Hoisting & Lowering Rod	14°00'	2.8 %	2.7 %				
	Hoisting & Lowering I.T.	63°00'	12.4 %	12.1 %	200 ~ 252 m	55.1 %	82.0 %	
	Miscellaneous	158°00'	31.1 %	30.3 %	Efficiency of Drilling			
	Repairing	6°00'	1.2 %	1.2 %	252.00 m/Working Period		14.8 m/day	
	Others	136°00'	26.7 %	26.2 %	252.00 m/Working Days		14.8 m/day	
	Sub Total	508°00'	100 %	97.7 %	252.00 m/Drilling Period		16.8 m/day	
	Removing	Preparation	12°00'	-	2.3 %	252.00 m/Net Drilling Days		16.8 m/day
		Moving	-	-	- %	Total workers/	252.00 m	1.71 Man/m
	Grand Total	520°00'	-	100 %	Total Drilling Workers/ 252.00 m		1.27 Man/m	
Casing Pipe Inserted	Pipe Size & Meterage	Inserted Length (%) Drilling Length	Recovery of Casing Pipe		Hoisting & Lowering Rod	9 Times	Hoisting & Lowering I.T.	252 Times
	HW 3.10 m	1.2 %	100 %		Remarks			
	NW 30.50 m	12.1 %	100 %		I.T.: Inner Tube			
	BW 125.60 m	49.8 %	100 %					

Table III-6 Operational results of drill hole, DDH-3

Working Period	Period			Number of Days	Actual Working Days	Day Off	Total Number of Workers	
Preparation	4th Aug.'80 ~ 19th Aug.'80			16	16	-	170	
Drilling	20th Aug.'80 ~ 9th Sep.'80			21	21	-	416	
Removing, Log.	10th Sep.'80 ~ 12th Sep.'80			3	3	-	55	
Total	4th Aug.'80 ~ 12th Sep.'80			40	40	-	641	
Drilling Length	Planned Length	150.00 m	Overburden	0.90 m	Core Recovery for each 100 m section			
	Increase or Decrease in Length		Core Length	145.85 m	Depth of Hole	Section	Total	
	Length Drilled	157.00 m	Core Recovery	93.3 %	0 ~ 100 m	92.5 %	92.5 %	
Working Time	Drilling	83°00'	17.1 %	12.5 %	100 ~ 157 m	94.2 %	93.3 %	
	Hoisting & Lowering Rod	12°00'	2.5 %	1.8 %				
	Hoisting & Lowering I.T.	89°00'	18.4 %	13.4 %				
	Miscellaneous	118°00'	24.3 %	17.8 %	Efficiency of Drilling			
	Repairing	3°00'	0.6 %	0.5 %	157.00 m/Working Period	3.93 m/day		
	Others	180°00'	37.1 %	27.1 %	157.00 m/Working Days	3.93 m/day		
	Sub Total	485°00'	100 %	73.1 %	157.00 m/Drilling Period	7.48 m/day		
	Removing	Preparation	76°00'	-	11.5 %	157.00 m/Net Drilling Days	7.48 m/day	
		Moving	102°00'	-	15.4 %	Total workers/ 157.00 m	4.08 Man/m	
	Grand Total	663°00'	-	100 %	Total Drilling Workers/ 157.00 m			2.64 Man/m
Casing Pipe Inserted	Pipe Size & Meterage	Inserted Length (%)	Recovery of Casing Pipe		Hoisting & Lowering Rod	Hoisting & Lowering I.T.		
	HW 3.10 m	2.0 %	100 %		8 Times	178 Times		
	NW 30.10 m	19.2 %	100 %		Remarks			
	BW 63.60 m	40.5 %	100 %		I.T.: Inner Tube			

Table III-8 Working time of each drill hole

Drill hole No.	Drilling	Hoisting & lowering of rod & I.T.		Miscellaneous			Repairs	Others	Moving operation	Total
		Rod	Inner tube	Casing insertion	Hole reaming	Others				
DDH-1	107°00'	7°30'	40°00'	29°00'	-	76°30'	188°00'	198°00'	32°00'	678°00'
DDH-2	131°00'	14°00'	63°00'	17°00'	-	141°00'	6°00'	136°00'	12°00'	520°00'
DDH-3	83°00'	12°00'	89°00'	24°00'	12°00'	82°00'	3°00'	180°00'	178°00'	663°00'
Total	321°00'	33°30'	192°00'	70°00'	12°00'	299°30'	197°00'	514°00'	222°00'	1,861°00'
					381°30'					

Table III-9 Drilling meterage of diamond bits

Item	Size	Type	Bit No.	Drilling meterage by drill hole. Unit meter			Total
				DDH-1	DDH-2	DDH-3	
Bit	HX	HQ-WL	E-1959			26.50	26.50
			E-2802		27.40		27.40
			C-8057	5.00			5.00
			Total	5.00	27.40	26.50	58.90
	NX	NQ-WL	OT-1			47.20	47.20
			OT-2			46.30	46.30
			J-1466	59.00			59.00
			J-1467	56.70			56.70
			18782		38.60		38.60
			18783		42.20		42.20
			18784		10.70		10.70
			Total	115.70	91.50	93.50	300.70
	BX	BQ-WL	OT-3			21.50	21.50
			OT-4			12.40	12.40
			OT-5	15.00			15.00
			J-1471	15.30			15.30
			J-1477		40.50		40.50
			J-1480		46.70		46.70
			873456		42.80		42.80
			Total	30.30	130.00	33.90	194.20

Table III-10 Specifications of diamond bits

Size	Type	Carats per bit	Matrix	Stones per carat	Water way	Number	Remark
HX	HQ-WL	40	T ₁		6	E-1959	Reset
		"	Z		6	E-2802	"
		"	Z		6	C-8057	"
NX	NQ-WL	30	T ₁		4	OT-1	Reset
		30	T ₁		4	OT-2	"
		30	Y		4	J-1466	"
		30	Z		4	J-1467	"
		30	E		4	18782	"
		30	E		4	18783	"
		30	E		4	18784	"
BX	BQ-WL	20	T ₁		4	OT-3	Reset
		20	T ₁		4	OT-4	"
		20	T ₁		4	OT-5	"
		20	Y		4	J-1471	"
		20	Z		4	J-1477	"
		20	Z		4	J-1480	"
		20	E		4	873456	"

Chapter 3 Geology and Mineralization of the Drill Holes

3-1 DDH-1

(1) Purpose: This drilling was made to identify possible downward extension of black gossan which has a high zinc grade. The drilling site was decided at the widest and richest part of the gossan.

(2) Location: The drilling site is about 200 m south of the Cumbre de Iscay Cruz. The altitude is 4,643.3 m. It was drilled to 80° with inclination of -50° and was completed down to 155 m. Two layers of the black gossan, 22 m and 5 m wide, are exposed at the surface site of this drill hole. The following assay values were obtained from the two layers.

	Ag (g/t)	Cu (ppm)	Pb (%)	Zn (%)
Footwall side one	tr	27	0.50	5.00
Hanging wall one	4	27	0.21	4.61

(3) Geology: The first recovered rock was seen at 4.3 m. The drill cores between 4.3 and 29.7 m are of Carhuaz formation which consists mainly of slaty shale intercalated with calcareous shale, sandstone and limestone. These rocks are pervasively argillized, silicified and pyrite disseminated.

From 29.7 m to the bottom is Santa formation of silicified carbonate rocks, which consist of siderite bed, silicified shale, and silicified and dolomitized marlstone. Limestone is expected, but is not seen due probably to remobilization of the calcium carbonate during the alterations.

Siderite bed is greyish in color and fine and crystalline in texture. It is brecciated and disseminated with galena and sphalerite. The fractures are filled with veinlets of white siderite (cf., CB-01-061, Table III-13). The siderite bed has sometimes brownish black color. The marlstone is grey and massive; the shale is black and slaty. Both the rocks are disseminated with pyrite.

The drilling seems to penetrate sheared zone from 113.8 m downwards, and only sludge core was obtained. Although it is difficult to identify the original rocks by drilling tips, oxidized and argillized siderite bed and dolostone are the main constituents. It is inferred that lower part of the Santa formation is sheared, thus the drilling is close to Chimu formation.

(4) Mineralization and ore grade: Dissemination of pyrite is seen all through the drill hole, and is particularly prominent in strongly silicified shale. When fine-grained pyrite is densely disseminated, the rock shows dark and spotty pattern.

Ore minerals of the siderite bed in the Santa formation are too fine to identify them with naked eyes. X-ray diffraction (c.f., CB-01-032, CB-01-057, Table III-13) indicates that the minerals are sphalerite and galena. Assay results on series of samples at two main mineralized horizons are as follows:

Depth (m)	Interval (m)	Number of samples	Ag(g/t)	Cu(%)	Pb(%)	Zn(%)
49.0-63.2	14.2	14	10	0.01	0.65	3.48
67.0-78.7	11.6	7	8	0.01	0.58	4.18

(5) Evaluation: It was identified by X-ray diffraction that host rock of the main mineralized parts is silicified siderite mass (c.f. CB-01-032, CB-01-057, Table III-13). The siderite peaks are however shifted to the low angles side. This is characteristic of manganiferous siderite and is confirmed also by chemical analysis (c.f. CB-01-032, CB-01-061, Table III-12). The chemical analysis indicates that molecular ratio of Mn:Fe is about 40:60.

It is concluded that black gossan at the surface is oxidized manganiferous siderite mass, so that it has been stained with Mn-oxides. The mineralization in the siderite mass is low grade but is large in quantity; thus has significant potentiality as future mineral resource and should be

considered carefully in future exploration. Thickness of the Santa formation had not been known because of terrace covers, but it is now identified to have about 80 m (c.f. Fig. III-4).

3-2 DDH-2

- (1) Purpose: This hole was drilled to explore downward extension of DDH-1.
- (2) Location: The same as DDH-1. The direction is 80°; the inclination is -75°. The depth is 252 m.
- (3) Geology: No coring up to 3.8 m. From 3.8 to 52.9 m, it is Carhuaz formation. This formation is composed of slaty shale with intercalated limestone, sandstone and dolostone. Pyrite disseminates throughout the rocks. Andesitic porphyry appears at 30 m.

From 52.9 m to the bottom, it is Santa formation. This formation consists of calcareous shale and marlstone with intercalated limestone and siderite bed down to 107.9 m. Pyrite is disseminated all through the rocks. From 107.9 m downwards, siderite prevails and is alternated with limestone, tuffaceous siltstone and shale. The siderite mass contains very fine-grained disseminated grains of galena and sphalerite.

From 200 m downwards, the drill hole may have cut through sheared zone, because of the poor core-recovery. But this part may also be composed of siderite and alternated marlstone and shale.

- (4) Mineralization and ore grade: Like the cores of DDH-1, rocks from this hole are disseminated with pyrite. Lead and zinc are seen in brecciated siderite mass. Assays of the main mineralized parts are shown as follows:

Depth (m)	Interval(m)	Number of samples	Ag(g/t)	Cu(%)	Pb(%)	Zn(%)
107.9-121.0	13.1	5	3	0.01	0.09	4.37
124.9-130.8	5.9	2	6	0.02	0.19	4.51
220.9-231.7	10.8	5	5	0.01	1.06	4.46
240.5-252.0	11.3	5	3	0.01	0.73	4.92

(5) Evaluation: The main mineralization is seen in the upper part of the Santa formation which is 20 to 40 m below the bottom of the Carhuaz formation. This mode of occurrence is somewhat different from that on the surface gossan. Lead-zinc mineralization in the siderite mass is controlled by bedding of the Santa formation, thus elongates in a north-south direction but is irregular locally. Genesis of the siderite mass is beyond the scope of this report. However, it is considered that, besides the original sedimentary accumulation, diagenetic processes and later hydrothermal alterations are responsible for the formation of the siderite mass.

3-3 DDH-3

(1) Purpose: This drilling was aimed at massive sulfide orebody that may exist underground. Thus it is located at northern fringe of distinct FE (frequency effect) and AR (apparent resistivity) anomalies. At surface, massive pyrite orebody accompanying galena crops out about 250 m at north of this drill hole.

(2) Location: About 400 m north of Cumbre de Limpe at 4,694.5 m above sea level. The direction is 60°, the inclination is -48°. The total length is 157 m. Small outcrop of sandstone and shale of Carhuaz formation was selected to start with the drilling, in order to avoid to pass through thick Quaternary sediments.

(3) Geology: From 0.9 to 92.1 m, present is Carhuaz formation, which consists mainly of black shale and subordinate amount of calcareous sandstone, limestone and red shale. The shale is pervasively silicified and is disseminated with pyrite.

Santa formation is seen from 92.1 m to the bottom. The bottom may be close to Chimu formation, because the rocks are sheared. The Santa formation is composed of limestone and marlstone with some amount of dolostone

and shale. The orebody was found between 104.6 m and 118.9 m. This 14.3 m thick orebody is massive aggregates of pyrite and pyrrhotite accompanying disseminated galena and sphalerite (cf. Fig. III-5).

(4) Mineralization and ore grade: Series of samples taken from the orebody give the following assay results:

Depth (m)	Interval (m)	No. of Sample	Ag (g/t)	Cu (%)	Pb (%)	Zn (%)	Fe (%)	S (%)
104.6-108.6 (high grade part)	4.0	4	89	0.03	6.74	14.17	30.47	32.86
108.6-116.8 (low grade part)	8.2	8	30	0.02	1.32	2.53	51.02	35.75
116.8-118.9 (intermediate grade part)	2.1	2	41	0.02	1.02	12.48	17.90	22.72
104.6-118.9 (total)	14.3	14	48	0.02	2.76	7.24	40.41	33.03

As is shown in the percentages of Fe and S, this orebody is rich in pyrite and pyrrhotite. If pyrrhotite/pyrite ratio increases, the grade of lead and zinc decreases. The highest content of lead and zinc is seen in porous and brecciated portion of the pyrite orebody.

This orebody occurs to replace the Santa calcareous rocks. Silicification and dolomitization are intense at margin of the orebody (cf. CB-03-100, CB-03-121, Table III-13). Gangue minerals are mainly siderite. Quartz and sericite are also seen (cf. CB-03-105, 107, 110, 114, Table III-13).

(5) Interpretation: Since this drill hole did not reach quartzite of Chimu formation, thickness of Santa formation is not known. However, the thickness is assumed to be about 50 m, for the general geologic structure in the area and measurement of bedding plane in the drill hole. The thickness is about 60 m at the Cumbre de Limpe, which is about 400 m to the south of the drill hole site. Although two layers of the gossan were observed at the Cumbre de Limpe, orebody was one layer in this drill hole.

3-4 Evaluation of the Mineralization

The massive sulfide orebody discovered by DDH-3 and lead-zinc dissemination found by DDH-1 and 2 are different in degree of concentration of the ore minerals. However, siderite and quartz seen in a low grade part of the massive sulfide orebody are the same as gangue minerals of the lead-zinc disseminated ore deposits. Both types are also similar in wall-rock alterations and brecciation of the host rocks. Thus the two types are considered to have similar genetic history. The lead-zinc disseminated siderite deposits tend to occur at fringe of the massive sulfide orebody.

The siderite may have been formed by diagenetic processes. Besides the sideritization and silicification, wall rock and horse stone in the massive sulfide orebody are free of intense alterations. Thus, a possibility of submarine-hydrothermal sedimentary genesis cannot be ruled out on the massive sulfide orebody, although no volcanic rocks were observed in the Santa formation, except for some acidic dikes.

Ore microscopy was made on ores from the massive sulfide orebody. Pyrite is strongly brecciated. Sphalerite and galena fill up the fractures and encircle the pyrite (cf. CB-03-118 etc). Pyrite is corroded and replaced and encircled by pyrrhotite (cf. CB-03-113). Pyrrhotite includes sphalerite and sometimes replace sphalerite (cf. CB-03-115). These textures of the ore minerals differ clearly from those of skarn ore deposits such as Chupa deposit.

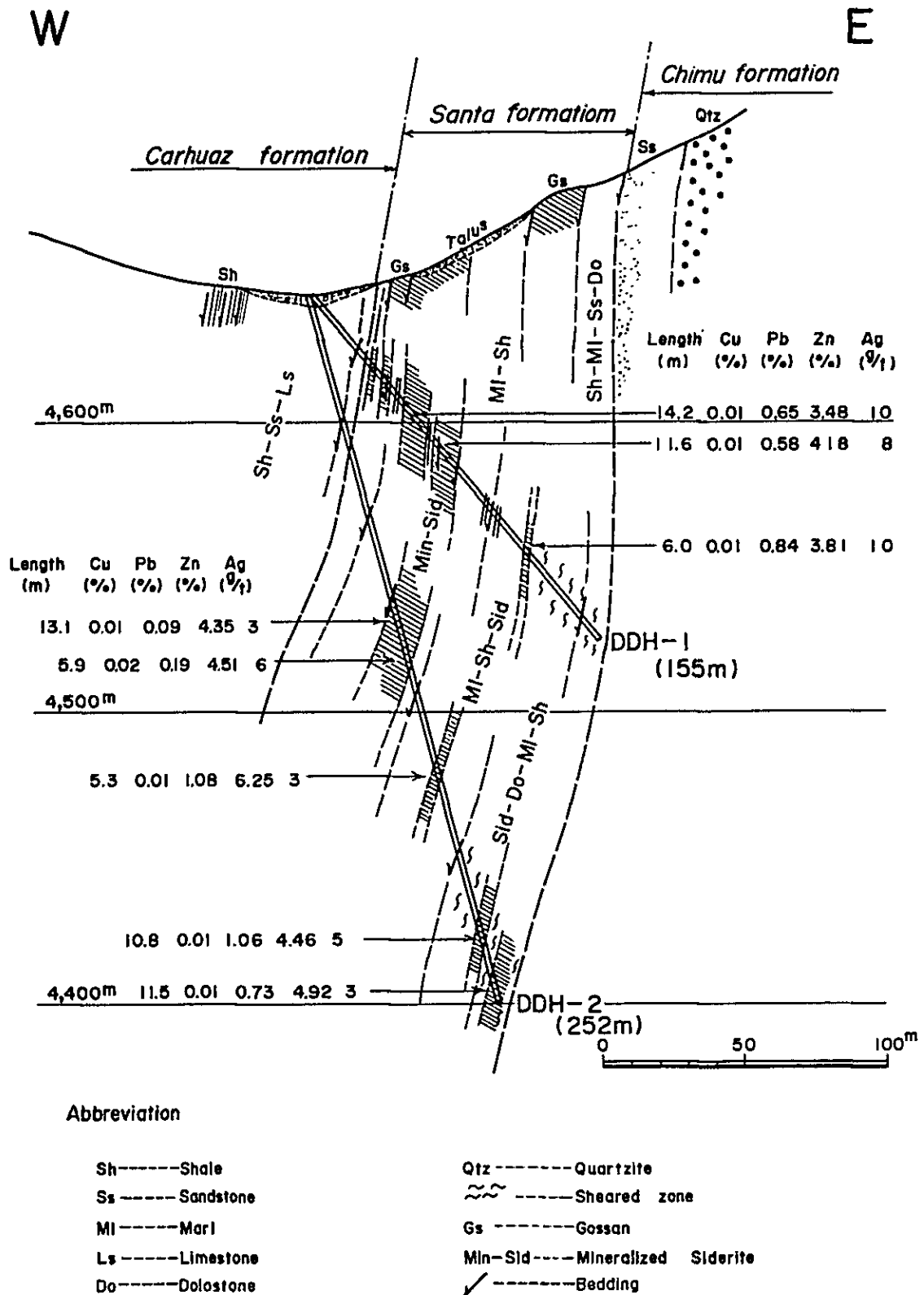
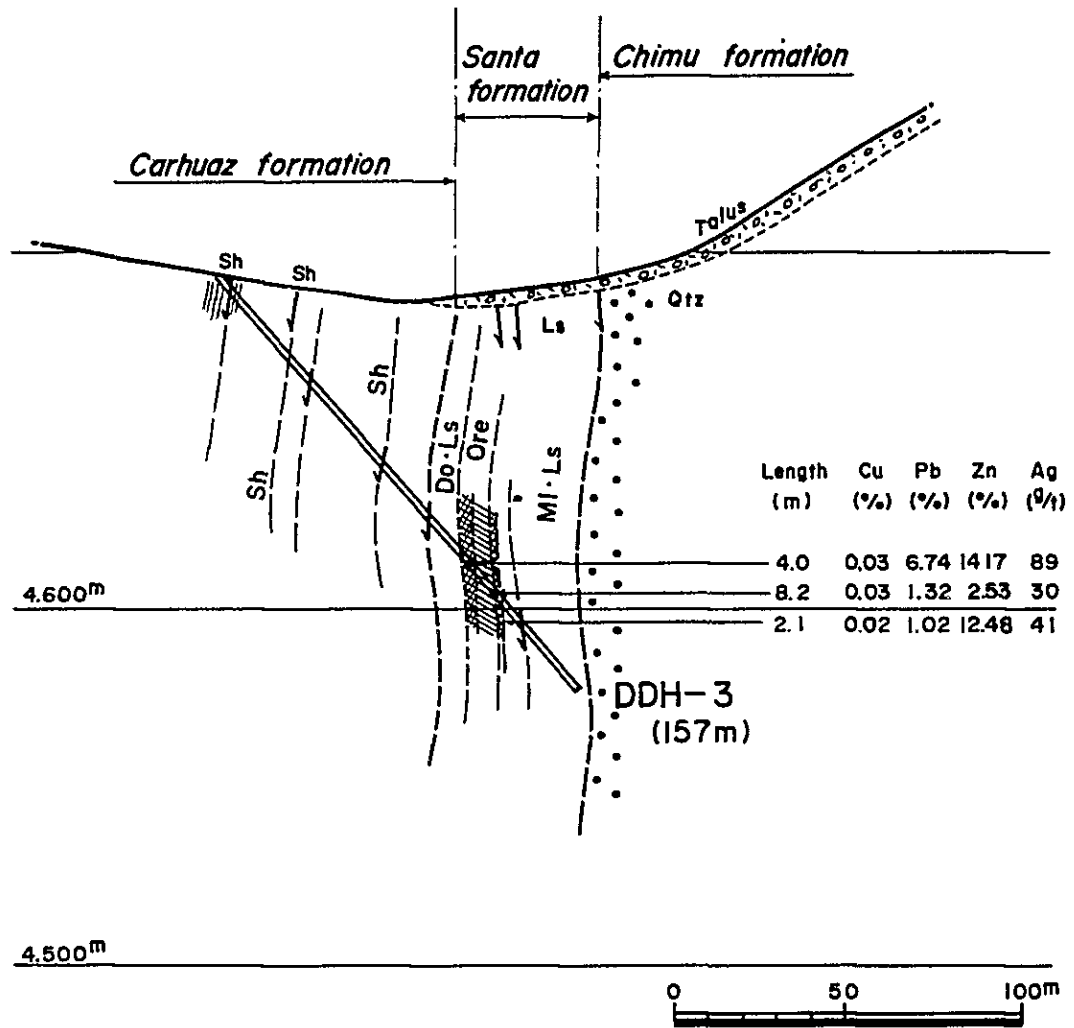


Fig. III-4. Geological Section for DDH-1 and DDH-2 (S80°W — N80°E)

WSW

ENE



Abbreviation

- Sh-----Shale
- MI-----Marl
- Ls-----Limestone
- Do-----Dolostone
- Qtz-----Quartzite
- High grade ore
- Low grade ore
- Bedding

Fig. III-5. Geological Section for DDH-3 (S60°W - N60°E)

Table III-11 Assay results of the drilled core

(1)

No.	Sample No.	Depth (m)	Rock Type	Cu (%)	Pb (%)	Zn (%)	Ag (g/t)	Fe (%)	S (%)
1	CB-01-031	29.7~31.1	Sid	0.006	2.50	7.05	10	21.59	2.43
2	CB-01-032	31.1~32.5	Sid	0.005	1.60	5.40	5	19.38	0.48
3	CB-01-039	38.1~39.3	Sid	0.008	1.20	6.25	7	8.53	0.76
4	CB-01-040	39.3~41.2	Sid	0.012	2.20	6.15	12	9.75	3.24
5	CB-01-050	49.0~50.0	Sid	0.014	2.00	4.80	26	-	-
6	CB-01-051	50.0~51.0	Sid	0.008	0.24	0.85	10	-	-
7	CB-01-052	51.0~52.0	Sid	0.007	0.61	2.80	3	-	-
8	CB-01-053	52.0~53.0	Sid	0.007	0.95	3.40	15	-	-
9	CB-01-054	53.0~54.0	Sid	0.005	0.72	4.70	7	-	-
10	CB-01-055	54.0~55.0	Sid	0.005	0.40	4.20	5	-	-
11	CB-01-056	55.0~56.0	Sid	0.006	0.42	2.60	7	-	-
12	CB-01-057	56.0~57.0	Sid	0.008	0.60	2.70	10	-	-
13	CB-01-058	57.0~58.0	Sid	0.008	0.92	2.00	9	-	-
14	CB-01-059	58.0~59.0	Sid	0.007	0.86	4.00	6	-	-
15	CB-01-060	59.0~60.0	Sid	0.006	0.28	3.50	5	-	-
16	CB-01-061	60.0~61.0	Sid	0.008	0.29	4.20	8	-	-
17	CB-01-062	61.0~62.0	Sid	0.005	0.35	3.40	2	-	-
18	CB-01-063	62.0~63.2	Sid	0.009	0.48	5.20	27	-	-

(2)

No.	Sample No.	Depth (m)	Rock Type	Cu (%)	Pb (%)	Zn (%)	Ag (g/t)	Fe (%)	S (%)
19	CB-01-068	67.0~68.5	Sid	0.007	0.13	4.10	7	-	-
20	CB-01-069	68.5~70.0	Sid	0.005	0.10	3.80	2	-	-
21	CB-01-071	70.0~72.0	Sid	0.006	0.20	6.40	16	-	-
22	CB-01-073	72.0~73.9	Sid	0.004	0.31	3.40	6	-	-
23	CB-01-075	73.9~75.8	Sid	0.005	0.73	4.00	9	-	-
24	CB-01-077	76.3~77.5	Sid	0.006	2.50	5.40	9	-	-
25	CB-01-078	77.5~78.7	Sid	0.015	0.40	1.60	8	-	-
26	CB-01-097	95.8~97.7	Sid	0.005	0.45	3.00	8	-	-
27	CB-01-112	111.6~112.7	Sid	0.006	0.58	3.00	4	-	-
28	CB-01-113	112.7~113.8	Sid	0.008	0.75	3.60	10	-	-
29	CB-01-114	113.8~117.2	Sid	0.010	0.98	4.20	13	-	-
30	CB-01-151	149.8~151.4	Sid	0.007	0.34	1.60	18	-	-
31	CB-01-152	151.4~155.0	Sid	0.025	0.42	13.98	59	-	-
32	CB-02-111	107.9~111.0	Sid	0.01	0.11	4.48	1	-	-
33	CB-02-114	111.0~114.0	Sid	0.01	0.07	4.30	2	-	-
34	CB-02-117	114.0~117.0	Sid	0.01	0.10	3.88	2	-	-
35	CB-02-119	117.0~119.0	Sid	0.01	0.11	4.60	2	-	-
36	CB-02-121	119.0~121.0	Sid	0.01	0.06	4.70	7	-	-

(3)

No.	Sample No.	Depth (m)	Rock Type	Cu (%)	Pb (%)	Zn (%)	Ag (g/t)	Fe (%)	S (%)
37	CB-02-127	124.8~127.7	Sid	0.03	0.08	4.20	2	-	-
38	CB-02-130	127.7~130.7	Sid	0.02	0.30	4.80	10	-	-
39	CB-02-148	144.7~148.3	Ls	0.02	0.22	1.50	2	-	-
40	CB-02-169	166.7~169.0	Sid	0.01	1.05	7.40	2	-	-
41	CB-02-172	169.0~172.0	Sid	0.01	1.10	5.36	3	-	-
42	CB-02-222	220.9~222.9	Sid	0.01	1.15	4.38	1	-	-
43	CB-02-224	222.9~224.9	Sid	0.02	0.70	4.39	2	-	-
44	CB-02-226	224.9~226.9	Sid	0.01	1.16	4.29	8	-	-
45	CB-02-228	226.9~228.9	Sid	0.02	1.38	4.80	8	-	-
46	CB-02-231	228.9~231.7	Sid	0.01	0.95	4.46	5	-	-
47	CB-02-241	240.5~243.0	Sid	0.01	0.79	4.26	3	-	-
48	CB-02-246	243.0~246.0	Sid	0.01	1.40	6.20	6	-	-
49	CB-02-248	246.0~248.0	Sid	0.02	0.62	4.90	2	-	-
50	CB-02-250	248.0~250.0	Sid	0.01	0.10	4.46	1	-	-
51	CB-02-252	250.0~252.0	Sid	0.01	0.39	4.29	1	-	-
52	CB-03-068	68.3~68.8	Sh	0.010	0.01	0.03	2	6.85	6.55
53	CB-03-098	98.0~98.5	Do	0.008	0.80	0.42	8	3.05	1.03
54	CB-03-103	103.0~103.8	M1	0.010	0.35	0.58	12	8.10	3.60

(4)

No.	Sample No.	Depth (m)	Rock Type	Cu (%)	Pb (%)	Zn (%)	Ag (g/t)	Fe (%)	S (%)
55	CB-03-104	103.8~104.6	Ore	0.009	1.85	2.30	27	11.30	5.53
56	CB-03-105	104.6~105.6	Ore	0.030	8.25	18.05	118	27.31	38.07
57	CB-03-106	105.6~106.6	Ore	0.042	11.00	16.36	95	17.17	37.44
58	CB-03-107	106.6~107.6	Ore	0.026	5.50	17.85	75	30.12	19.82
59	CB-03-108	107.6~108.6	Ore	0.023	2.20	4.40	68	47.29	36.12
60	CB-03-109	108.6~109.6	Ore	0.028	0.70	1.30	30	56.63	33.88
61	CB-03-110	109.6~110.6	Ore	0.024	1.10	2.10	28	54.82	37.72
62	CB-03-111	110.6~111.6	Ore	0.020	1.00	1.80	20	51.71	36.92
63	CB-03-112	111.6~112.6	Ore	0.014	1.65	3.60	32	46.69	34.43
64	CB-03-113	112.6~113.6	Ore	0.016	2.05	3.30	30	51.91	36.82
65	CB-03-114	113.6~114.6	Ore	0.093	2.10	2.70	32	44.48	31.36
66	CB-03-115	114.6~115.7	Ore	0.010	1.52	3.40	35	50.20	37.48
67	CB-03-116	115.7~116.8	Ore	0.012	0.50	2.00	30	51.71	37.09
68	CB-03-117	116.8~117.9	Ore	0.030	1.35	12.29	38	28.26	30.75
69	CB-03-118	117.9~118.9	Ore	0.008	0.65	12.69	45	6.50	13.89
70	CB-03-119	118.9~120.1	Do	0.012	0.07	1.75	4	4.45	3.63
71	CB-03-120	120.1~121.3	Do	0.008	0.55	2.50	6	5.65	21.27
72	CB-03-125	125.0~125.5	Ml	0.008	0.01	0.01	4	12.10	13.90

Ls --- Limestone, Sh --- Shale, Ml --- Marl, Do --- Dolostone, Sid --- Siderite

Table III-12 Assay results of rock forming elements in the drilled core

No.	Sample No.	Depth (m)	Rock Type	Ca (%)	Mn (%)	Fe (%)	Mg (%)	Ba (%)	Sr (%)	SiO ₂ (%)	Co (%)
1	CB-01-008	7.5-8.5	Ss	6.00	0.13	2.50	0.75	-	-	66.54	-
2	CB-01-032	31.1-32.5	Sid	1.05	12.70	19.48	1.23	-	-	19.43	-
3	CB-01-057	56.0-57.0	Sid	1.04	4.85	6.80	0.50	-	-	65.96	-
4	CB-01-061	60.0-61.0	Sid	1.35	16.20	26.40	0.48	-	-	3.54	-
5	CB-01-081	80.5-81.5	Ml	15.45	0.12	2.15	0.70	-	-	25.54	-
6	CB-01-151	149.8-151.4	Altered r.	0.11	0.03	0.80	0.01	-	-	75.95	-
7	CB-03-065	64.8-65.0	Ss	9.00	0.06	1.45	0.60	-	-	74.49	-
8	CB-03-086	85.8-86.0	Ss	7.00	0.13	6.25	0.72	-	-	59.78	-
9	CB-03-095	94.8-95.0	Ls	38.22	0.07	0.70	0.85	-	-	5.03	-
10	CB-03-100	99.8-100.0	Do	16.29	0.26	2.75	3.50	0.010	0.032	21.38	0.005
11	CB-03-105	104.8-105.0	Ore	0.37	0.17	2.45	0.18	-	-	76.82	-
12	CB-03-114	113.8-114.0	Ore	0.16	2.20	28.92	0.55	0.003	0.038	37.01	0.004
13	CB-03-121	120.8-121.0	Do	17.53	5.80	6.45	3.20	0.003	0.018	8.61	0.005
14	CB-03-124	123.8-124.0	Ls	20.49	0.09	0.90	3.50	-	-	22.41	-
15	CB-03-131	130.8-131.0	Sh	0.30	0.11	3.45	0.60	-	-	65.25	-
16	CB-03-139	138.8-139.0	Ls	30.90	0.07	1.10	1.25	0.010	0.050	11.67	0.007
17	CB-03-145	144.8-145.0	Ml	14.49	0.05	1.95	2.90	-	-	31.91	-
18	CB-03-153	152.8-153.0	Ls	23.29	0.09	1.40	3.75	0.007	0.058	14.70	0.004

Ss ---- Sandstone, Ml ---- Marl, Ls ---- Limestone, Do ---- Dolostone, Sid ---- Siderite, Sh ---- Shale

Table III-13 Summary of X-ray diffraction test in the drilled core

Sample No.	Mineral		Quartz	Calcite	Dolomite	Siderite	Fluorite	Gypsum	Kunahorite	Serpente	Chlorite	Kaolinite	Sphalerite	Galena	Pyrite	Pyrrhotite
	Rock Name															
CB-01-032	Siderite		⊙			⊙							○	○		
CB-01-057	Siderite		⊙			⊙						○	○	○		
CB-01-061	Siderite		○			⊙	●					●				
CB-01-151	Altered r.		⊙									⊙	○	○		
CB-03-100	Dolostone		⊙	●	⊙					●					●	
CB-03-105	Ore		⊙								⊙					
CB-03-107	Ore		○			⊙				○			⊙	⊙	○	
CB-03-110	Ore		●			○				●			○	○	○	⊙
CB-03-114	Siderite		⊙			⊙						○	●		●	
CB-03-121	Dolostone		○			○		○	⊙				○		○	

⊙ Very abundant ○ Common ● Very rare

⊙ Abundant ○ Rare

APPENDICES
PART I
GEOLOGICAL DATA

A. I - 1 List of geochemical samples

Index of Geological Units

Qt----- Quaternary
 Cs ---- Casapalca formation
 Cd ---- Celendin formation
 Jm ---- Jumasha formation
 Ph ---- Pariahuanca formation
 Cz ---- Carhuaz formation
 St ---- Santa formation
 Cm ---- Chimu formation
 Ig ---- Igneous rocks

Index of Analysis

G ---- Geochemical assay
 T ---- Thin section
 P ---- Polished section
 X ---- X-ray diffraction test
 E ---- EPMA (electron probe microanalysis)
 O ---- Assay of ore
 R ---- Complete analysis of rock
 D ---- Isotopic age determination
 M ---- Analysis of rock-forming elements

List of Geochemical Samples (1)

NO.	Sample NO.	Location	Geological Unit	Rock Name	G	T	P	X	E	O	R	D	M
1	NO-301	IC-5	St	Limestone	○								○
2	NO-302	IC-5	St	Crystalline limestone	○								
3	NO-303	IC-5	St	Gossan	○								
4	NO-304	IC-5	St	Ore (Zn, Py)		○		○		○			
5	NO-305	IC-5	St	Limestone									○
6	NO-306	IC-5	St	Green skarn (Py)		○				○			
7	NO-307	IC-5	St	Siderite ore (Zn, Py)						○			
8	NO-308	IC-5	St	Ore (Py, Zn, Cu)			○			○			
9	NO-309	IC-5	St	Oxide ore				○					
10	NO-310	IC-5	St	Limestone	○								○
11	NO-311	IC-5	Gm	Brecciated quartzite	○								
12	NO-312	G4	St	Gossan (Py, Cp)	○			○					
13	NO-313	G4	St	Altered rock	○			○					
14	NO-314	IC-4	St	Skarn (Py, Cp)		○				○			
15	NO-315	IC-4	St	Skarn (Py, Cp)		○				○			
16	NO-317	G4	St	Dolostone	○	○							
17	NO-319	G4	Ph	Limestone									○
18	NO-320	G4	St	Ore (Py, Zn, Pb, Cp)			○			○			
19	NO-321	G4	Jm	Limestone									○
20	NO-322	IC-5	St	Brecciated gossan				○					
21	NO-323	IC-5	St	Limestone									○
22	NO-324	IC-5	St	Gossan	○			○					

List of Geochemical Samples (2)

NO.	Sample NO.	Location	Geological Unit	Rock Name	G	T	P	X	E	O	R	D	M
23	NO-325	IC-5	St	Hematite gossan	○			○					
24	NO-329	G4	St	Limestone	○								○
25	NO-330	G4	St	Limestone	○								
26	NO-332	G4	Ig	Phylolite	○	○							
27	NO-333	G4	Cm	Gossan	○			○					
28	NO-334	G4	Ig	Altered rhyolite	○	○		○			○		
29	NO-335	G4	Cm	Quartzite	○								
30	NO-341	G4	Jm	Limestone	○								
31	NO-342	G4	Cz	Gossan						○			
32	NO-343	G4	Ig	Granite prophyry	○	○					○		
33	NO-345	G4	St	Limestone	○								
34	NO-346	G4	St	Skarn				○					
35	NO-347	G4	St	Siliceous limestone	○	○							
36	NO-350	G4	Ig	Granodiorite	○	○				○		○	
37	NO-351	G4	St	Gossan (Py)						○			
38	NO-352	G4	St	Skarn		○				○			
39	NO-361	G3	Jm	Stibnite ore			○						
40	NO-364	G4	Cd	Marl	○								
41	NO-367	G4	Cs	Red shale		○							
42	NO-368	G4	Ig	Granite porphyry		○							
43	NO-369	G4	Ph	Ore (Pb, Zn)			○			○			
44	NO-373	G4	Ig	Diorite		○						○	

List of Geochemical Samples (3)

NO.	Sample NO.	Location	Geological Unit	Rock Name	G	T	P	X	E	O	R	D	M
45	NO-374	G4	Ig	Granodiorite		○							
46	NO-375	G3	St	Limestone	○	○						○	
47	NO-376	G3	Ig	Granite porphyry									
48	NO-381	IC-1	St	Gossan		○		○					○
49	NO-382	IC-1	St	Gossan				○					
50	NO-383	IC-1	St	Gossan				○					
51	NO-384	IC-1	St	Gossan				○					
52	NO-385	IC-1	St	Siderite patch in Gs.				○					
53	NO-387	IC-1	St	Gossan with barite		○							
54	NO-388	IC-1	St	Dolostone				○					○
55	NO-389	IC-1	St	Gossan				○					
56	NO-392	IC-2	St	Dolostone									○
57	NO-394	IC-2	St	Calcite vein in Is.				○					
58	NO-395	IC-2	St	Quartz network in Do.				○					
59	NO-401	G4	Jm	Ore (Zn)		○		○		○			
60	NO-402	G4	Jm	Actinolite skarn (Zn)						○			
61	NO-403	G4	Jm	Epidote skarn (Pb, Zn)						○			
62	NO-404	G4	Jm	Garnet skarn						○			
63	NO-405	G4	Jm	Massive pyrite ore						○			
64	SO-206	G4	St	Limestone	○								
65	SO-208	G4	Ig	Rhyolite	○								
66	SO-215	G4	Ig	Quartz porphyry		○							

List of Geochemical Samples (4)

NO.	Sample NO.	Location	Geological Unit	Rock Name	G	T	P	X	E	O	R	D	M
67	SO-216	IC-4	St	Altered shale				○					
68	SO-217	G4	Jm	Limestone	○								
69	SO-218	G4	Ph	Limestone	○								
70	SO-219	G4	St	Limestone	○								
71	SO-220	G4	St	Limestone	○								
72	SO-221	G4	St	Limestone	○								
73	SO-222	G4	Ph	Limestone	○								
74	SO-223	G4	Ph	Limestone	○								
75	SO-224	G4	Ph	Limestone	○								
76	SO-226	G4	Ph	Limestone (skarn)						○			
77	SO-227	G4	Ig	Diorite	○								
78	SO-228	G4	St	Siliceous limestone						○			
79	SO-229	G4	Ph	Limestone	○								
80	TO-227	G4	Cz	Rhodochrosite (Pb, Zn)				○					
81	IC-501	IC-4	St	Gossan	○								
82	IC-502	IC-4	St	Gossan	○								
83	IC-503	IC-4	St	Gossan	○								
84	IC-504	IC-4	St	Gossan	○								
85	IC-505	IC-4	St	Gossan	○								
86	IC-506	IC-4	St	Gossan	○								
87	IC-507	IC-4	St	Gossan	○								
88	IC-508	IC-4	St	Gossan	○								

List of Geochemical Samples (5)

NO.	Sample NO.	Location	Geological Unit	Rock Name	G	T	P	X	E	O	R	D	M
89	IC-509	IC-4	St	Skarn	○								
90	IC-510	IC-4	Qt	Gossan (limonite)	○								
91	IC-511	IC-3	St	Gossan	○								
92	IC-512	IC-3	St	Gossan	○								
93	IC-514	IC-4	St	Gossan	○								
94	IC-515	IC-4	St	Gossan	○								
95	IC-516	IC-4	St	Gossan	○								
96	IC-517	IC-4	St	Gossan	○								
97	IC-518	IC-4	St	Gossan	○								
98	IC-519	IC-4	St	Gossan	○								
99	IC-520	IC-4	St	Gossan	○								
100	IC-601	IC-5	St	Gossan	○			○					
101	IC-602	IC-5	St	Gossan	○								
102	IC-603	IC-5	St	Gossan	○								
103	IC-604	IC-5	St	Gossan	○								
104	IC-605	IC-5	St	Gossan	○								
105	IC-606	IC-5	St	Gossan	○								
106	IC-607	IC-5	St	Gossan	○								
107	IC-608	IC-5	St	Gossan	○								
108	IC-609	IC-5	St	Gossan	○								
109	IC-610	IC-5	St	Gossan	○								
110	IC-611	IC-5	St	Gossan	○								

List of Geochemical Samples (6)

NO.	Sample NO.	Location	Geological Unit	Rock Name	G	T	P	X	E	O	R	D	M
111	IC-612	IC-5	St	Gossan	○								
112	IC-613	IC-5	St	Gossan	○								
113	IC-614	IC-5	St	Gossan	○								
114	IC-615	IC-5	St	Gossan	○								
115	IC-616	IC-5	St	Gossan	○								
116	IC-617	IC-5	St	Gossan	○								
117	IC-618	IC-5	St	Gossan	○								
118	IC-619	IC-5	St	Gossan	○								
119	IC-620	IC-5	St	Gossan	○			○					
120	IC-621	IC-5	St	Gossan	○								
121	IC-622	IC-5	St	Gossan	○								
122	IC-623	IC-5	St	Gossan	○								
123	IC-624	IC-5	St	Gossan	○								
124	IC-625	IC-5	St	Gossan	○								
125	IC-626	IC-5	St	Gossan	○								
126	IC-627	IC-5	St	Gossan	○								
127	IC-628	IC-5	St	Gossan	○								
128	IC-629	IC-5	St	Gossan	○								
129	IC-630	IC-5	St	Gossan	○								
130	IC-631	IC-5	St	Gossan	○								
131	IC-632	IC-4	St	Gossan	○								
132	IC-633	IC-5	St	Gossan	○								

List of Geochemical Samples (7)

NO.	Sample NO.	Location	Geological Unit	Rock Name	G	T	P	X	E	O	R	D	M
133	IC-634	IC-5	St	Gossan	○								
134	IC-635	IC-5	St	Gossan	○								
135	IC-636	IC-5	St	Gossan	○								
136	IC-637	IC-5	St	Gossan	○								
137	IC-638	IC-5	St	Gossan	○								
138	IC-639	IC-5	St	Gossan	○								
139	IC-640	IC-5	St	Gossan	○								
140	IC-641	IC-5	St	Gossan	○			○					
141	IC-642	IC-5	St	Gossan	○								
142	IC-643	IC-5	St	Gof an	○								
143	IC-644	IC-5	St	Gossan	○			○					
144	IC-645	IC-5	St	Gossan	○								
145	IC-646	IC-5	St	Gossan	○								
146	IC-647	IC-5	St	Gossan	○								
147	IC-648	IC-5	St	Gossan	○								
148	IC-649	IC-5	St	Gossan	○								
149	IC-650	IC-5	St	Gossan	○								
150	IC-651	IC-5	St	Gossan	○								
151	IC-652	IC-5	St	Gossan	○								
152	IC-653	IC-5	St	Gossan	○								
153	IC-654	IC-5	St	Gossan	○								
154	TP-201	G4	Ph	Ore (Zn, Pb)						○			

List of Geochemical Samples (8)

NO.	Sample NO.	Location	Geological Unit	Rock Name	G	T	P	X	E	O	R	D	M
155	TP-202	G4	Ph	Ore						○			
156	TP-203	G4	Ph	Ore (Zn)			○			○			
157	TP-204	G4	Ph	Ore (Zn)		○		○		○			
158	TP-205	G4	Ph	Ore						○			
159	TP-206	G4	Ph	Ore				○		○			
160	TP-207	G4	Ph	Ore (Zn)			○			○			
161	TP-208	G4	Ph	Ore (Zn)		○				○			
162	TP-209	G4	Ph	Ore (Zn)						○			
163	TP-210	G4	Ph	Ore (Zn)						○			
164	TP-211	G4	Ph	Ore (Zn, Py)			○			○			
165	TP-212	G4	Ph	Ore (Zn, Po)						○			
166	TP-213	G4	Ph	Ore (Zn)						○			
167	TP-214	G4	Ph	Ore (Zn, Po)						○			
168	TP-215	G4	Ph	Ore						○			

A. I-2 Microscopic observation of the thin sections

(1)

Sample No.	Rock Type	Microscopic Observation
NO-306	Silicified rock (St)	The rock is composed of quartz, chlorite and opaque minerals which are mainly pyrite, and shows clastic texture. Granular quartz is surrounded by chlorite and fine-grained felsic minerals. Opaque minerals occurs in dotted euhedral form.
NO-314	Skarnized limestone (St)	Quartz, carbonate, limonite, chlorite, apatite, zircon and opaque minerals are observed in this section. Quartz shows various grain size from 6 mm of single crystal to 0.05 mm in aggregate. Carbonate contains limonite and chlorite. Chlorite shows fibrous aggregates. Opaque minerals exist often with carbonates.
NO-315	Tremolite skarn (St)	Main constituent minerals are amphibole, carbonate, epidote, quartz and chlorite. Amphibole occurring in aggregated form is mostly altered to chlorite and carbonates. Epidote occurs together with amphibole. Coarse crystals of quartz are up to 3 mm in diameter and carbonate up to 2 mm contain subhedral amphibole and epidote grains. Apatite, limonite and opaque minerals are also observed.
NO-317	Dolostone (St)	The rock is composed of carbonates and talc, and shows granular texture. Carbonates of 0.05 ~ 0.2 mm grain size and needle-shaped talc of 0.05 mm size coexist.
NO-332	Altered rhyolite (Ig)	The rock is composed of fine-grained quartz and sericite. Their grain sizes are about 0.01 ~ 0.05 mm. Pseudomorphs of feldspar which has been completely replaced by sericite are observed in parts.
NO-334	Altered rhyolite (Ig)	This rock is composed of fine-grained quartz and pyrophyrite. Their grain sizes are about 0.02 mm.

Microscopic Observation of the Thin Sections

(2)

Sample No.	Rock Type	Microscopic Observation
NO-343	Granite porphyry (Ig)	<p>Porphyritic texture is seen. Main minerals are plagioclase, quartz, orthoclase and biotite. Phenocrystic euhedral plagioclase shows zonal structure and albite twinning. Quartz crystals are subhedral and up to 2 mm in size. Biotite is usually subhedral and brown to light yellow in color. Groundmass is composed of fine-grained plagioclase, quartz and orthoclase. Accessory minerals are apatite, zircon and opaque minerals.</p>
NO-347	Siliceous limestone (St)	<p>Clastic texture and microfolding are observed. Constituent minerals are quartz, opaque minerals, epidote, chlorite and glassy materials. Their grain sizes are very fine less than 0.1 mm. Veinlet of prehnite occurs in this section.</p>
NO-350	Granodiorite (Ig)	<p>Main constituent minerals are plagioclase, quartz, orthoclase, hornblend and biotite. Porphyritic texture is seen. Phenocrysts of plagioclase are up to 40 mm, which show zonal structure and albite twinning. Quartzs are up to 1.5 mm in size. Orthoclases, up to 4 mm, include plagioclase crystals. Hornblend is replaced by felsic minerals in parts. Biotite of brown and light yellow colors is partly altered to chlorite. Groundmass is composed of quartz and feldspar. Sphene, apatite and opaque minerals are observed as accessory minerals.</p>
NO-352	Garnet skarn (St)	<p>Garnet, carbonates and quartz are main minerals. Garnet of pale green shows anomalous anisotropism and banding structure in the margin. Garnet is weakly altered to chlorite in parts. Carbonates and quartz occur among euhedral garnets.</p>
NO-367	Red shale (Cs)	<p>The rock is composed of carbonates seemed to be dolomite and minor quartz. Carbonates occur as aggregate. Fine-grained limonite occurs in dotted-form.</p>

Microscopic Observation of the Thin Sections

(3)

Sample No.	Rock Type	Microscopic Observation
NO-368	Granite porphyry (Ig)	This rock is nearly same with the sample NO-343. However, the groundmass is coarser and alteration is stronger. Carbonitization of plagioclase and mafic minerals is characteristic.
NO-373	Diorite (Ig)	Plagioclase and hornblende are main minerals and porphyritic texture develops. Phenocrysts of plagioclase are subhedral up to 4 mm in size and show albite twinning. In the Groundmass plagioclase exists with minor amount of quartz and orthoclase. Feldspare are partly altered to sericite. Hornblende is mostly altered to chlorite. Epidote occurs in parts. Opaque minerals occur in dotted-form. Apatite and sphane are also observed.
NO-374	Granodiorite (Ig)	The rock shows granular texture composed of plagioclase, quartz, orthoclase and hornblende. Subhedral grains of plagioclase have albite twinning and contain mirmekitic quartz and orthoclase in the marginal parts. Quartz is anhedral and exists with orthoclase in intergraphic relation. Hornblende is strongly altered to chlorite accompanied with opaque minerals. Apatite and sphane are contained as accessory minerals.
NO-375	Limestone (St)	Main constituent minerals are carbonates with small amount of opaque minerals. Carbonates show very fine-grained, less than 0.01 mm making aggregates. Coarser grains of carbonates occur in dotted-form and veintets in parts.
NO-381	Black gossan (St)	Main minerals are opaque minerals seemed to be limonite and chalcedonic quartz.
NO-387	Barite in black gossan (St)	Aggregates of barite accompanied with opaque minerals which seems to be limonite are observed. Barite shows euhedral elongated crystals about 1 mm in length.

Microscopic Observation of the Thin Sections

(4)

Sample No.	Rock Type	Microscopic Observation
NO-401	Zn ore (Jm)	Sphalerite, chlorite, epidote and opaque minerals are main constituent minerals. In sphalerite, zonal structure is observed showing various colors from colorless to dark brown. Anhedral epidote exists with chlorite.
SO-215	Altered quartz porphyry (Ig)	Typical porphyritic texture develops in this rock. Quartz and pseudomorph of feldspar which is completely altered to sericite are occasionally observed as phenocrysts. Groundmass is composed of fine-grained feldspar, quartz, sericite and a small amount of chlorite.
TP-204	Zn ore (Ph)	Sphalerite, chlorite, quartz, carbonates and opaque minerals are recognized in this section. Brownish sphalerite is sometimes enclosed by quartz grains. Chlorite and carbonates coexist closely.
TP-208	Tremolite skarn (Ph)	The rock is tremolite-epidote skarn. Subhedral tremolite shows elongated up to 3 mm in length and also fibrous in parts, and pale green to colorless. Reddish sphalerite and opaque minerals occur in parts. Minor amount of quartz and carbonates is also observed.

A. I-3 Microscopic observation of the polished sections (1)

Sample No.	Rock Type	Microscopic Observation
NO-304	Zn-pyrite ore (St)	<p>This is composed of sphalerite, hematite, magnetite, pyrite and minor amount of galena and chalcopyrite. Very small inclusions of chalcopyrite can be seen in sphalerite of large euhedral crystals. Galena is minor amount and occurs in coexisting with sphalerite and pyrite.</p>
NO-308	Zn-pyrite ore (St)	<p>Constituent minerals are pyrite, sphalerite, galena and chalcopyrite. Sphalerite shows euhedral to subhedral, up to 2 mm, and contains many exsolution bodies of chalcopyrite and a minor amount of galena. On the other hand, pyrite of euhedral crystals contains a small amount of inclusions of sphalerite and galena.</p>
NO-314	Pyrite ore (St)	<p>This is mainly composed of iron oxides, magnetite and hematite. Sulfide minerals can't be seen. Magnetite shows medium-grained granular crystals, up to 0.3 mm across, sometimes forming aggregates. Hematite shows acicular, up to 0.2 mm across, and occurs in coexisting with magnetite.</p>
NO-320	Pb-Zn pyrite ore (St)	<p>It is mainly composed of pyrrhotite, pyrite and marcasite, with subordinate amount of sphalerite and galena. Pyrrhotite is almost replaced by marcasite which partly produce so called "bird's eye" texture. Marcasite shows colloform texture and forms alternating layers with pyrite. Sphalerite shows subhedral to euhedral and occurs in coexisting with pyrrhotite and marcasite.</p>
NO-361	Stibnite ore (Jm)	<p>There is a minor amount of ore minerals in this sample. It is composed of pyrite and pyrrhotite, with subordinate amount of chalcopyrite. Pyrite and Pyrrhotite show very fine-grained size, up to 0.05 mm</p>

Microscopic Observation of the Polished Sections

(2)

Sample No.	Rock Type	Microscopic Observation
NO-361 (Cont.)	Ag-Pb-Zn ore (Ph)	across, and are scattered in gangue minerals. Sphalerite and galena can not be seen in this section.
NO-369	Ag-Pb-Zn ore (Ph)	<p>It is mainly composed of pyrite and galena, with subordinate sphalerite and chalcopyrite.</p> <p>Galena shows euhedral to subhedral forms and contains a minor amount of two unknown minerals in the large crystal.</p> <p>In reflected light one is pale greenish grey and shows distinct anisotropy. The other is grey to brownish grey in reflected light, but the anisotropy is not present.</p> <p>Sphalerite contains many inclusions and blebs of pyrite and galena, and is partly replaced by galena. There is a small amount of chalcopyrite.</p>
NO-401	Ag-Pb-Zn ore (Jm)	<p>Main constituent minerals are sphalerite, galena and pyrite with accessory chalcopyrite.</p> <p>Sphalerite shows large crystals and contains a little exsolution bodies of chalcopyrite.</p> <p>Subhedral to anhedral galena is embedded in coexisting with sphalerite and pyrite.</p>
NO-402	Pb-Zn ore (Jm)	<p>It is mainly composed of sphalerite and galena, with subordinate amount of pyrite and chalcopyrite.</p> <p>Sphalerite after forming large crystals contains exsolution bodies of chalcopyrite and occurs in coexisting with galena, chalcopyrite and pyrite. Galena commonly show euhedral to subhedral forms and is partly embedded in large crystals of pyrite.</p>
TP-203	Zn-magnetite ore (Ph)	<p>It is mainly composed of sphalerite and magnetite, accompanied with pyrrhotite, chalcopyrite and pyrite. Large crystals of sphalerite enclose many medium-grained magnetite in euhedral granular crystals and also contain exsolution bodies of chalcopyrite and pyrrhotite.</p> <p>Pyrite is partly replaced by marcasite.</p>

Microscopic Observation of the Polished Sections (3)

Sample No.	Rock Type	Microscopic Observation
TO-203 (Cont.)		<p>There is a minor amount of unknown mineral like galena, which shows strong anisotropy. It seems to be a kind of Pb-Bi-S minerals.</p>
TP-207	Zn ore (Ph)	<p>It is mainly composed of sphalerite and pyrite, with subordinate amount of pyrrhotite and chalcopyrite. Sphalerite contains a lot of exsolution bodies of pyrrhotite and chalcopyrite. Pyrrhotite and pyrite are mostly replaced by marcasite, and marcasite partly produce so called "bird's eye" texture. There is a minor amount of unknown minerals like to be Pb-Bi-S minerals.</p>
TP-211	Zn pyrite ore (Ph)	<p>It is mainly composed of pyrite, sphalerite and chalcopyrite, with subordinate amount of pyrrhotite and galena. Coarse grained sphalerite contains exsolution bodies, partly orientated, of chalcopyrite, pyrrhotite and pyrite. A small amount of chalcopyrite veinlets is embedded in sphalerite. Pyrite is weakly replaced by marcasite.</p>

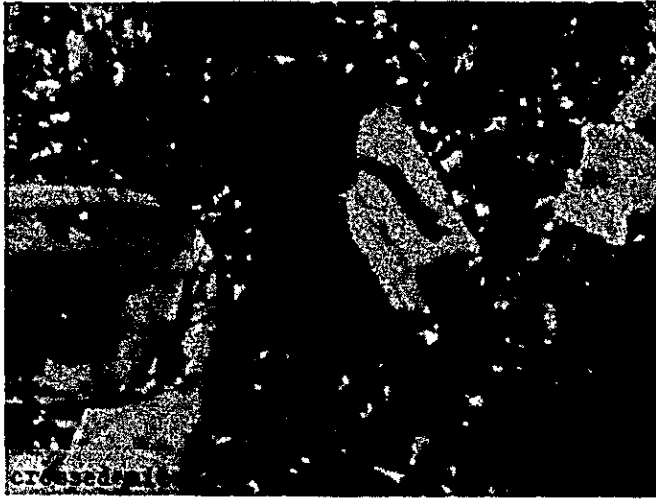
A. I-4 Photomicrographs of rock and ore samples

A. I-4-1 Thin section

Sample No.	Location	Geological Unit	Rock Type
NO - 343	G 4	Ig	Granite porphyry
NO - 350	G 4	Ig	Granodiorite
NO - 373	G 4	Ig	Diorite
NO - 387	IC - 1	St	Barite in black gossan
SO - 215	G 4	Ig	Altered quartz porphyry
TP - 208	G 4	Ph	Tremolite skarn

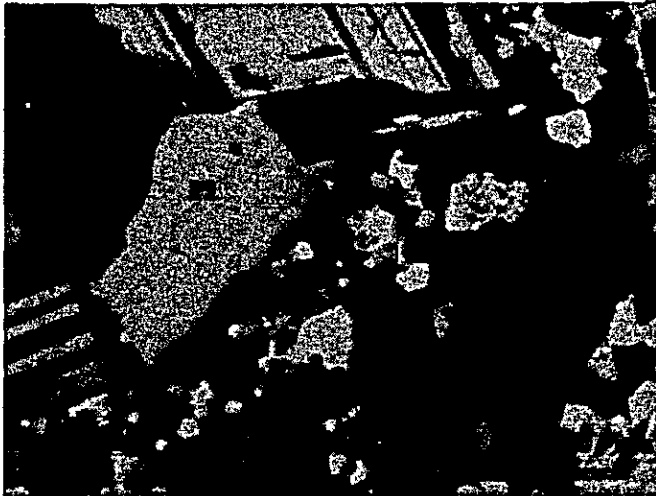
Abbreviations

Qt : Quartz
 Pl : Plagioclase
 Bt : Biotite
 Hb : Hornblende
 Ep : Epidote
 Ba : Barite
 Tr : Tremolite
 Ser : Sericite
 Cal : Calcite



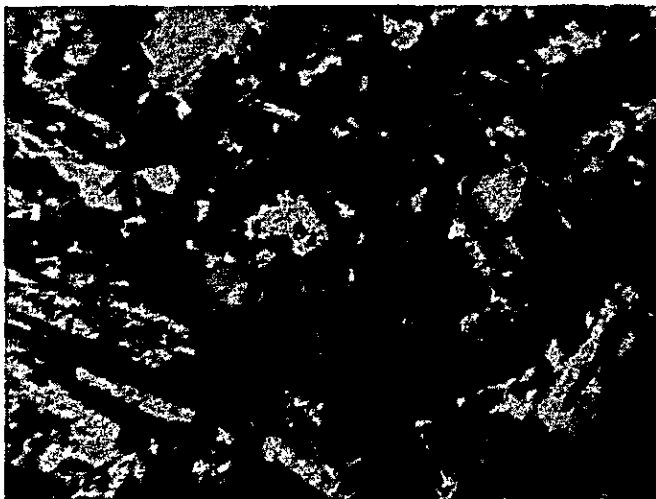
Sample No. NO-343

Rock Type: Granite porphyry



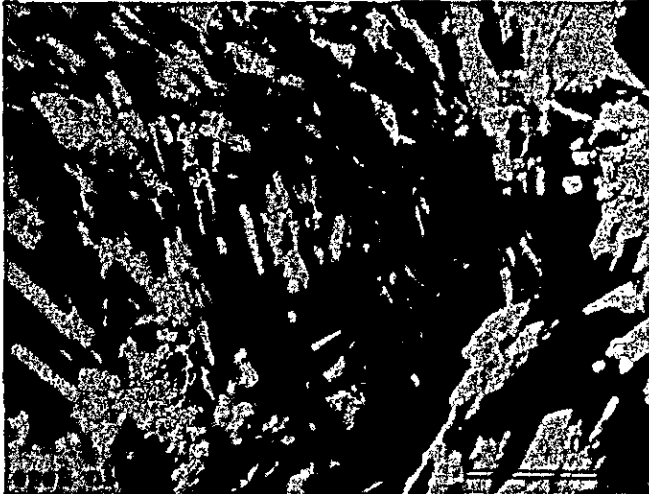
Sample No. NO-350

Rock Type: Granodiorite



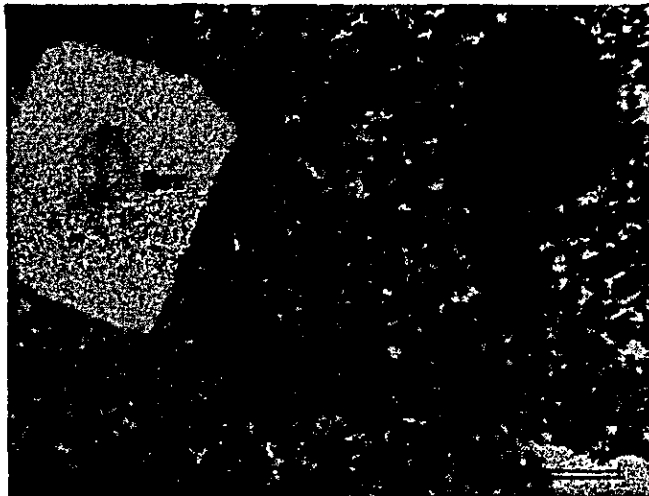
Sample No. NO-373

Rock Type: Diorite



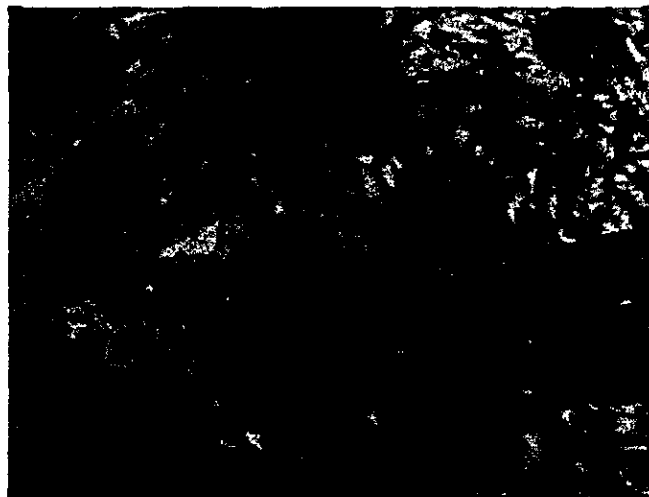
Sample No. NO-387

Rock Type: Barite in
black gossan



Sample No. SO-215

Rock Type: Altered
quartz porphyry



Sample No. TP-208

Rock Type: Tremolite skarn

A. I-4-2 Polished section

Sample No.	Location	Geological Unit	Rock Type
NO - 304	G 4	St	Sphalerite - pyrite ore
NO - 314	IC - 4	St	Pyrite ore
NO - 369	G 4	Ph	Ag - galena - sphalerite ore
NO - 401	G 4	Jm	Ag - galena - sphalerite ore
TP - 203	G 4	Ph	Sphalerite - magnetite ore
TP - 211	G 4	Ph	Sphalerite-pyrite ore

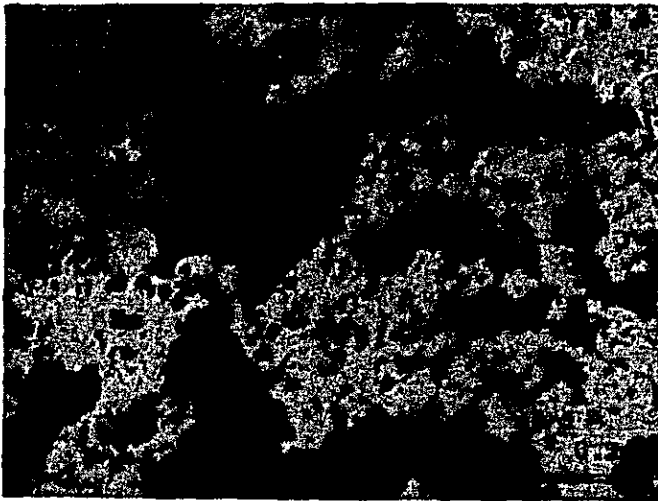
Abbreviations

Cp : Chalcopyrite
 Gl : Galena
 Sp : Sphalerite
 Py : Pyrite
 Po : Pyrrhotite
 Mg : Magnetite
 Hm : Hematite
 Bis : Bismuthinite
 Tet : Tetrahedrite



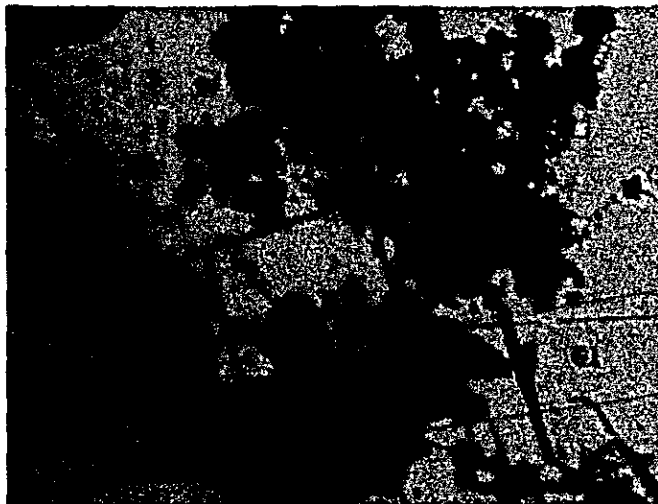
Sample No. NO-304

Rock Type: Zn pyrite ore



Sample No. NO-314

Rock Type: Pyrite ore



Sample No. NO-369

Rock Type: Ag-Pb-Zn ore